UNIVERSITÀ DEGLI STUDI DI CAMERINO

School of Advanced Studies

DOCTORAL COURSE IN

Physical and Chemical Processes in Earth Systems

XXXV cycle

MODELLING HISTORICAL EARTHQUAKES SCENARIOS IN THE APENNINES: IMPLICATIONS FOR SEISMIC HAZARD ASSESSMENT

PhD Student
Veronica Gironelli

Supervisor
Prof. Emanuele Tondi

Co-Supervisors
Dr. Lucia Luzi
Dr. Tiziano Volatili

ACKNOWLEDGEMENTS

I would like to express my gratitude to my supervisor Prof. Dr. Emanuele Tondi, whose support and encouragement gave me precious insight into not only my future academic life but also the rest of my life. This thesis would not have been possible without his guidance and foresight.

I extend sincere gratitude to my Co-Supervisors, Dr. Lucia Luzi and Dr. Tiziano Volatili, whose invaluable guidance and supervision have been instrumental in shaping the trajectory of my academic journey. I am truly fortunate to have benefitted from their expertise and mentorship.

A special debt of gratitude is owed to my Reviewers, Dr. Andrea Rovida and Dr. Francesca Pacor, for their valuable suggestions and insights. Their constructive feedback has significantly enhanced the quality of my work.

Lastly, my gratitude extends to the colleagues of the National Institute of Geophysics and Volcanology of Milan division. I am truly grateful for the collaborative environment and for their support and assistance throughout my research period.

ABSTRACT

This thesis, conducted in collaboration with the National Institute of Geophysics and Volcanology (INGV) of Milan Division, is supported by the Marche Region and by the University of Camerino as part of the FAR Project “NoHard - Novel approach for seismic hazard analysis and earthquake damage scenarios”.

The primary objective of this research is to investigate historical earthquake seismogenic sources by means of ground motion simulations. The aim is to reduce uncertainties related to unknown or debated sources in areas affected by historical earthquakes. To achieve this, a novel methodology for simulating historical earthquake scenarios is proposed, utilizing a combination of empirical methods such as Ground Motion Models (GMMs) and Ground Motion Intensity Conversion Equations (GMICEs), with observed macroseismic intensity data. This approach enables the determination of the 3D geometry of the seismogenic sources, ultimately leading to the estimation of ground motion that is consistent with the source. Such an estimation is paramount for effective emergency planning, particularly in regions with a long seismic history, such as the Italian peninsula.

The research focuses on three historical earthquakes that occurred in Central Italy during the XVIII century: the 1741 Fabriano (Imax 9 MCS, Mw 6.17), the 1799 Camerino (Imax 9-10 MCS, Mw 6.18), and the 1706 Maiella (Imax 10-11 MCS, Mw 6.84) earthquakes. Furthermore, to simulate historical earthquake scenarios at sites, the soil amplification is considered through the averaged shear-wave velocity of the uppermost 30 m (Vs,30). To enhance the accuracy of ground motion simulations, a Vs,30 map is developed for the study area, as detailed in Chapters 5 and 6.

TABLE OF CONTENTS

LIST OF FIGURES

LIST OF TABLES

ABBREVIATIONS

***PGA** : Peak Ground Acceleration*

***PGV** : Peak Ground Velocity*

***Mw** : Moment Magnitude*

***Vs,30** : Time-average shear-wave velocity to a depth of 30 m*

***SA** : 5% damped Spectral Acceleration*

***MCS** : Mercalli-Cancani-Sieberg Intensity Scale*

***DEM** : Digital Elevation Model*

***GMPEs** : Ground Motion Prediction Equations*

***GMMs** : Ground Motion Models*

***IPEs** : Intensity Prediction Equations*

***GMICEs** : Ground Motion to Intensity Conversion Equations*

***USGS** : United States Geological Survey*

***INGV** : National Institute of Geophysics and Volcanology*

***DISS** : Database of Individual Seismogenic Sources*

***ISSs** : Individual Seismogenic Sources*

***CSSs** : Composite Seismogenic Sources*

***CFTI** : Catalogue of Strong Earthquakes in Italy*

***ASMI** : Italian Archive of Historical Earthquake Data*

***DBMI** : Macroseismic Database of Italian Earthquakes*

***CPTI** : Parametric Catalogue of Italian Earthquakes*

***IDPs** : Intensity Data Points*

CHAPTER 1

INTRODUCTION

1. Introduction

The Italian Peninsula is characterised by high seismic hazard due to its location at the boundary between the Eurasian and African tectonic plates (Danciu et al., 2021) referring to the seismic hazard map of Europe available at (http://hazard.efehr.org/en/home/).

The computation of seismic hazard relies on a multidisciplinary approach based on the knowledge of recent (i.e., instrumental) and historical (i.e., pre-instrumental) seismicity, the tectonic and structural setting, and the theory of seismic source and wave propagation (e.g., Baker et al. 2021). In particular, the seismicity models used for the evaluation of seismic hazard are based on the statistics of the earthquakes that occurred in the past. Since modern seismic networks capable of accurately detecting the microseismicity and major earthquakes date back to the '70s, earthquakes of the past centuries can only be described using historical documents or paleoseismology.

Historical seismology in Italy relies on a long-standing tradition, and today the most known macroseismic catalogues are the Italian Macroseismic Database (*Database Macrosismico Italiano* - DBMI, Locati et al., 2022) and the Parametric Italian Earthquake Catalogue (*Catalogo Parametrico Terremoti Italiani* – CPTI, Rovida et al., 2022; https://emidius.mi.ingv.it/CPTI15-DBMI15/), that are regularly updated. The CPTI ensures the completeness and correct parameterization of all earthquakes of interest for Italy with Imax $\geq$ 5 or M $\geq$ 4.0 starting from 1000.

Another important catalogue is the Catalogue of Strong Earthquakes in Italy (*Catalogo dei Forti Terremoti Italiani* - CFTI, Guidoboni et al., 2018, 2019; https://storing.ingv.it/cfti/cfti5/), which focuses on detailing the strongest earthquakes occurring in Italy and the Mediterranean basin since very remote epochs.

In the parametric catalogue, the epicentral location and the earthquake magnitude are based on macroseismic observations because of the absence of instrumental data, (e.g., Bakun and Wentworth, 1997; Gasperini et al., 1999; 2010; Provost and Scotti, 2020, among others). However, epicentral location and magnitude could be affected by some

bias, while the earthquake focal depth is always missing since it cannot be estimated from macroseismic data.

Despite these limitations, the parametric catalogue is considered an essential tool for representing long-term seismicity within the Italian territory for countless research endeavors and applications, such as seismic hazard estimations and the definition of seismogenic processes, the identification and characterisation of areas and fault lines that are seismically active. The identification process of active faults involves a combination of geological, geophysical, and geodetic techniques, paleo-seismic analysis, and the integration of historical and instrumental earthquake data.

An example of active fault repository is the project ITHACA (ITaly HAzard from CApable faults; ITHACA Working Group, 2019) developed in the second half of the '90s by ISPRA (*Istituto Superiore per la Protezione e la Ricerca Ambientale*) which focuses on the identification of active faults capable of generating strong earthquakes. Currently, the last version of the catalogue is available online on the Italian Geological Survey's (SGI) portal (https://sgi.isprambiente.it/ithaca/viewer/). However, this catalogue has limitations, including a lack of information about the 3D geometry of the seismic sources and the absence of individual sources of historical (i.e., pre-instrumental) earthquakes, while it provides only a representation of the fault trace evidences at the surface.

A Database of Individual Seismogenic Sources (*Database delle Sorgenti Sismogeniche Individuali* – DISS; DISS Working Group, 2021; https://diss.ingv.it/) was compiled by the National Institute of Geophysics and Volcanology (*Istituto Nazionale di Geofisica e Vulcanologia* - INGV). This database, initially published in 2000, has the aim of investigating and organizing knowledge regarding the sources of earthquakes in Italy. This database provides the 3D geometry and extent of the seismogenic sources for moderate-to-large earthquakes. Nevertheless, in this repository are observed some incompleteness. For example, not all ISSs are associated with a seismic event, as evident in the case of ITIS027 (Sulmona Basin) and ITIS038 (Gubbio North) seismogenic sources. Similarly, not all seismic events are associated to a defined seismogenic source (e.g., 1706 event). Additionally, the downdip fault extension for

some ISSs remains uncertain due to the lack of focal depth information. This is particularly relevant for historical earthquakes.

1.1. Objective and scope of the thesis

To address the limitations of the historical/macroseismic and seismic sources catalogues, the seismological methods may be integrated with more geological aspects.
The aim of the research project is to introduce a novel approach that involves the integration of observed macroseismic intensity data, existing seismogenic source catalogues, and empirical Ground Motion Models (GMMs) to define the 3D geometries of historical earthquake sources. In the proposed methodology, the empirical prediction models represent a crucial tool for correlating the historical and geological data. GMMs are calibrated on ground motion recordings of instrumental earthquakes and relate ground motion parameters to a set of variables (e.g., earthquake magnitude, source-to-site distances, and local site conditions).
To investigate the 3D geometry of historical earthquake sources, Ground Motion Intensity Conversion Equations (GMICEs) are employed to convert observed macroseismic intensity into ground motion parameters.

Moreover, another important objective of this research is the reconstruction of ground motion scenarios that are useful for the evaluation of their potential impact on today's urban setting. This is particularly true for historical earthquakes characterised by long return periods, for developing more accurate land-use planning, and emergency response strategies aimed at mitigating the impact of future earthquakes on the population and infrastructures.

According to the current literature, one of the reference approaches for calculating the shaking scenarios is the ShakeMap model (Worden et al., 2020, Wald et al., 2021), a software distributed by the US Geological Survey (USGS). ShakeMap is a ground motion interpolator that avails of recorded data and seismological and geotechnical knowledge to produce ground shaking maps. Allen et al. (2008) developed an atlas of shaking maps for recent and historical global earthquakes. In Italy, the application of this methodology was proposed by Michelini et al. (2020), and very recently adopted by Oliveti et al. (2023) to develop an Italian atlas of historical earthquakes shaking maps.

However, this approach has limitations, relying on an empirical prediction model for macroseismic intensity calibrated based on epicentral distance and a ground motion model calibrated using the distance from the surface projection of the fault. Consequently, both methods neglect the three-dimensional geometries of the seismogenic sources. Additionally, the ShakeMap approach incorporates site effects through soil categories (e.g., Eurocode 8 - EC8).

For these reasons, the integration of a geological approach with the seismological contribution given by the empirical prediction models allowed to investigate the location and parametrization of historical earthquake sources and subsequently generate reliable ground motion scenarios. Differently from the commonly adopted ShakeMap-based approach, the proposed methodology allows to calculate the shaking scenarios for historical earthquakes at a site by using a map of the averaged shear-wave velocities in the uppermost 30m (Vs,30). With this aim, a large effort is spent in this thesis to develop a Vs,30 map.

This doctoral thesis is organised as a collection of scientific papers. The Chapters 2, 3, and 4 provide a description of the geological and seismotectonic settings of the study area and an overview of the input data. The Chapters 5, 6, and 7 constitute the bulk of the thesis, detailing the approach used to develop a Vs,30 map and the application of the methodology to two distinct case studies. A summary outlining the content of these chapters and delineating my contributions into each work is presented below:

- ***Chapter 5 – Dual-proxy estimation of Vs30: the case study of the Marche Region (central Italy)***

  "Published in Journal of Maps"

This chapter illustrates the procedure to create a Vs,30 map as a proxy to account for site effects in ground motion models. In this work, I collect existing data of shear-wave velocity profiles for the Marche Region that are used to compile a dataset of Vs,30. Each Vs,30 point has been associated to a lithology and to a value of topographic slope from a Digital Elevation Model. To this aim, a lithological classification was conducted to homogenize and organize the original geological formations into complexes based on prevailing lithologies. A statistical analysis was conducted to obtain an empirical

equation relating Vs,30 to lithology and topographic slope. This procedure is calibrated for the Marche Region, is propaedeutic for a subsequent creation of the Vs,30 map of the entire study area.

- ***Chapter 6 – Ground motion simulations of historical earthquakes: the case study of the Fabriano (1741, Mw = 6.1) and Camerino (1799, Mw = 6.1) earthquakes in central Italy***

  "Published in Bulletin of Earthquake Engineering"

This chapter presents the methodology for generating ground motion simulations and determining the seismogenic sources of two case studies in the Marche Region (Central Italy): the "Fabrianese" event on April 24th, 1741 (Imax 9 MCS; Mw 6.17) and the "Appennino Marchigiano" event on July 28th, 1799 (Imax 9-10 MCS; Mw 6.18), hereinafter called "Fabriano" and "Camerino" earthquakes, respectively. The approach utilizes recent GMMs for Italy (ITA18, Lanzano et al., 2019) to predict ground motion in terms of Peak Ground Acceleration (PGA) and Peak Ground Velocity (PGV), and a Ground Motion Intensity Conversion Equation (GMICE, Gomez Capera et al., 2020) to convert ground motion parameters into macroseismic intensities and vice-versa. The 3D seismogenic sources of these earthquakes are identified through a residual analysis between simulated and observed macroseismic intensities. The presented procedure has been developed as a MATLAB code that is used to investigate both the seismogenic source geometries and shaking scenarios.

- ***Chapter 7 - Elusive seismogenic sources of historical earthquakes: Insights from the Mw 6.8, 1706 Maiella earthquake (Central Italy)***

  "Submitted to Bulletin of Earthquake Engineering"

This chapter presents the application of the methodology introduced in Chapter 6 to identify the source of the "Maiella" event on November 3rd, 1706 (Imax 10-11; Mw 6.84) in the Abruzzi Region (Central Italy). Many seismogenic sources are attributed to this seismic event (e.g., De Nardis et al., 2008; Galli and Pallone, 2019; Bordoni et al., 2023) and in this work some of them have been tested to constrain the most reliable causative fault and calculate an earthquake scenario. My contribution in this work is the

analysis for the identification of the 3D seismogenic source and the modelling of shaking scenarios.

Conclusions and final considerations are presented in Chapter 8.

CHAPTER 2

GEOLOGICAL AND SEISMOTECTONIC SETTING OF THE CENTRAL APENNINES

This Chapter presents a general description of the central Apennines with an overview of the main geological and seismotectonic features of the area considered as case study.

2. Geological and seismotectonic setting of the central Apennines

The central Apennines (central Italy) are part of a NW-SE trending, east-verging fold-and-thrust belt developed during the Cenozoic time (Centamore and Rossi, 2009; Cosentino et al. 2010). The present-day structural framework of this sector derives from the succession of contractional, and extensional deformation events related to the emplacement of the Apennine chain (e.g., Mazzoli et al., 2002; Butler et al., 2006; Di Domenica et al., 2014 among others). Starting from the Late Miocene a two-stage compressional tectonic phase was active until the beginning of Early Pliocene. The first stage involved the formation of NW-SE thrust and fold systems (Patacca et al., 1990, 2008, and references therein), while the second stage caused the eastward migration of the orogenic front and the foredeep-foreland system. Successively, a post-orogenic Plio-Quaternary extensional phase involved the area due to the diffuse back-arc stretching affecting the Tyrrhenian side of the orogen (Carminati and Doglioni, 2012) and caused the collapse of the inner domains of the thrust belt. Such a tectonic setting controlled the origin and the evolution of the tectonic units of the Umbria-Marche and Latium-Abruzzi sectors. During the evolution of the central Apennines, these sectors are characterised by a shallow marine environment and carbonate sedimentation. Successively, the formation of sin-sedimentary normal faults dissected the carbonate platform and creating a deepening of the Umbria – Marche sector with the sedimentation of turbiditic deposits. The Umbria-Marche domain is characterised by a Meso-Cenozoic sedimentary sequence mainly composed of Jurassic-Paleogene calcareous and marly units, followed by arenaceous Oligo – Miocene units and the Plio-Pleistocene peri-adriatic sequence (Pierantoni et al., 2013). After the emersion of this sector, the sedimentation is exclusively continental and influenced by Quaternary climatic phases, resulting in the formation of erosion surfaces and alluvial terraces. Whereas the Latium-Abruzzi domain is characterised by deposition of a thick stratigraphic sequence composed of Mesozoic-Tertiary shallow-water and transitional platform-to-basin carbonates of the Adriatic-Apulian margin (Vezzani and Ghisetti, 1998; Antonellini et al., 2008).

The central Apennines are among the most seismically active areas of Italy. The seismic activity in this area is strongly influenced by an extensional tectonic regime in the axial

sector of the chain and by a compressional tectonic regime in the Peri-Adriatic area. As evidenced by seismological data and the available focal mechanisms of the major earthquakes reported in Monachesi et al. (2021), shallow seismic events (depth < 10 km), with strike-slip and thrust fault plane solutions, are localised in the easternmost Adriatic area (Mazzoli et al., 2015). Whereas in the axial sector of the central Apennines, the Plio-Quaternary extensional tectonics is superimposed on the previous compressional one (Galadini and Galli, 2000; Roberts and Michetti, 2004; among others) as shown in Fig. 2.1. Therefore, in this context, the seismicity related to extensional processes is localised in the upper crustal levels (depth of 7-15 km) and is consistent with normal fault kinematics (Collettini, 2002; Collettini et al., 2003; Lavecchia et al., 2004), while a few compressive earthquakes are localised in sub-crustal levels at depth range of 30-90 km (Pauselli et al., 2006).

The present-day extensional processes active in the axial sector of central Apennines developed a network of fault systems. The surface expression of these fault systems is represented by a set of mainly NW-SE trending, normal or oblique fault segments with lengths ranging from a few km to 15–20 km, mostly steeply dipping towards the SW (Pizzi and Galadini, 2009).

The major fault system of the study area is represented by the Central Apennines Fault System (CAFS; Cello et al., 2000; Tondi, 2000), which extends from Colfiorito to L'Aquila, over a total length of 100 km (Tondi, 2000). These structures usually border the eastern side of the Mio-Pliocene extensional basins infilled by Plio-Quaternary continental deposits controlling their evolution (e.g., Norcia, Castelluccio, Cascia, Rieti, L'Aquila, Fucino, and Sulmona basins). After the 1997 seismic events, the CAFS has been the subject of several studies, as well as of detailed geological, geophysical, and paleo-seismological field investigations (e.g., Barchi et al., 2000; Galadini and Galli, 2000; Tondi, 2000; Tondi et al., 2020; Galli et al., 2008, 2022) and based on these studies, most of the historical and instrumental seismicity of the area was associated with CAFS-related structures.

The central Apennines, given the huge amount of seismological data, both historical and instrumental, represents a key region in Italy for the investigation of seismogenic sources related to historical earthquakes. According to current seismic catalogues (e.g., CPTI15; Rovida et al., 2022), the central Italy suffered at least 50 destructive

earthquakes of a magnitude in the range of Mw 5.5-6.5 over the last seven centuries (*Appendix A*). The last three major seismic sequences occurred in 1997 (Mw = 6.0) Colfiorito, in 2009 (Mw = 6.3) L'Aquila, and in 2016 (Mw = 6.5) Amatrice-Visso-Norcia (Fig. 2.1). Specifically, in this PhD dissertation the following historical earthquakes, are investigated: i. April 24th, 1741 "Fabrianese" (Imax 9 MCS; Mw 6.17), ii. July 28th, 1799 "Appennino Marchigiano" (Imax 9-10 MCS; Mw 6.18), hereinafter called "Fabriano" and "Camerino", iii. November 3rd, 1706 "Maiella" (Imax 10-11 MCS; Mw 6.84). These seismic events, among the strongest earthquakes occurred in the Marche and Abruzzi regions in the past, did not manifest recurrence in instrumental times. Their geological characteristics are further described in Chapters 6 and 7.

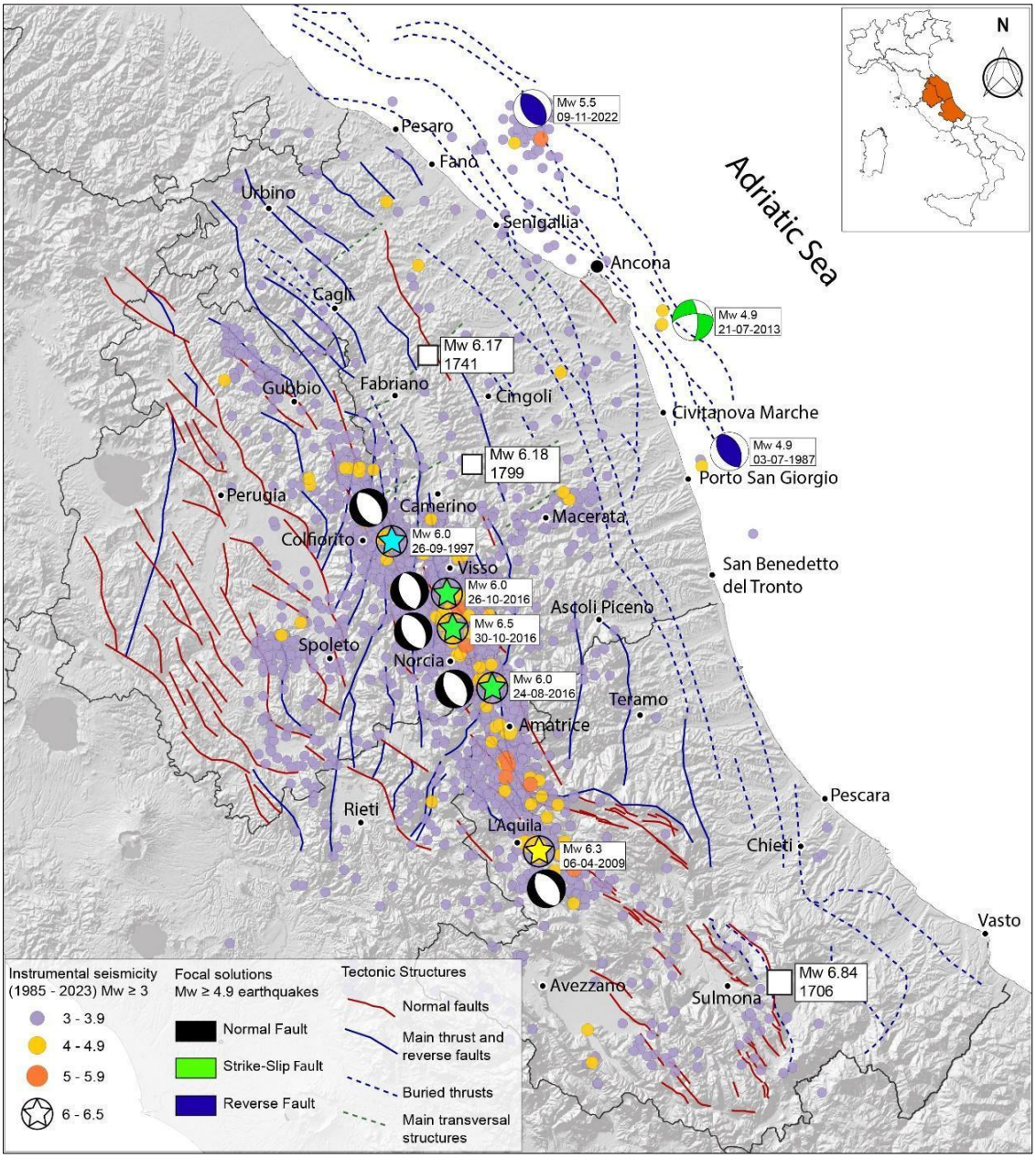

Figure 2.1. Main tectonic structures of central Apennines (modified after Mazzoli et al., 2002 and Galli and Pallone 2019) and related instrumental seismicity Mw ≥ 3 from ISIDe Working Group, 2007. The focal mechanisms relative to the main events are representative of the extensional and compressional tectonic structures of the area. White squares represent the investigated historical earthquakes.

CHAPTER 3

DATA COLLECTION

This Chapter provides an overview of the data employed in this research: *individual seismogenic sources, historical macroseismic data,* and *shear-waves velocity profiles* .

3. Data Collection

3.1. Database of Individual Seismogenic Sources

Among the existing databases, the Database of Individual Seismogenic Sources (DISS Working Group, 2021) has been selected for the scope, due to its completeness at the National scale and for the presence of historical earthquake sources. DISS differentiates the seismogenic sources into Composite Seismogenic Sources (CSSs) and Individual Seismogenic Sources (ISSs), as shown in Fig. 3.1. The CSSs identify zones containing an unspecified number of seismogenic sources, while the ISSs are a 3D representation of sources of occurred earthquakes. ISSs are provided for well-recorded instrumental earthquakes, as well as historical ones, and have a different level of accuracy related to the availability of data. DISS provides information about the latitude and longitude, and a full set of geometrical (strike, dip, length, width, and depth of the fault vertices), kinematic (rake) and seismological parameters (average displacement, magnitude, slip rate and recurrence interval). In particular, for instrumental earthquakes, the causative sources are determined accurately using a set of information, such as a surface expression, if evident, the occurrence of aftershocks, and the calculation of moment tensor. Whereas, for historical earthquakes, all such information are often unavailable, and the identification of the seismogenic source relies on limited data and regional tectonic knowledge.

Figure 3.2. Representation of the Composite Seismogenic Sources (CSSs) and Individual Seismogenic Sources (ISSs) within the DISS database (DISS Working Group, 2021).

In the current release of the DISS database (version 3.3.0), the two highly damaging historical events in the Marche Region, the 1741 Fabriano earthquake (Imax 9 MCS; Mw 6.17) and the 1799 Camerino earthquake (Imax 9-10 MCS; Mw 6.18), are characterised by a source geometry. The Fabriano seismic source (ITIS048) lacks evidence of fault surface, leading to controversial interpretations of the fault

mechanisms. DISS suggests the ITIS048 source as a NW–SE dipping SW low-angle reverse fault; other authors suggest a NE–SW strike-slip mechanism, sub-perpendicular to the Apennine axis (e.g., Cello et al. 1997; Materazzi et al. 2022). On the other hand, the Camerino seismic source (ITIS049) presents a definite fault mechanism and geometry, although the focal depth is uncertain. DISS identifies the ITIS049 as a NW-SE structure characterised by the typical normal faulting mechanism of the Apennine faults.

Differently, the 1706 Maiella earthquake (Imax 10-11; Mw 6.84) that occurred in the Abruzzi Region, is not associated with any source. Several hypotheses have been proposed, including superficial normal faults (Pizzi and Galadini, 2009; De Nardis et al., 2011; Bordoni et al., 2023) and deep reverse tectonic structures (Galli and Pallone, 2019). Whereas DISS suggests that this event may be related with the largest and proximal Sulmona Basin source (ITIS027). This ISS is associated with the Mt. Morrone fault, a dip-slip fault with surface expression consistent with a maximum magnitude of 6.7 ± 0.1 as reported by Galli et al. (2015).

For these earthquakes, the geometrical parameters of the source (i.e., strike, dip, length, width, and depth of the fault vertices) provided by DISS are mainly derived from available observational geological data and empirical relationships due to the lack of significant instrumental seismicity. The fault scaling relations of Wells and Coppersmith (1994) are used in the ISS construction to obtain the seismic source dimensions (length or width or both) that are consistent with the size of the associated earthquake. Specifically, the scaling relationships from Wells and Coppersmith (1994) used in DISS for deriving source length and width from moment magnitude are as follows:

$$\mathrm{Log_{10}L} = \mathrm{a} + \mathrm{b} * \mathrm{Mw} \quad (3.1)$$

$$\mathrm{Log_{10}W} = \mathrm{a} + \mathrm{b} * \mathrm{Mw} \quad (3.2)$$

where $\boldsymbol{L}$ and $\boldsymbol{W}$ are the source length and width, respectively, $\boldsymbol{Mw}$ is the moment magnitude, and $\boldsymbol{a}$ and $\boldsymbol{b}$ are the coefficients for the fault mechanisms.

The geometrical parameters of the sources associated with these historical earthquakes are listed in the following table (Table 3.1), while individual seismogenic sources (ISSs) are illustrated in Fig. 3.2. These sources are plotted on top of the seismic hazard map of Italy (Mappa di Pericolosità Sismica - MPS04; Meletti et al., 2006), highlighting that the study area is located in one of the most hazardous areas in Italy. Therefore, the identification of poorly-known sources of historical earthquakes, is of paramount importance for future hazard studies.

Table 3.1. The geometrical parameters of the seismogenic source of the 1741 Fabriano, 1799 Camerino, and 1706 Maiella earthquakes from DISS (DISS Working Group, 2021).

Seismogenic Source	***FABRIANO***	***CAMERINO***	***SULMONA BASIN***
ID_DISS	ITIS048	ITIS049	ITIS027
Length [km]	13.0	14.0	20.0
Width [km]	9.0	9.5	12.2
Min_depth [km]	14.0	3.0	1.0
Max_depth [km]	17.1	7.8	11.6
Strike [°]	135	153	135
Dip [°]	20	30	60
Associated Event	24 April 1741	28 July 1799	/

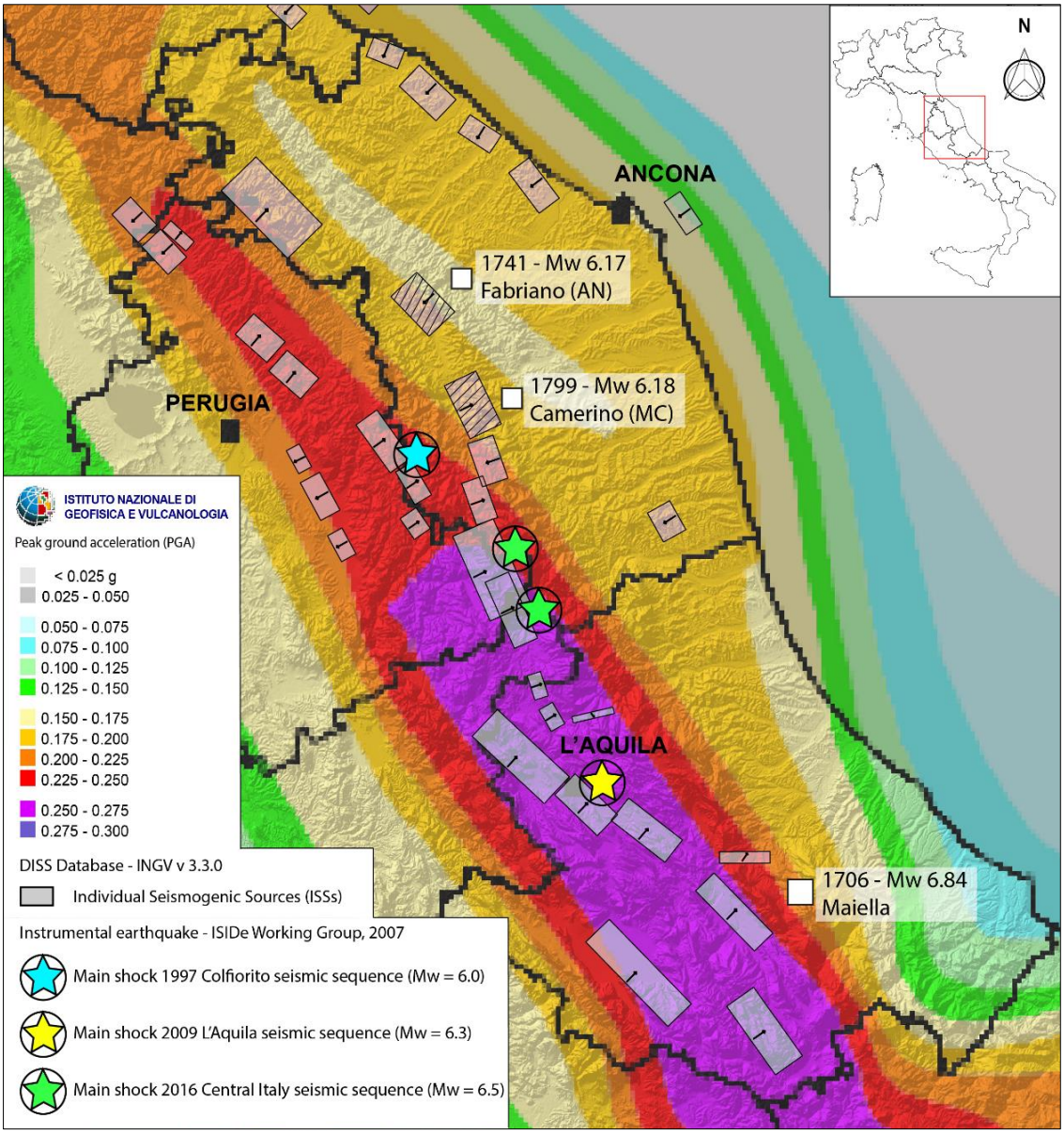

Figure 3.2. Seismic hazard map of central Italy (MPS04 modified after Stucchi et al. 2004). The main shocks of the major seismic sequences affecting the central Apennines in the last decades are plotted using the location from the ISIDe database (ISIDe Working Group, 2007). White squares represent the investigated historical earthquakes (Mw ≥ 6) from CPTI15 catalogue (Rovida et al., 2022). The rectangles with a dashed pattern represent the individual seismogenic sources ITIS048 and ITIS049 from the Database of Individual Seismogenic Sources (DISS; Basili et al., 2008; DISS Working Group 2021).

3.2. Macroseismic Intensity Data

The severity of earthquakes can be assessed through macroseismic intensity which quantifies the earthquake effects at different localities on humans, objects, buildings, and the environment (Cancani, 1904).

The evaluation of the observed seismic effects at a site is performed through macroseismic intensity scales. In general, most of the intensity scales used in Europe are constituted by a series of twelve damage scenarios organized in an increasing order based on the severity of the effects (e.g., MCS, Sieberg, 1932; MSK, Medvedev et al., 1964; MM, Stover and Coffman, 1993; EMS98, Grünthal, 1998). Each scenario is associated to an ordinal number and is accompanied by a description of the observed seismic effects. The assessment of an intensity value is performed through a comparison of the observed seismic effects at a site and the scenarios proposed in the adopted scale. In the Italian Macroseismic Database (DBMI) the intensity values are attributed/provided according to the Mercalli-Cancani-Sieberg (MCS) scale of Sieberg (1932).

The intensity value attributed to a specific location, identified through geographic coordinates, and related to a specific earthquake, is defined as Intensity Data Point (IDP).

The whole distribution of IDPs referred to a specific event is known as the macroseismic intensity distribution, which is a representation of the area interested by the earthquake effects. Referring to historical earthquakes, the macroseismic intensity distribution represents the only information available which are inferred from historical documentation.

In Italy, the practice of collecting macroseismic data has a long tradition and much effort are spent to archive these data into historical seismic catalogues. The first benchmark catalogue was compiled by Mario Baratta in 1901. The ‘80s and ‘90s represent an intense period dedicated to historical seismic studies by two distinct working groups: the CNR-National Group for the Defense against Earthquakes (GNDT), and the ING-SGA History Geophysics Environment. Both these entities eventually merged into the National Institute of Geophysics and Volcanology (INGV),

culminating in the initial version of the Parametric Catalogue of Italian Earthquakes (CPTI99; Boschi et al., 1999).

The National Institute of Geophysics and Volcanology (INGV) is at present the largest institution in Italy that collects macroseismic data. The information related to the historical earthquake studies contained in the Italian Archive of Historical Earthquake Data (*Archivio Storico Macrosismico Italiano* – ASMI; Rovida et al., 2017; https://emidius.mi.ingv.it/ASMI/index_en.htm), after a careful review on the content and quality, are used for the compilation of the Italian Macroseismic Database (*Database Macrosismico Italiano* - DBMI15; Locati et al., 2022). The current version of this database (version 4.0), available at https://emidius.mi.ingv.it/CPTI15-DBMI15/, provides a collection of 123.981 IDPs related to 3229 Italian earthquakes that occurred in the time-period 1000-2020, as illustrated in Fig. 3.3.

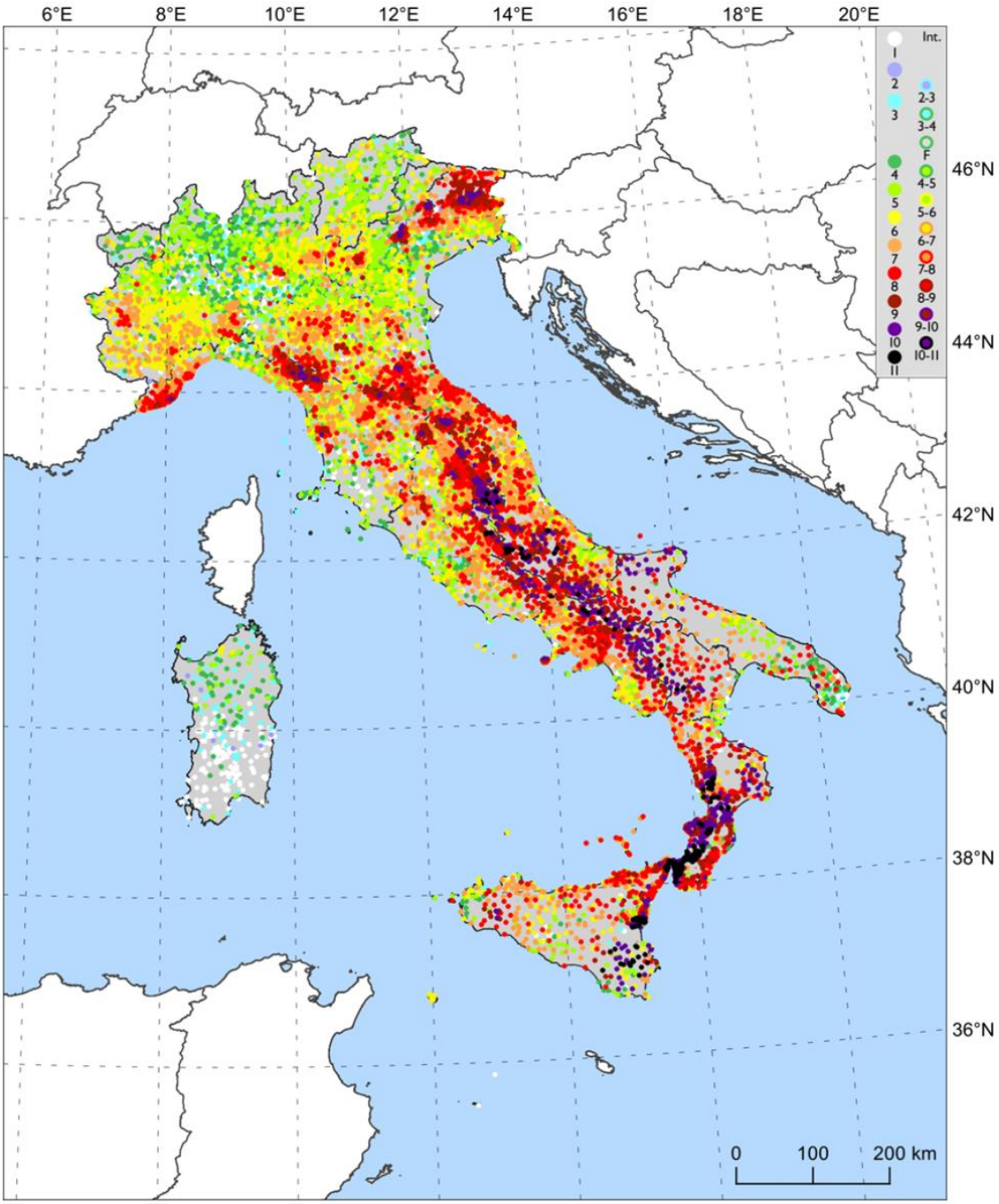

Figure 3.3. Representation of the maximum observed intensities distribution in Italy from DBMI15 (Locati et al., 2022).

The data contained in the DBMI15 (Locati et al., 2022) are used for compiling the associated Parametric Catalogue of Italian Earthquakes (*Catalogo Parametrico dei Terremoti Italiani* – CPTI15; Rovida et al., 2022) which contains 4894 earthquakes that have occurred in Italy and neighbouring areas in the time-period 1000-2020, and for deriving the earthquake parameters.

In detail, for historical earthquakes the spatial distribution of IDPs can be considered for the characterisation of the epicentral location and magnitude due to the absence of instrumental data (e.g., Bakun and Wentworth, 1997; Gasperini et al., 1999, 2010; Musson and Jiménez, 2008; Provost and Scotti, 2020).

The source parametrization in CPTI15 is determined using the Boxer method proposed by Gasperini et al. (1999, 2010). Considering the distribution of largest macroseismic intensities, Boxer calculates the epicentral location (or macroseismic epicentre) as the barycentre of the localities with the highest seismic intensities as in Gasperini et al. (2010). Boxer is also employed to compute the epicentral intensity, reported as I_0, and the macroseismic magnitude. The macroseismic magnitudes determined using Boxer are calculated through two different approaches. The first is the isoseismal method which calculates a magnitude for each intensity class using a recalibration of Boxer method with a new dataset and the following equation based on the formula by Sibol et al. (1987):

$$Mi = ai + bi \log^2 (Ai) + ci\ I_0^2 \qquad (3.3)$$

where ***M*** represents the magnitude, ***Ai*** is the area of a circle with a radius equal to the average epicentral distance of places whose observed intensity belongs to the i-th intensity class, $\boldsymbol{I_0}$ is the epicentral intensity, and ***ai***, ***bi***, ***ci*** are the empirical coefficients in CPTI15 (Rovida et al., 2022). The resulting magnitude, expressed as moment magnitude, is the weighted mean of the magnitudes obtained for each of intensity classes.

Whereas the second approach is adopted in cases of sparse intensity distributions and is based on a conversion from I_0 to Mw that is calibrated using the same dataset of the first approach. The empirical relation is the following:

$$Mw = (0.4667 \pm 0.0191) * I_0 + (1.8267 \pm 0.1571) \qquad (3.4)$$

For my research purpose, the macroseismic intensity data are useful for the computation of the residual analysis between the observed macroseismic data and the synthetic intensities predicted by the ground motion model. Subsequently, these intensity data are also employed to generate the shaking scenarios.

The macroseismic data related to the examined historical earthquakes are extracted from the latest release of the DBMI15, version 4.0 (Locati et al., 2022). A total of 304 Intensity Data Points (IDPs) were collected, including 135 for the 1741 Fabriano earthquake (Monachesi, 1987), 70 for the 1799 Camerino earthquake (Guidoboni et al., 2007), and 99 for the 1706 Maiella earthquake (Guidoboni et al., 2007), respectively. The magnitude values from the CPTI15 catalogue were considered for the shaking prediction. It assigns a moment magnitude of 6.17 to the Fabriano earthquake, 6.18 to the Camerino earthquake, and 6.84 to the Maiella earthquake (Table 3.2).

Table 3.2. Macroseismic data from the CPTI15 catalogue (Rovida et al., 2022). Mw is the moment magnitude obtained from macroseismic intensity and NMO is the number of macroseismic observations from DBMI15 (Locati et al., 2022).

Historical Earthquake	***Date***	***Epicentral location***	***Imax***	***Mw***	***NMO***
Fabriano	24 April 1741	43.426 / 13.005	9	6.17	135
Camerino	28 July 1799	43.193 / 13.151	9-10	6.18	70
Maiella	3 November 1706	42.076 / 14.080	10-11	6.84	99

The spatial distribution of the 135 IDPs related to the 1741 Fabriano earthquake (Imax 9) is represented in Fig. 3.4. The macroseismic intensity data are derived from Monachesi (1987) and ranges from $3 \leq I_{MCS} \leq 9$, with the maximum macroseismic intensity value (I_{MCS} 9) assigned to the Fabriano, Mergo, Sasso, and Serra San Quirico localities. Approximately 87% of the macroseismic data falls within the range $5 \leq I_{MCS} \leq 8.5$. Lower macroseismic intensities are assigned to localities at greater distances (≥ 100 km) from the earthquake epicentre, such as Ascoli Piceno, Cesena, and Rimini. The wide macroseismic intensity field, along with the estimated magnitude of 6.17 and the absence of documented aftershocks, suggests that the earthquake may have had a considerable hypocentral depth.

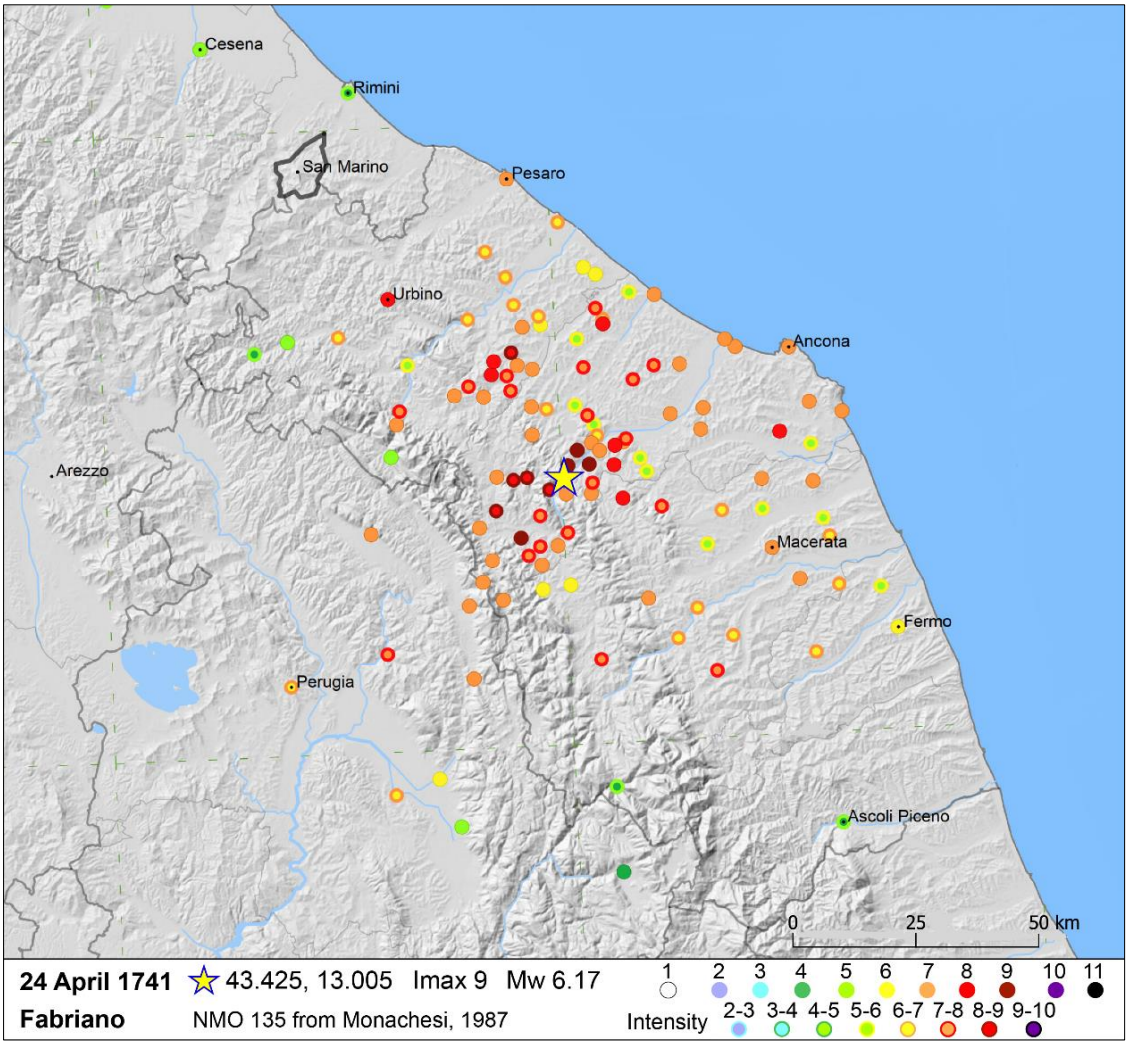

Figure 3.4. Spatial distribution of the macroseismic intensities for the 1741 Fabriano earthquake (Imax 9; Mw 6.17) modified from DBMI15 (Locati et al., 2022).

Differently from the Fabriano earthquake, the 1799 Camerino earthquake (Imax 9-10) is characterised by a narrower distribution, as shown in Fig. 3.5. The majority of macroseismic intensity values fall within the range of $7 \leq I_{MCS} \leq 9$. The highest macroseismic intensity value (I_{MCS} 9) is attributed to Camerino, San Ginesio, and other smaller localities, including Cessapalombo, Letegge, Pozzuolo, Cesolo, where extensive damage has been documented (Monachesi et al., 2016). However, the macroseismic intensity distribution of this event is characterised by a scarcity of low-intensity values ($I_{MCS} \leq 4$) and areas devoid of macroseismic intensity data, suggesting that the earthquake went unnoticed in those areas. This absence may be attributed to a lack of

available data, possibly due to sparse population or limited testimonies collected in those areas during that period.

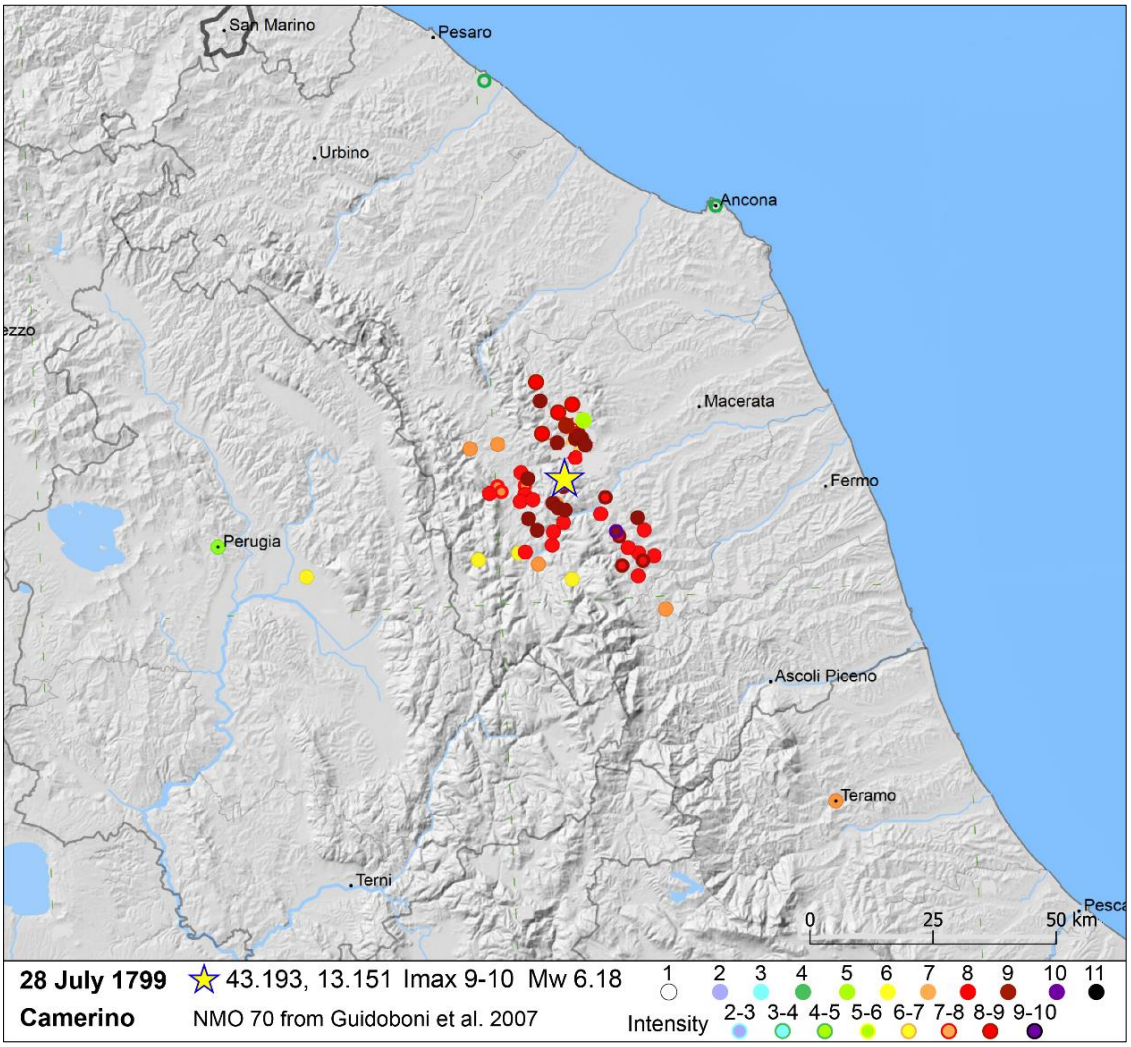

Figure 3.5. Spatial distribution of the macroseismic intensities for the 1799 Camerino earthquake (Imax 9-10; Mw 6.18) modified from DBMI15 (Locati et al., 2022).

The macroseismic intensity field illustrated in Fig. 3.6 provides a comprehensive overview of the spatial distribution of macroseismic intensities related to the 1706 Maiella earthquake (Imax 10-11). The macroseismic intensity field is mostly concentrated around the Maiella Massif, with values that fall within the range of $6 \leq I_{MCS} \leq$ 10-11. The highest macroseismic intensity value (I_{MCS} 10-11) has been assigned to the smaller villages of Lama dei Peligni, Manoppello, and Palena localities. While Sulmona, that was one of the most heavily damaged inhabited centres, has been assigned a macroseismic intensity value of I_{MCS} 9-10.

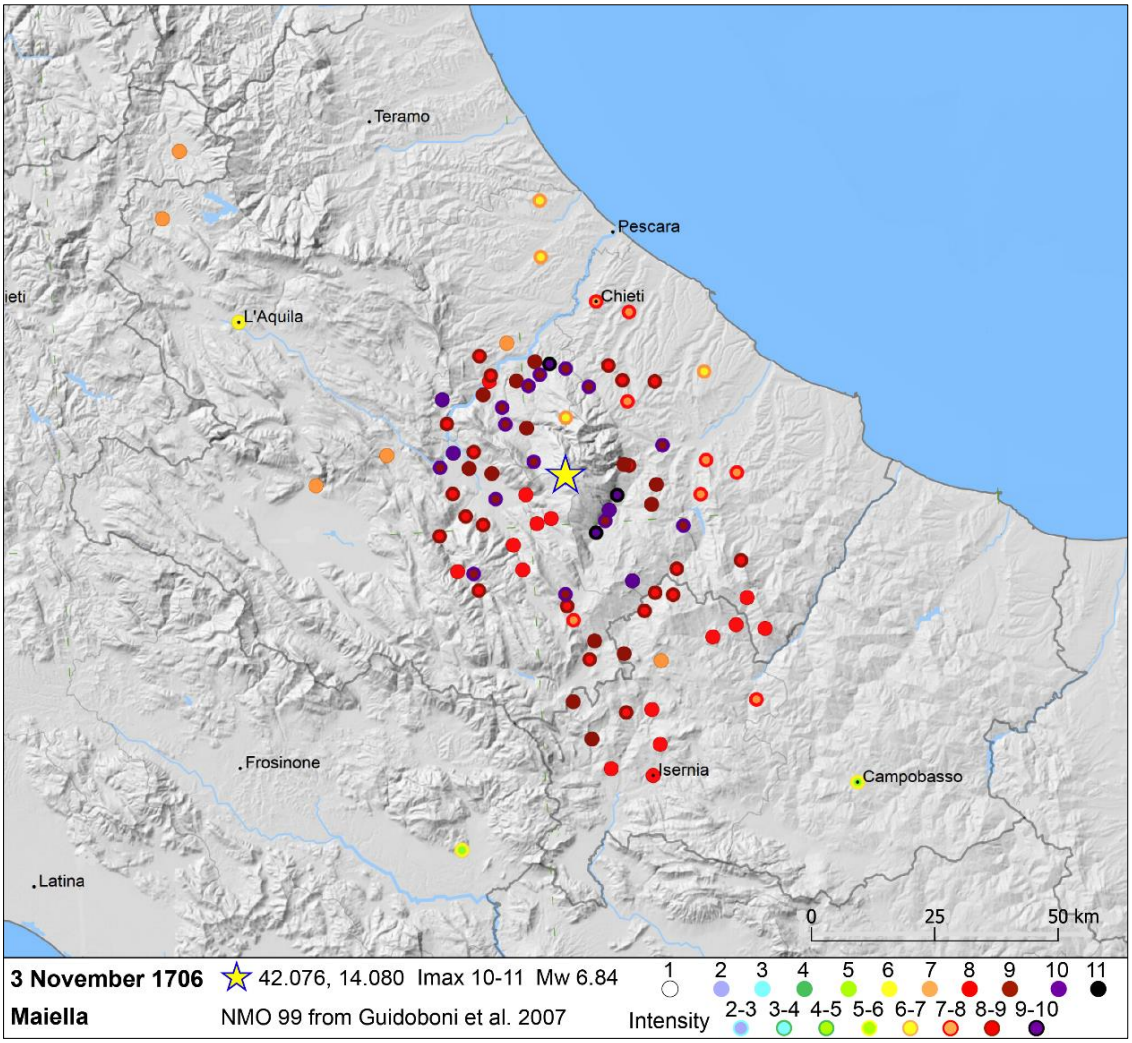

Figure 3.6. Spatial distribution of the macroseismic intensities for the 1706 Maiella earthquake (Imax 10-11; Mw 6.84) modified from DBMI15 (Locati et al., 2022).

3.3. Data Collection for local site effects estimation

Local site conditions can significantly affect various aspects of earthquake ground motion, including amplitude, frequency content, and duration. The complexity of the subsoil geology produces a complex seismic wave propagation, and site response modelling is required to characterise soil dynamics. However, in the literature, a simplified parameter to account for site response in ground motion modelling is the average shear-wave velocity of the upper 30 m (Vs,30; e.g., Borcherdt, 1994). This parameter was introduced as a practical alternative by the Federal Emergency Management Agency (FEMA; FEMA 273, 1997).

Most Ground Motion Models (GMMs) refer to Vs,30 either by considering the Vs,30 value in the functional form (Campbell and Bozorgnia, 2014; Lanzano et al., 2019), categorising the soil behaviour (i.e., stiff or soft soil) depending on Vs,30 intervals (e.g., Akkar and Bommer, 2010), or allowing both of these strategies (e.g., Bindi et al., 2014).

In this research, to calculate the shaking scenarios of investigated earthquakes and account for local site amplifications through Vs,30 values, a Vs,30 map is needed in the computation. Tinsley and Fumal (1985) were pioneers of site condition mapping. Since then, several approaches have been developed in the literature to calculate the Vs,30 using several proxies. For example, Park and Elrick (1998) observed a correlation between the Vs,30 and the grain size characteristics of geological unit in southern California, and developed a Vs,30 map categorizing the geologic units into eight different categories based on grain size and age.

In more recent studies, alternative methods for predicting Vs,30 have also been suggested, focusing on correlations with explanatory variables, such as topographic and geomorphologic proxies (e.g., Wald and Allen, 2007; Yong et al., 2008; Iwahashi et al., 2010; Yong et al., 2012). Wald and Allen (2007) introduced a topography-based Vs,30 estimation. Utilizing data from the shuttle radar topography mission (SRTM) (Farr et al., 2007), they investigated correlations between topography and Vs,30. They provided two sets of coefficients, one for active tectonic regions and another for stable continental regions, that can be employed as predictors for estimating Vs,30 globally.

At present, conventional methods for determining shear-wave velocity consist of borehole methods (down-hole, up-hole, cross-hole), active seismic methods (refraction,

multichannel surface wave analysis, seismic analysis of surface waves) and passive seismic methods (refraction microtremor, f-k analysis of noise array measurements). For example, Lee and Tsai (2008) established the spatial relationship between the shear-wave velocity (Vs) and the N value of the standard penetration test (SPT-N) and adopted the kriging with varying local means to update the Vs,30 maps in Taiwan.
For Italy, Forte et al. (2019) and Mori et al. (2020) provided soil classification maps based on site-specific measurements, geological and geomorphological information. Forte et al. (2019) calibrated two maps of seismic shallow soil classification based on soil class (e.g., EC8) and Vs,30 from Vs measurements and a large-scale geological map. Mori et al. (2020) correlated geological and geomorphological data with Vs,30 values from in-situ geophysical tests to derive a Vs,30 map for Italy. Similar approaches to Forte et al. (2019) and Mori et al. (2020) have been used for specific regions within Italy, like Molise and Campania (Cantore et al., 2010; Fabbrocino et al., 2015).

Although different Vs,30 maps exist for Italy, a significant aspect of this research is represented by the creation of a Vs,30 map specifically for the study area (further discussed in Chapter 5 and 6). This map is developed using a new dataset of shear-waves velocities profiles obtained from publicly accessible Italian seismic microzonation datasets, available at (https://sisma2016data.it/microzonazione/) and the web portal (https://qmap-protciv.regione.marche.it/cs/), as well as from private collections. A total of 2180 Vs profiles are collected for the Umbria and Marche regions and their distribution is illustrated in Fig. 3.7. The Vs profiles were measured using both invasive and non-invasive geophysical techniques, such as borehole methods (Down-Hole and Cross-Hole) and seismic refraction and surface-waves surveys (e.g., Multichannel Analysis of Surface Waves, MASW; Spectral Analysis of Surface Waves, SAWS; and REfraction MIcrotremors, REMI).
As shown in Fig. 3.7, the largest percentage of Vs profiles (47%) are executed in the Quaternary continental deposits, followed by clayey soils (21%), arenaceous (12%), marly (6%), and evaporitic soils (6%).

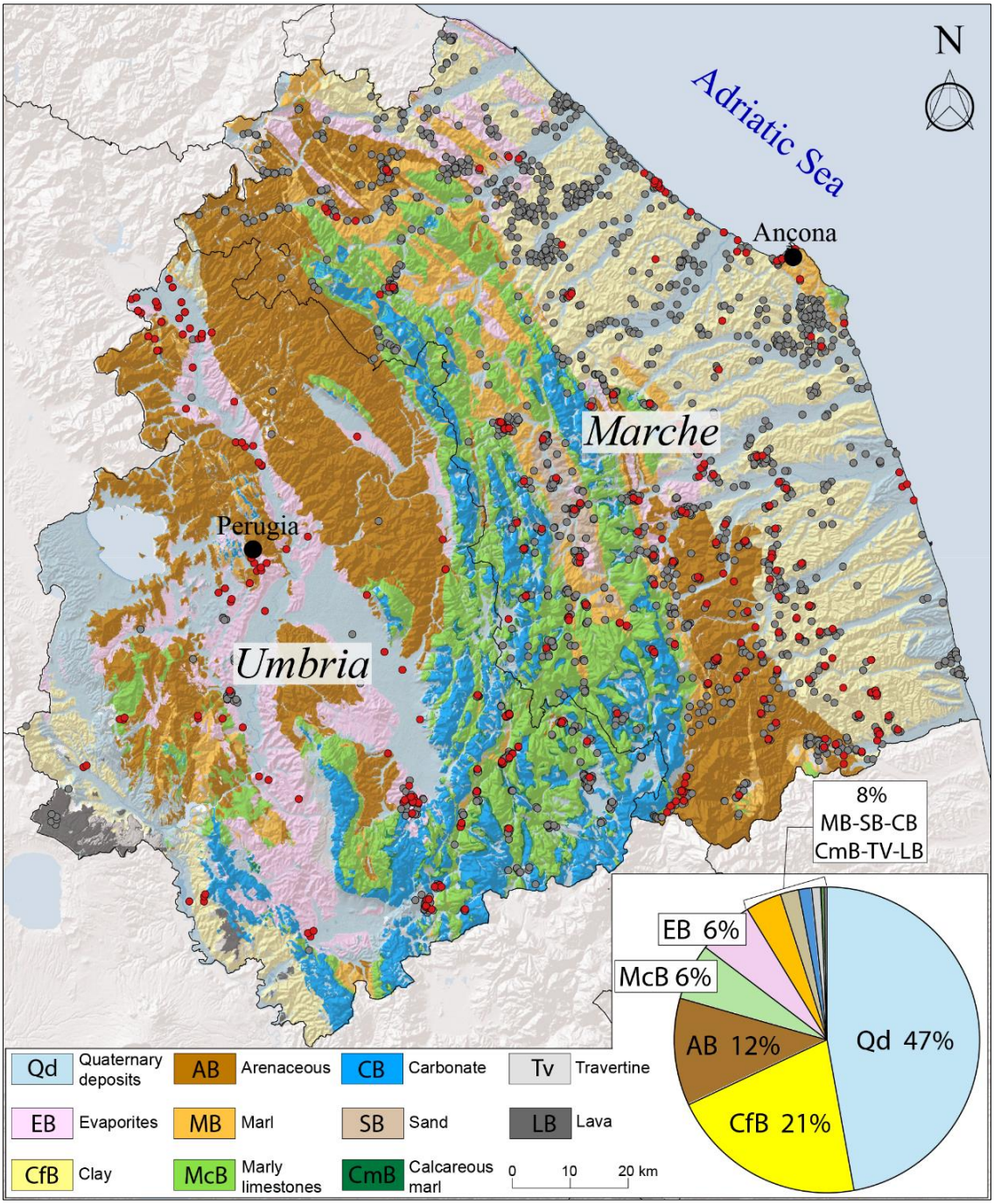

Figure 3.7. Distribution of shear wave velocity (Vs) profiles collected from the Italian seismic microzonation dataset for the Umbria and Marche regions. Red dots are in-hole tests, and grey dots are surface tests. The pie chart shows the percentage of Vs profiles for each lithological complex.

The Vs,30 values were calculated from these profiles using a MATLAB code that performs a data quality checks, to identify invalid or incomplete profiles characterised by missing or incorrect values (e.g., missing coordinates or inconsistent layers). Additionally, controls were executed to check for velocity inversions within profiles,

that have been disregarded. For each profile, the code calculates the averaged shear wave velocity in the uppermost 30 m (i.e., Vs,30) as defined by following equation:

$$\mathrm{Vs},30 = \sqrt{\frac{30}{\sum \mathrm{i} = 1,\mathrm{N}\frac{\mathrm{hi}}{\mathrm{vi}}}} \tag{3.5}$$

where ***hi*** and ***vi*** are the thickness (m) and shear-wave velocity of the i-th layer, respectively.

These Vs,30 values are used to create the Vs,30 map for the study area with the procedure described in Chapter 5 for the Marche Region. The details about the Vs,30 map of the Umbria-Marche regions and the application of the map are described in the Chapters 6. The Vs,30 dataset is provided in *Appendix B*.

CHAPTER 4

GROUND MOTION MODELLING

This Chapter introduces ground motion prediction methods and outlines the specific methods and parameters employed in this research.

4. Ground Motion Modelling

The generation of ground shaking scenarios is generally based on different computational techniques that simulate the propagation of seismic waves and predict the resulting ground shaking during an earthquake.

At present, there are many methods for predicting ground motions. They can be summarised into four main categories: (i) stochastic-process-based methods (ii) numerical methods, (iii) hybrid methods, and (iv) empirical prediction methods (Fig. 4.1). Stochastic-process-based, numerical, and hybrid methods predict the time history of the ground motion, whereas empirical prediction methods predict a single intensity measure (IM) representing the ground motion (i.e., Peak Ground Acceleration – PGA, Peak Ground Velocity – PGV, etc.). The current state of practice is based mainly on the adoption of the numerical approach, which is based on physical principles, and the empirical one, which is based on observed data.

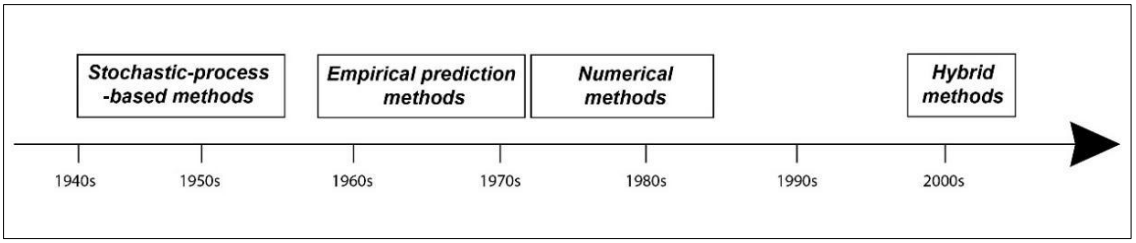

Figure 4.1. Summary of the approximate date when each simulation method was developed (modified after Douglas and Aochi, 2008). Boxed methods are the four main categories of ground motion simulation methods.

Stochastic-process-based methods can be classified also as black-box approaches (e.g., Housner, 1947; Dowrick, 1977; Thrainsson and Kiremidjian, 2002; Pousse et al., 2006). These methods are generally characterised by simple formulations with few input parameters that are used to simulate the ground motion time histories. Specifically, these techniques do not involve rigorous considerations of the physics of the earthquakes but simply modify the white noise to replicate specific characteristics observed in strong motion records. They were developed by using the small datasets of observations of past earthquakes available.

Regarding the numerical approaches, the physics-based ground motion simulations (PBS) are largely adopted, and differently from the former category of techniques, physics-based methods strictly rely on the underlying mechanics of earthquakes to provide a physical representation of the finite fault rupture process and seismic wave propagation and attenuation (e.g., McCallen et al., 2021; Komatitsch et al., 2002; Graves et al., 2010; Huang et al., 2020). These techniques often consist of two stages: (1) simulation of the generation of seismic waves (through fault rupture), and (2) simulation of wave propagation. Due to this separation, it is possible to couple the same source model with differing wave propagation approaches or different source models with the same wave propagation code (Aochi and Douglas 2006).
PBS can be divided into three main categories: (i) finite-fault methods (e.g., Joyner and Boore, 1986; Tumarkin et al., 1994; Zeng et al., 1994; Motazedian and Atkinson, 2005), (ii) kinematic methods (e.g., Herrero and Bernard, 1994; Hutchings, 1994; Hartzell et al., 1999, 2005; Ruiz et al., 2007), and (iii) dynamic methods (e.g., Guatteri et al., 2003, 2004; Schmedes et al., 2010; Kozdon and Dunham, 2013).Despite these approaches being more realistic in simulating the time histories of events due to advances in the understanding of earthquake source and wave propagation they usually include significant epistemic uncertainties besides being highly computationally demanding.

Hybrid methods allow to simulate a ground motion time history by combining two or more of methods to take advantage of their differing strengths (e.g., Hartzell et al., 1999; Graves and Pitarka, 2010; Mai et al., 2010; Schmedes et al., 2010). A common hybrid method is to splice a stochastic finite-fault method at short periods to a kinematic method at long periods. The resulting seismogram is more realistic across a wide frequency range, which is important for engineering applications such as the analysis of tall buildings that are excited at multiple frequencies.

Empirically-based approaches are the most straightforward way for ground motion prediction. Intensity Prediction Equations (IPEs) are used to predict the macroseismic intensities, whereas Ground Motion Prediction Equations (GMPEs) or Ground Motion Models (GMMs) are employed to predict ground motions in physical parameters, such as peak ground acceleration (PGA), peak ground velocity (PGV), or spectral acceleration at multiple periods (Sa(T)). In general, IPEs are based on observations of

the effects of earthquakes and GMMs are based on the observed ground motion parameters. These models have been used for the generation of shaking scenarios and are described in detail in the following sections. Finally, the conversion from ground motion parameters to macroseismic intensity is performed using Ground Motion Intensity Conversion Equations (GMICEs).

4.1. Intensity Prediction Equations - IPEs

The Intensity Prediction Equations (IPEs) predict the macroseismic intensity as a function of magnitude or epicentral intensity and source-to-site distance, and are widely adopted for local seismic hazard assessment (e.g., Albarello and Mucciarelli, 2002; D'Amico and Albarello, 2008), earthquake loss estimation (e.g., Kircher et al., 2006), and in the parameterization of historical events (e.g., Bakun and Wentworth, 1997; Gasperini et al., 1999, 2010; Sbarra et al., 2019, 2023).

In the literature, different empirical equations exist to estimate the macroseismic intensity. These equations calibrated based on the observed intensity data from recorded earthquake can differ for the type of the selected data. Examples of regional or local intensity prediction equations are Bakun (2006) for Western North America; Bakun and Scotti, (2006) for France; Stromeyer and Grunthal, (2009) for Central Europe; Bindi et al., (2011) for Central Asia; Oros et al., (2019) for Romania; and Peruzza (1996), Albarello and D'Amico (2004), Gómez Capera (2006), Pasolini et al. (2008), and Oliveti et al. (2022) for Italy. Moreover, the statistical approaches for calibrating these IPEs can be different. For example, Sorensen et al., (2009) adopted a regression technique whereas Pasolini et al., (2008) used a fully probabilistic method.

Generally, to quantify the source, IPEs adopt either the epicentral intensity (e.g., Pasolini et al., 2008) or the moment magnitude (e.g., Oros et al., 2019). Whereas to characterise the distance between the seismic source and the site, IPEs adopt the epicentral distance (***Repi***), which measures the radial distance between the macroseismic epicentre and the intensity data point, or the hypocentral distance which is the distance between the hypocentre and the intensity data point, calculated as follow:

$$D = \sqrt{(\mathrm{Repi})^2 + (\mathrm{h})^2} \tag{4.1}$$

where ***h*** is the hypocentral depth.

However, in the literature, some IPEs consider different distances borrow from the Ground Motion Models (GMMs), including the Joyner-Boore distance (*Rjb*) that is the closest horizontal distance to the vertical projection of the rupture (i.e., surface projection), or rupture-plane distance (*Rrup*) the closest distance to the rupture surface as input in their formulation (e.g., Albarello and D'Amico, 2004). The different distance measures are displayed in Fig. 4.2.

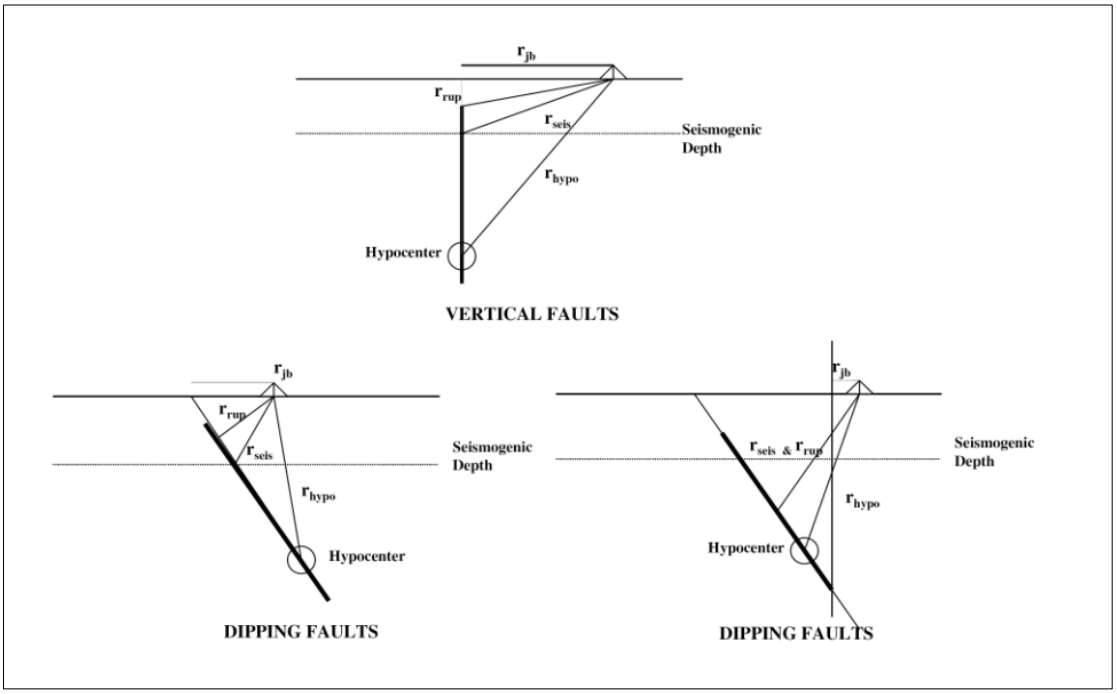

Figure 4.2. Definition of the different source-to-site distance measures used in predictive equations (After Abrahamson and Shedlock, 1997).

IPEs are generally based on simple functional forms, accounting for magnitude/intensity and distance, and do not specifically account for site effects because they are included in the macroseismic intensity values. Moreover, the IPEs based on the epicentral intensity might introduce an error in the prediction since they underestimate the real source-to-site distance.

4.2. Ground Motion Prediction Equations - GMPEs

Ground Motion Prediction Equations (GMPEs) or Ground Motion Models (GMMs) are empirical equations to predict peak ground motion (Peak Ground Acceleration - PGA, and Peak Ground Velocity - PGV, and spectral ordinates) as a function of several explanatory variables related to an earthquake and are calibrated based on observed ground motion data from recorded past earthquakes.

The basic predictor (explanatory) variables included in the GMMs are the earthquake magnitude (i.e., Source), the source-to-site distance measure (i.e., Path), and soil conditions (i.e., Site) as shown in Fig. 4.3.

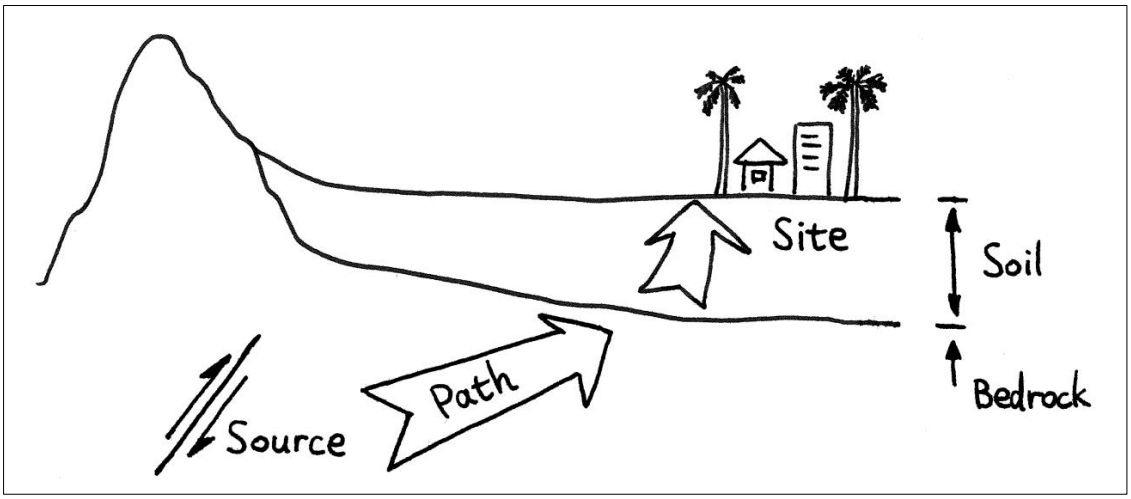

Figure 4.3. Three main aspects affecting the earthquake ground motions: source, path, and site. This picture reflects the typical near-surface geology of many Italian cities: sedimentary soils underlain by bedrocks. (Modified after Kramer, 1996).

In early GMMs, earthquake magnitude was used as a unique parameter to characterise the seismic source. However, recent equations have included additional variables such as Style of Faulting (*SoF*), to enhance source characterisation. The most appropriate magnitude scale used in the calibration of these predictive equations is the moment magnitude (*Mw*) since it is strictly related to the seismic moment (*Mo*) of the earthquake. Nevertheless, alternative magnitude scales, such as surface-wave magnitude (*Ms*) and local magnitude (*Ml*), have also been considered.

The source-to-site distance (i.e., Path) represents the geometric separation between the earthquake seismic source and the site of interest. Different metrics, including epicentral distance (*Repi*) and hypocentral distance (*Rhyp*), are used to characterise wave propagation. *Repi* represents the distance to the epicentre, while *Rhyp* represents the distance to the hypocentre. Additional metrics, such as the Joyner-Boore distance (*Rjb*) that is the closest horizontal distance to the vertical projection of the rupture (i.e., surface projection) and the closest distance to the rupture surface (*Rrup*) are used (see Fig. 4.2).

Moreover, considering the significant influence of site-specific factors on ground motion characteristics, most GMMs incorporate local site conditions in their formulation using different proxies. In early predictive models, local site conditions were categorised as either rock or soil. Campbell, (1981) used a more refined classification by subdividing in shallow soil, soft soil, soft rock, and hard rock. In modern GMMs, local site conditions are defined in terms of site geology and shear-waves velocity categories. The average shear-wave velocity in the uppermost 30 m of soil (Vs,30) is a commonly used parameter in predictive equations (e.g., Boore et al., 1997; Boore and Atkinson, 2008; Campbell and Bozorgnia, 2008, 2014; Lanzano et al., 2019).

A comprehensive review of such equations has been undertaken by Campbell, (1985, 2003), Joyner and Boore, (1988) and Douglas and Aochi, (2008). A comprehensive repository of GMMs suitable worldwide is available at http://www.gmpe.org.uk/gmpereport2014.html.

The functional forms and coefficients for these equations are usually derived using regression analyses on strong motion data (e.g., Joyner and Boore, 1981; Spudich and Hartzell, 1985). The distribution of ground motion in GMMs is described in terms of a median and a logarithmic standard deviation (Strasser et al., 2009).

One of the main hypotheses in GMMs formulation is ergodicity, that is the variability at a single site from a specific source is supposed to be identical to that derived from multiple sites over large regions (Al Atik et al., 2010).

In a non-ergodic approach, systematic contributions to ground motion variability are identified through statistical decomposition of total residuals (Al Atik et al., 2010). The

variability, represented by the residuals, is usually separated into between-event variability (ΔB) and within-event variability (ΔW). The former (ΔB) represents the average difference between observed ground motion from a single earthquake and the median ground motion as predicted by the ground-motion model across a number of earthquakes, while the latter (ΔW) represents the deviation between a single observation of ground motion at a specific station (i.e., site) and the predicted median ground motion for that earthquake. The ΔW component is decomposed into smaller parts related to site- and path-effects, that are used to correct the median GMM prediction (Al Atik et al., 2010). An example of a fully non-ergodic methodology for shaking scenarios in the Italian context is provided by Sgobba et al. (2019, 2021).

In the present PhD research, the recent GMM calibrated for Italian territory (ITA18) by Lanzano et al. (2019) is adopted to predict the ground motion of the investigated historical earthquakes. The Lanzano et al. (2019) equation predicts peak parameters (PGA and PGV) and the ordinates of spectral acceleration at 5% damping (SA) in the period range 0.01- to 10-seconds for shallow crustal events (e.g., depth < 30 km) in the magnitude range 4 < Mw < 7 and distance range 0-200 km.
The choice of ITA18 was motivated by the crucial advantage of taking into account the closest distance from the rupture surface plane (*Rrup*), allowing to consider the 3D geometry of the seismogenic sources. Additionally, it allows to consider the soil amplification through Vs,30.

The functional form of the ITA18 is the following:

$$\mathrm{Log}_{10}(\mathrm{Y}) = \mathrm{a} + \mathrm{F_M}(\mathrm{M_w}, \mathrm{SoF}) + \mathrm{F_D}(\mathrm{M_w}, \mathrm{R}) + \mathrm{F_S}(\mathrm{Vs},30) + \varepsilon \qquad (4.2)$$

where $\boldsymbol{Y}$ represents the predicted ground motion parameter, $\boldsymbol{a}$ is a constant; $\boldsymbol{F_M(M_W, SoF)}$ is the earthquake source function, where $\boldsymbol{M_W}$ is the moment magnitude and ***SoF*** indicates the style of faulting; $\boldsymbol{F_D(M_W, R)}$ is the distance function (Path), where ***R*** can be the rupture distance or the Joyner-Boore distance; $\boldsymbol{F_S(Vs,30)}$ is the site term represented through the average shear-waves velocity in the uppermost 30 m; $\boldsymbol{\varepsilon}$ represents the error associated with the median prediction.

The $\boldsymbol{F_M}$ and $\boldsymbol{F_D}$ functions are expressed as:

$$F_M(M_W) = \begin{cases} b_1(M_W - M_h) & for\ M_W \leq M_h \\ b_2(M_W - M_h) & for\ M_W > M_h \end{cases} \quad (4.3)$$

$$F_M(SoF) = f_j SoF_j \quad (4.4)$$

$$F_D(M_W, R) = [c_1(M_W - M_{ref}) + c_2]\log_{10}\sqrt{R_i^2 + h^2} + c_3\sqrt{R_i^2 + h^2} \quad (4.5)$$

where the coefficients b_1 and b_2 in equation (4.3) control the magnitude scaling, while the SoF coefficients in equation (4.4) provide the correction for focal mechanism. In equation (4.3), M_W and M_h are the moment magnitude and the hinge magnitude, respectively.

In equation (4.5), M_{ref} is the reference magnitude, c1-c3 are the path coefficients, R_i can be either the rupture distance (*Rrup*) and the Joyner-Boore distance (*Rjb*), and h is the pseudodepth (km) estimated by the regression.

The functional form $\boldsymbol{F_S}$ is expressed as:

$$F_S(V_S,30) = k\log_{10}\left(\frac{V_0}{800}\right) \quad (4.6)$$

in which $V_0 = Vs,30$ when $Vs,30 \leq 1500$ m/s, otherwise $V_0 = 1500$ m/s.

The coefficients of ITA18 used in this research to calculate the PGA and PGV are found in the electronic supplement of Lanzano et al. (2019).

4.3. Ground Motion Intensity Conversion Equations - GMICEs

Predictive relationships between macroseismic intensity scales and instrumental parameters are largely used worldwide for making comparisons between ground motion parameters (GMPs) and macroseismic intensity. In early studies, the conversion between macroseismic data to peak parameters (PGA and PGV) and vice-versa was performed through intensity-to-ground motion conversion equations (IGMCEs; e.g., Trifunac and Brady, 1975a, b; Murphy and O'Brien, 1977). At present, the development of seismic networks and the abundance of strong motion records has led to a reverse tendency based on the use of ground motion-to-intensity conversion equations (GMICEs; Wald et al., 1999; Kaka and Atkinson, 2004; Atkinson and Kaka, 2007; Dangkua and Cramer, 2011).

Several empirical relationships have been published, and various correlation models have been proposed in the past for Italy (e.g., Margottini et al., 1992; Panza et al., 1997; Faccioli and Cauzzi, 2006).

In the last decade, linear relationships based on a set of GMPs (PGA, PGV, and SA at different period range) and Mercalli-Cancani-Sieberg (MCS) intensity have been proposed for Italy by Faenza and Michelini, (2010, 2011), and Gomez Capera et al. (2015, 2018).

Faenza and Michelini (2010, 2011) conducted a correlation analysis between MCS-PGA and MCS-PGV and SA at 0.3, 1.0 and 2.0 seconds using an orthogonal distance regression technique. The dataset is composed of 66 earthquakes between 1972 and 2004 within the range of $3.9 \leq Mw \leq 6.9$ and $2 \leq I_{MCS} \leq 8$, with 266 pairs of Intensity-recorded GMPs. Gomez Capera et al. (2018) used a calibration dataset of 127 Intensity-recorded GMPs pairs from 55 Italian earthquakes in the period 1976-2016 with $3.9 \leq Mw \leq 6.8$ and $3\text{-}4 \leq I_{MCS} \leq 11$. However, some existing linear correlations such as Faccioli and Cauzzi (2006) and Gomez Capera et al. (2015, 2018) reveal PGA saturation. Therefore, alternative correlations between macroseismic intensity and GMPs that enable conversions for higher macroseismic intensity levels into PGA values is needed to avoid this issue.

Recently, Gomez Capera et al. (2020) proposed a non-linear reversible GMPs-macroseismic intensity relationships for Italy using regression analyses between macroseismic intensity and PGA, PGV, and spectral acceleration (SA) at 0.2, 0.3, 1.0

and 2.0 seconds. The dataset comprises 67 Italian earthquakes between 1972 and 2016 within the range of $4.2 \leq Mw \leq 6.8$ and $2 \leq I_{MCS} \leq 10–11$ which results in 240 macroseismic intensity-GMP pairs correlated within a range of 2 kilometres from each other.

In this research, the most recent GMICEs of Gomez Capera et al. (2020) for Italy are used for the conversion of observed macroseismic intensity data to GMPs and vice-versa. The equations are employed in two distinct stages: firstly, to determine the most appropriate seismogenic sources by calculating the differences between observed and predicted macroseismic intensities and then to calculate the shaking scenarios in terms of PGA, PGV, and macroseismic intensity. Specifically, the conversion from GMPs to macroseismic intensity is performed using the following exponential relation:

$$I_{MCS} = a\, e^{(b\, LogGMP)} \tag{4.3}$$

For the conversion into macroseismic intensity, only the PGV is used as it is the best parameter to predict the intensity according to the authors.
Conversely, the inverse empirical relation is used to convert macroseismic intensity to GMPs:

$$LogGMP = a' + b'\, Log(I_{MCS}) \tag{4.4}$$

For both relations, $\boldsymbol{I_{MCS}}$ represents the macroseismic intensity expressed in the Mercalli-Cancani-Sieberg scale, ***LogGMP*** is the mean value of the GMP (log10 unit), ***a-a'*** and ***b-b'*** are the correlation coefficients proposed by Gomez Capera et al. (2020). The coefficients used to convert the macroseismic intensity into PGA and PGV, and vice-versa are listed in Table 4.1.

Table 4.1. Regression coefficients (a, b), (a', b'), and standard deviation of the data of the Eq. (4.3) and (4.4) for the GMPs used for the conversions from Gomez Capera et al. (2020).

GMP	a	b	σ
PGA	2.276	0.546	1.13
PGV	4.514	0.502	1.04

GMP	a'	b'	σ
PGA	-1.446	4.134	0.35
PGV	-2.912	4.462	0.36

CHAPTER 5

DUAL-PROXY ESTIMATION OF Vs,30: THE CASE STUDY OF THE MARCHE REGION (CENTRAL ITALY)

This Chapter presents a description of the methodology adopted for the creation of a Vs,30 map with an application to the Marche Region. The same methodology has been extended to the Umbria Region and adopted to calculate the shaking scenarios of historical earthquakes descripted in Chapter 6. From the literature, two commonly acknowledged parameters, i.e., the topographic slope and the geological classification are usually adopted to compute the Vs,30 map. In this work, the Vs,30 has been computed in function of lithology, based on a reclassification of the geo-lithological map of Italy provided by the Italian Institute for Environmental Protection and Research - ISPRA, and the topographic slope derived from the ASTER Global Digital Elevation Model (GDEM) with a resolution of 30 m.

The present article has been published in Journal of Maps. DOI: 10.1080/17445647.2024.2349787

.

5. Dual-proxy estimation of Vs,30: the case study of the Marche Region (central Italy)

Veronica Gironelli [1,2], Tiziano Volatili [1], Lucia Luzi [3], Giulio Brunelli [1,3], Emanuele Tondi [1,2]

[1]*School of Science and Technology – Geology Division, University of Camerino, Italy*

[2]*National Institute of Geophysics and Volcanology, Seismology and Tectonophysics Division, Camerino, Italy*

[3]*National Institute of Geophysics and Volcanology, Milan, Italy*

Abstract

This study focuses on generating a shear-wave velocity averaged within the uppermost 30 m of the ground surface (Vs,30) map for the Marche region (central Italy) using two commonly acknowledged proxies: topographic slope and lithological classification. The analysis is based on a comprehensive dataset of geophysical tests from the Italian seismic microzonation dataset, employed as a training set. Through regression analysis, Vs,30 values are modelled as a function of lithology and topographic slope, with a random effect accounting for the combination of these variables. The resulting Vs,30 raster map illustrates the spatial distribution of shear-wave velocities across the region, offering a representation of the subsurface seismic characteristics essential for various applications, including local seismic hazard assessment, prediction of seismic ground motion parameters, microzonation mapping, real-time shakemap generation, and seismic design of engineering structures.

Keywords: *Seismic Hazard; Shear-wave velocity; Vs,30 map; Marche region.*

5.1. Introduction

The determination of the ground shaking induced by destructive earthquakes is becoming a crucial aspect of seismic hazard assessment. The complexity of the soil conditions at a site might induce seismic wave amplification which influences the local seismic response. Thus, mapping the geophysical characteristics of soil is essential to predict the effects of an earthquake, due to site amplification. The shear-wave velocity averaged within the uppermost 30 m of the ground surface (Vs,30) is the most used parameter for the site classification and the evaluation of the soil amplification for the seismic design (Wald and Allen, 2007; Stewart et al., 2014; Parker et al., 2017). In addition, most of the ground motion models (GMMs) use Vs,30 as data input representing the local site conditions (Abrahamson and Silva, 2008; Boore and Atkinson, 2008; Campbell and Bozorgnia, 2008; Chiou and Youngs, 2014; Lanzano et al., 2019).

Since Vs,30 is considered a key factor for ground motion prediction, it is fundamental to evaluate its spatial distribution to calculate shaking scenarios. Vs,30 is a measure directly calculated from the shear-wave velocity (Vs) profiles obtained by geophysical investigations. Borehole methods (i.e., Down-Hole, DH; Cross-Hole, CH), seismic refraction, Multichannel Analysis of Surface Waves (MASW), Spectral Analysis of Surface Waves (SAWS), and REfraction MIcrotremors (REMI) are well-known invasive and non-invasive techniques for estimating Vs (Kramer, 1996; Xia et al., 2002; Comina et al., 2020; Wang et al., 2022). Since detailed geophysical investigations are expensive and time-consuming, it is unrealistic to perform very dense geophysical characterisation of an area, therefore, various proxy-based methods have been proposed for mapping Vs,30 over a large region. These methods are typically based on data available for the area, such as the topographic slope and geomorphology-based terrain categories obtained from a digital elevation model (Wald and Allen, 2007; Allen and Wald, 2009; Yong et al., 2012), or geotechnical categories and surface geology (Chiou et al., 2014; Wills and Clahan, 2006; Wills et al., 2015) obtained from geological maps at various scales.

In Italy, systematic seismic microzonation (MS) studies have been carried out after the 2009 L'Aquila earthquake as part of the National Programme for seismic risk

prevention and mitigation, an initiative led by the Department of Civil Protection (DPC). These studies provide a considerable amount of data, and therefore, alternative Vs,30 maps of the whole national territory are present in the literature. (e.g., Forte et al., 2019; Mori et al., 2020). These maps are mainly based on surface geology at 1:100.000 scale, and geological and geomorphological information. Forte et al. (2019) calibrated two maps of seismic shallow soil classification based on soil class (e.g., EC8) and Vs,30 from Vs measurements, and a large-scale geological map of Italy. Mori et al. (2020) proposed a Vs,30 map for Italy using the 1:100,000 geological map and geomorphological classes as proxies of Vs,30 obtained by multiple in-situ geophysical tests from the Italian seismic microzonation dataset.

In this study, we present a Vs,30 map (Main Map) tailored for the Marche region, Central Italy, according to its distinct geological and topographic characteristics. The adopted approach differs from previous studies for the implementation of a reclassification of geological formations and a higher-resolution Digital Elevation Model (DEM) to ensure a better representation of the lithology and topography of the region. Moreover, the public microzonation data are integrated for the Marche region with additional data (curtesy of local freelance geologists), and the dataset of the Engineering Strong motion (ESM) database (Luzi et al., 2016, 2020) to ensure a comprehensive representation of the seismic site characteristics. However, the Vs,30 measurements are limited by a nonuniform spatial distribution, with a higher amount of data in populated areas, possibly leading to an underrepresentation of Vs,30 values for certain lithologies and/or slope classes. The final Main Map is a spatial mapping of the results of regression analysis between Vs,30, lithology, and topographic slope.

5.2. Geological and geomorphological setting of the Marche Region

The Marche region belong to the Umbria-Marche Apennines, a fold-and-thrust belt, that resulted from the convergence between the continental of Corsica-Sardinia European margin to the west, and the Adria margin of African origin to the east (e.g., Malinverno and Ryan, 1986; Carmignani and Klingfield, 1990; Mazzoli et al., 2002; Pierantoni et al., 2013). The Umbria-Marche Apennines constitute the external sector of the Northern Apennines and is characterised by an arcuate shape and by the presence of asymmetrical

anticlines, that are mostly faulted, verging mainly to the north-east. The study area is characterised by a Mesozoic-Tertiary sedimentary succession represented by the so-called Umbria-Marche Sedimentary Succession. This continuous stratigraphic sequence can be divided into three main geological units: i., Meso-Cenozoic carbonates and hemipelagic limestones; ii., Oligo-Miocene siliciclastic turbiditic deposits; and iii., Plio-Pleistocene peri-adriatic succession (Bigi et al., 1997; Mazzoli et al., 2002; Pierantoni et al., 2013). The Meso-Cenozoic portion of the sedimentary succession crops out extensively in the western part of the Marche region, in the so-called Umbria-Marche and Marche ridges, respectively, which merge to the south to form the Sibillini Mountains (e.g., Calamita and Deiana, 1988). This portion is characterised by a prevalence of carbonate lithotypes (e.g., Calcare Massiccio, Corniola, Calcari Diasprigni, and Maiolica Fms.) and marly lithotypes (e.g., Marne a Fucoidi, Scaglia Bianca, Scaglia Rossa, Scaglia Variegata, and Scaglia Cinerea Fms.) indicating the transition from shallow water to deep marine and hemipelagic environments. Siliciclastic turbiditic marine deposits which constitute the upper portion of the sedimentary succession are distinguishable in the long intra-Apennine synclinal structure represented by the Camerino basin and in the southernmost part of the Marche region. This portion of the sequence involves the Bisciaro, and Schlier Fms., and the Miocene turbidites of the Camerino and Laga Fms. In the eastern Adriatic sector of the Marche region, the Plio-Pleistocene peri-Adriatic succession characterised by the Argille Azzurre Fm., crops out (Pierantoni et al., 2013). Finally, the late Quaternary continental deposits are widely distributed in the foothill zone along the alluvial plains of the Marche region. However, for the purpose of the study, the geological formations are grouped into lithological complexes according with the Vs,30 values as in Table 5.1.

From a topographic point of view, the landscape of the Marche region is characterised by the presence of higher relief with steeper slopes on the western side, in correspondence of the Sibillini Mountains ridge which is characterised by stiffer lithologies (i.e., calcareous formations). On the Adriatic side, the region is characterised by a predominantly high-hilly territory consisting of soft lithologies and dominated by relatively wide valley floors (Bisci and Dramis, 1991). The main geomorphological features are those connected with fluvial processes. The Marche valleys are characterised by several orders of alluvial terraces of Quaternary age and located at

elevation ranging from a few meters (fourth order terrace) up to more than 100 meters (first order terrace) above the present-day valley floor.

5.3. Data Collection and Analysis

The data collection consists of the geological, geotechnical, and geophysical tests carried out in the framework of microzonation studies acquired by publicly accessible datasets, available at (https://sisma2016data.it/microzonazione/) and (https://qmap-protciv.regione.marche.it/cs/), in-situ investigations, and the shear-wave velocity profiles available in the ESM database (http://esm.mi.ingv.it; Luzi et al., 2016, 2020). The dataset consists in 1806 shear-wave velocity (Vs) profiles. The dataset is validated and processed to eliminate the Vs profiles that are incomplete, without coordinates, with marked velocity inversions and unreliable Vs values (e.g., Vs < 80 m/s). The Vs,30 values are calculated and converted into a point map with the following attributes: point ID that is a combination of the Italian Census Codes and the geophysical test ID, coordinate of the survey location, type of geophysical tests, and Vs,30 values (Figure 5.1).

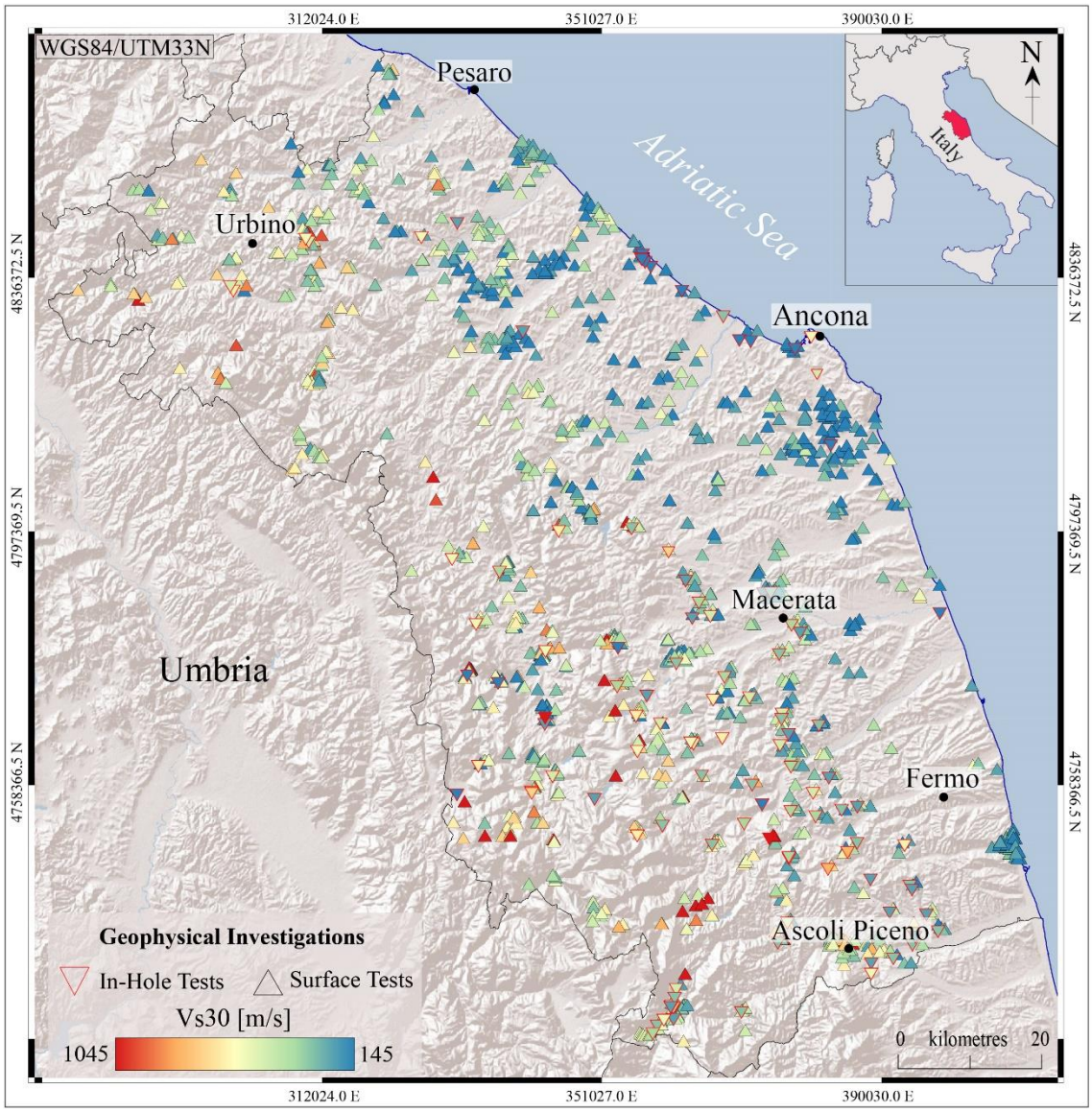

Figure 5.1. Distribution of the Vs,30 values obtained from the geophysical tests carried out in the Marche region as part of the seismic microzonation studies (DPC 2019). The geophysical tests are categorised into two types: red triangles with the tip pointing downwards for in-hole tests (DH and CH), while black triangles with the tip pointing upwards for surface tests (MASW, REMI, and SAWS), (Projected coordinate system UTM zone N33 expressed in meters).

The geo-lithologic information is obtained from the 1:100.000 geo-lithological map of Italy (courtesy of the Italian Institute for Environmental Protection and Research, ISPRA – Italian Geological Survey; Servizio Geologico d'Italia, 2004). For the sake of simplicity, the original categories described by ISPRA for the whole Italian territory were grouped into a set of homogeneous lithological complexes consistently constraining the lithological framework of the study area. The original categories are reclassified into 10 subclasses, including two "Quaternary deposits" and eight different

types of “geologic bedrock” (Jurassic to Pleistocene) encompassing the prevailing lithotypes and similar expected geotechnical behaviour (Table 5.1). The thematic map representing the lithological complexes outlined in Table 5.1 is obtained and presented in Figure 5.2. Approximately the 30% of the total area is represented by sandy-clayish lithotypes, whereas marly-arenaceous lithotypes and Quaternary deposits cover 24% and 22% of the total area, respectively. The complexes corresponding to prevailing calcareous lithotypes cover 18% of the total area, while the remaining 4% corresponds to the AfC complex, which represents evaporitic rocks. The lithological complexes with a percentage of area lower than 1% are not considered.

The first step of the procedure consisted of the overlay of the Vs,30 data with the geo-lithological units cropping out in the Marche region. Since microzonation studies aim to characterise lithologies that can be affected by seismic amplification, Quaternary deposits and soft rocks have a large number of observations. On the contrary, very few geophysical tests are performed in correspondence of stiff rocks such as limestones (CC class, Table 5.1), where amplification is not expected.

The mean and standard deviation of Vs,30 values derived for each lithology subclass are reported in Table 5.1. An analysis of variance (ANOVA test) is carried out to verify whether the lithological complexes listed in Table 1 significantly differ from each other in terms of Vs,30 values and the relative box-plot is shown in Figure 5.3. The Anova test revealed a statistically significant difference of Vs,30 between the complexes (overall P-value = 3.99e-40), although some lithological subclasses (e.g., McC and AC1; QC1 and QC2) exhibit similar Vs,30 values.

Table 5.1. List of the lithological complexes identified in the study area.

Name of Lithology	Lithological subclass	Description	Number of observations	Mean Vs30 (m/s)	Standard deviation of Vs30 (σ)
Carbonate	CC	Limestones, dolomitic limestones, micritic limestones	8	492.6	264.7
Marls	MC	Marlstones	2	537	67.9
Calcareous marl	CmC	Marly limestones, calcareous marlstones	55	600.7	212
Argillaceous marl	McC	Marlstones and silty marlstones	63	474.8	174.3
Arenaceous	AC1	Arenaceous-marly clayey turbidites (well-cemented sandstones)	171	471.9	147
	AC2	Arenaceous-silty turbidites (poorly cemented sandstones)	30	373	132.5
Arenaceous flysch	AfC	Resedimented gypsum, gypsum arenites, clays with interbedded sandstones and conglomerates	44	430	107.8
Clays	ClC	Mudstones, silty clays interbedded with sandstones and conglomerates	328	349.8	93.8
Quaternary deposits	QC1	Continental deposits, alluvial and terraced deposits, colluvium, alluvial fan	603	427.2	141.4
	QC2	Shallow water marine deposits, travertine, and soft limestone	22	430.6	101

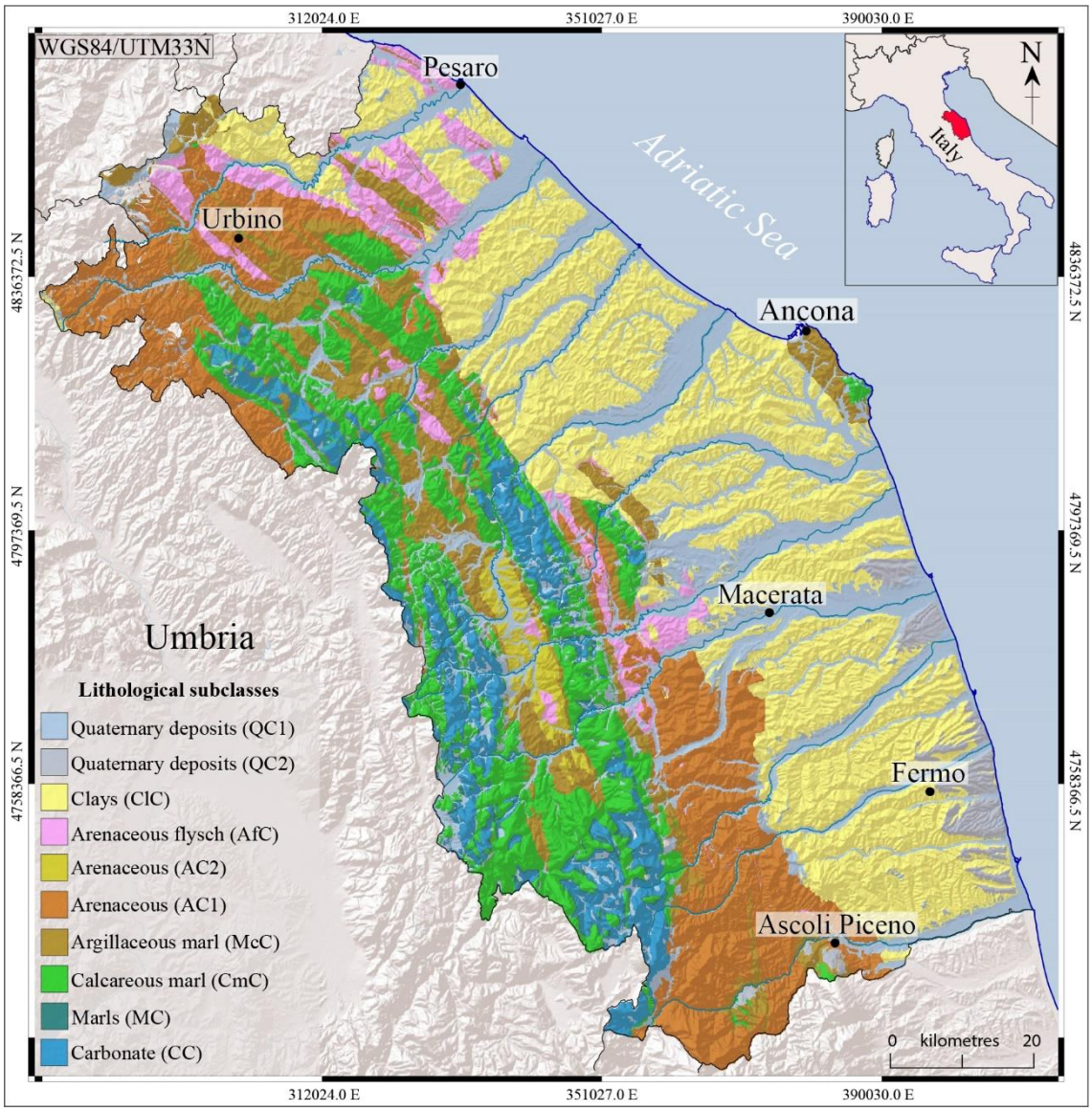

Figure 5.2. Map of the Marche region showing the identified lithological subclasses of Table 1, (projected coordinate system UTM zone N33 expressed in meters).

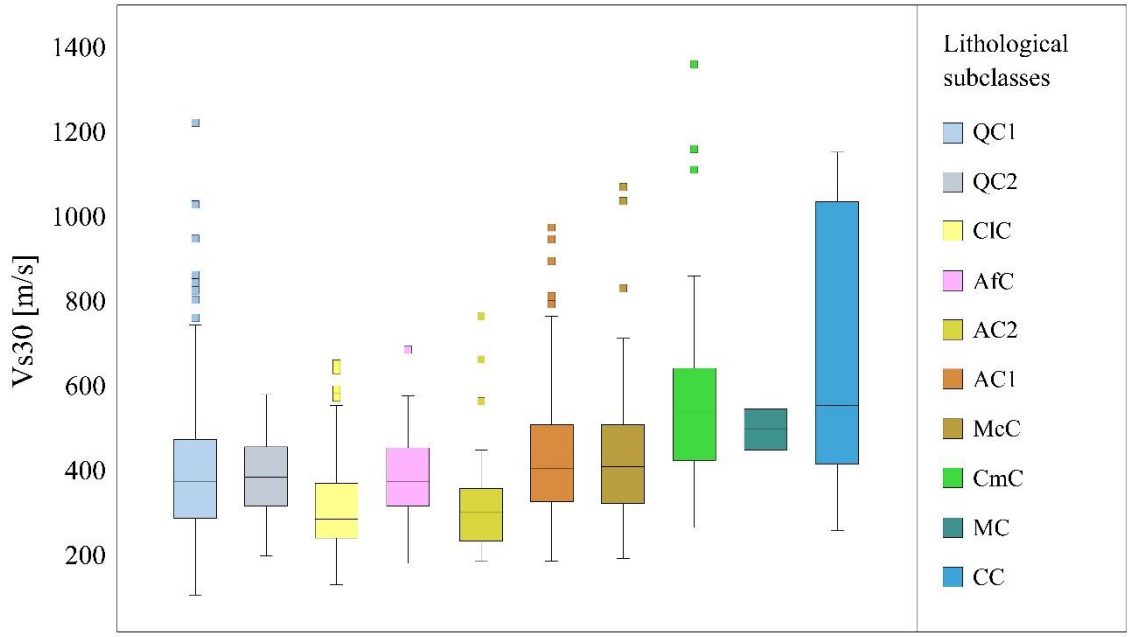

Figure 5.3. Box-plot showing the distributions of Vs,30 for the lithological subclasses listed in Table 5.1. The first quartile, the median value, and the third quartile are reported with the minimum and maximum values of the distribution and the outliers.

An additional analysis is performed to verify the correlation between Vs,30 and topographic slope.

The topographic data are derived from an ASTER Global Digital Elevation Model (GDEM) with a pixel size of 30 m, which is compatible with the regional scale of the work. The topographic slopes are calculated using the "Slope" tool of the ArcGIS software and are expressed in degrees. This tool employs an algorithm that uses the eight adjacent pixels associated with a specific weighting matrix, as proposed by Horn (1981). The different classes of slope in degrees and their description are shown in the Main Map. In the Marche region, the slope ranges from 0° to more than 35° (i.e., very gentle to very steep).

Given the limited number of observations and the similarity in Vs,30 values for certain lithological classes (i.e., McC and AC1; QC1 and QC2), we further investigated whether these classes could be distinguished based on morphological characteristics. The zonal statistics are performed using the ArcGIS Zonal Function to calculate the slope variability inside each lithological subclass. The mean, median, and standard deviation values obtained from the zonal statistics for each lithological subclass are listed in Table 5.2.

Table 5.2. Results of the zonal statistics.

Lithological subclass	Slope Mean [°]	Slope Median [°]	Slope Standard Deviation (σ)
CC	31.5	32	14.1
MC	28.3	28	13.6
CmC	24.3	23	13.4
McC	16.6	15	10.2
AC1	20.5	19	11.4
AC2	14.3	13	8.9
AfC	15.4	14	8.6
ClC	13	12	8.1
QC1	8	5	9.4
QC2	15.3	14	9.8

The zonal statistics revealed that the abovementioned subclasses (i.e., McC and AC1; QC1 and QC2), which share similar Vs,30, appear to be dissimilar in terms of topographic slope. Therefore, in the subsequent analysis they are kept as separate complexes. On the contrary, we could have joined the subclasses AC2 and ClC, as the distribution of Vs,30 values and slope proves to be comparable. However, we kept them separated because they have different lithological composition.

The Vs,30 data points are overlain to slope to obtain the final dataset. A linear regression using the mixed-effects model (Abrahamson and Youngs 1992) is used to obtain an empirical equation to predict Vs,30 values as a function of lithology and slope, and using the random effect on the combination lithology and slope.

We obtain the following equation:

$$Vs,30_{\mathrm{n}} = a_0 + S_{Ln} * \beta + L_n + \varepsilon \qquad (5.1)$$

where a_0 is a constant equal to 457; S_{Ln} is the slope coefficient for each geo-lithological complex (obtained by the mixed-effect regression); L_n is the coefficient of the geo-lithological complex; β is the topographic slope, in degrees, and n is the number of complexes; ε is the error. The total root mean square error is 134.79, while the root mean square error of each lithological subclass is listed in Table 5.3. Following the approach proposed by Karimzadeh et al. (2019), we also tested the log-normal distribution variable of the Vs,30 in relation with the Log10(slope), without obtaining a significant improvement in prediction accuracy. The Main Map is processed with a spatial resolution of 30 m using the ArcGIS Map Algebra tool.

Table 5.3. Regression coefficients of Eq. 1 for the geo-lithological complexes (Ln) and the slope coefficients for each geo-lithological complex (SLn), and the root mean square error (RMSE) obtained for each geo-lithological complex.

Lithological subclass	L_n	S_{Ln}	Number of observations	RMSE
CC	-16.48	2.40	8	248.8
MC	27.19	-0.11	2	66.1
CmC	132.38	0.007	55	212.1
McC	-2.16	1.38	63	173.1
AC1	11.77	0.15	171	146.9
AC2	-72.22	-0.17	30	132.3
AfC	-29.85	0.34	44	107.7
ClC	-122.17	1.49	328	92.9
QC1	-52.74	3.15	603	138.9
QC2	-26.12	0.25	22	100.9

5.4. Discussion

The final Main Map that represents the spatial distribution of Vs,30 can be subdivided into three main zones that share similar shear-wave velocities. The Vs,30 distribution reflects the gradual transition from the Apennine mountains, with the predominance of Jurassic-Cretaceous calcareous geological formations, to a hilly area with the

prevalence of terrigenous deposits of Miocene-Pleistocene age. The highest Vs,30 values are associated with calcareous lithotypes which constitute the Umbria-Marche ridge. This zone shows average shear-wave velocities of 620-800 m/s. The intermediate Vs,30 values in the 440-520 m/s interval are representative of the main arenaceous complex (AC1) in the north-western and southern parts of the region. On the Adriatic side, the silty-clayish complex (ClC) is characterised by lower Vs,30 values (≤ 320 m/s). The Quaternary complex represented by the QC1 subclass formed by conglomerates and finer alluvial sediments shows slightly lower Vs,30 values (320-400 m/s), while the subclass (QC2) represented by shallow water marine of sands and conglomerates shows a Vs,30 range 420-470 m/s.

The analysis of the Vs,30 residuals as a function of the lithological complexes and topographic slope is illustrated in Figures 5.4 a-b. The distribution of the residuals as a function of the lithological subclasses, in Figure 5.4a, shows that the complex MC represented by Marls is the class with large positive residuals. Nevertheless, since this complex is characterised by only two observations, and represents less than 1% of the total area, the error could be acceptable. The distribution of the Vs,30 residuals as a function of the topographic slope has zero mean and no trend with the slope, as illustrated in Figure 5.4b.

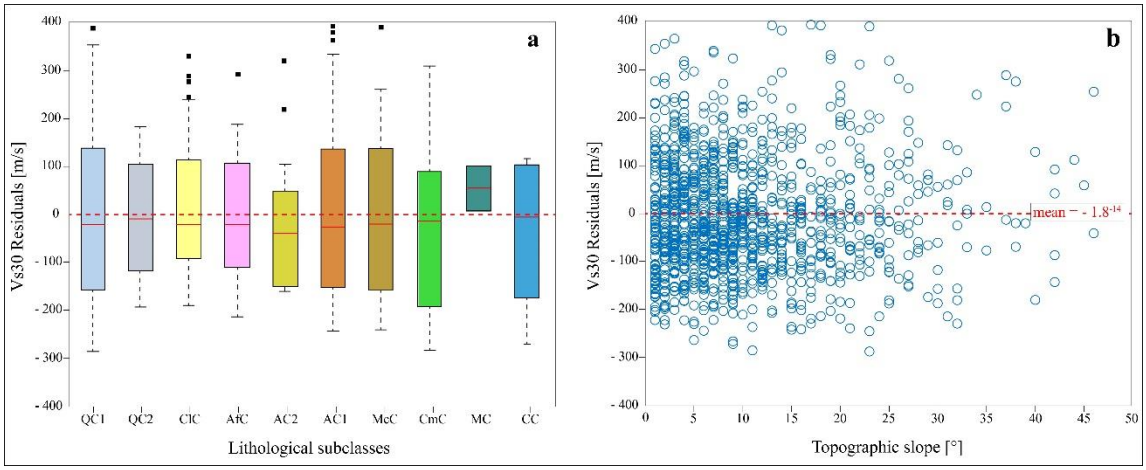

Figure 5.4. (a) Box-plot illustrating the distribution of Vs,30 residuals across the lithological subclasses of Table 1; (b) Distribution of the Vs,30 residuals across the topographic slope. The red dashed line is the residuals mean.

Finally, to investigate if the 30 m resolution of the Main Map is significant in terms of Vs,30 variability, the focal statistic using the ArcGIS Focal Function tool is performed on the final map. This function calculates a statistic for the input cells within a neighborhood. The Vs30 variability of the Main Map raster is calculated in terms of standard deviation (σ) using different neighborhood shapes (i.e., 10x10, 5x5, and 3x3). Small neighborhoods (e.g., 3x3 or 5x5) share similar variability, in terms of standard deviation (with maximum observed standard deviation of 172). Increasing the size of the neighborhood, the focal statistic reveals a reduction in variability in terms of standard deviation (with maximum observed variability equal to 158). Therefore, a Vs30 resampling from 30 m to 150 m does not alter the ground motion variability, with the advantage of a reduction of size of the map. A resampling of the Vs30 map to 300 m could reduce the variability of ground motion.

5.5. Conclusions

In this work, the variability of the local site conditions that might induce a seismic wave amplification is explored in terms of the spatial distribution of the average shear-wave velocity in the uppermost 30 m, a proxy commonly used for soil amplification in ground motion models. A set of shear-wave velocity profiles is used as a training dataset to calibrate an empirical relation to predict Vs30 based on lithology and topographic slope. The Vs30 Main Map is obtained by linear regression, with the random effect on the lithology-slope combination. The distribution of Vs30 reflects the predominant lithotypes characteristic of the Marche region, as depicted in Figure 5.3, with the topographic slope contributing to the variation within each lithological complex. The map is distributed with 30 m resolution and a resampling to 150 m does not alter the original Vs30 variability. However, it is worth noting that since Vs30 are punctual values, the presented methodology, aimed at the spatialization of Vs,30 covering unsampled areas is likely affected by possible inaccuracy due to other factors (e.g., the geological basemap scale, DEM inaccuracy, other proxies not considered in this study). Therefore, the final Vs,30 map can be employed in the framework of modelling or even other studies at a regional scale (e.g., shakemaps), but it is not designed for site-local scale purposes, possibly leading to an inaccurate estimation of the site response if employed at this site-scale.

References

Abrahamson, N., & Silva, W. (2008). Summary of the Abrahamson & Silva NGA ground-motion relations. Earthquake Spectra, 24(1), 67-97. https://doi.org/10.1193/1.2924360

Allen, T. I., & Wald, D. J. (2009). On the use of high-resolution topographic data as a proxy for seismic site conditions (VS 30). Bulletin of the Seismological Society of America, 99(2A), 935-943. https://doi.org/10.1785/0120080255

Bigi, S., Cantalamessa, G., Centamore, E., Didaskalou, P., Micarelli, A., Nisio, S., & Potetti, M. (1997). The periadriatic basin (Marche-Abruzzi sector, central Italy) during the Plio-Pleistocene. Giornale di Geologia, 59(1-2), 245-259.

Bisci, C., & Dramis, F. (1991). La geomorfologia delle Marche. L'ambiente Fisico delle Marche. Regione Marche, Giunta Regionale, Assessorato Urbanistica e Ambiente, SELCA, Firenze, 81-113.

Boore, D. M., & Atkinson, G. M. (2008). Ground-motion prediction equations for the average horizontal component of PGA, PGV, and 5%-damped PSA at spectral periods between 0.01 s and 10.0 s. Earthquake Spectra, 24(1), 99-138. https://doi.org/10.1193/1.2830434

Calamita, F., & Deiana, G. (1988). The arcuate shape of the Umbria-Marche-Sabina Apennines (Central Italy). Tectonophysics, 146(1-4), 139-147. https://doi.org/10.1016/0040-1951(88)90087-X

Campbell, K. W., & Bozorgnia, Y. (2008). NGA ground motion model for the geometric mean horizontal component of PGA, PGV, PGD and 5% damped linear elastic response spectra for periods ranging from 0.01 to 10 s. Earthquake Spectra, 24(1), 139-171. https://doi.org/10.1193/1.2857546

Carmignani, L., & Kligfield, R. (1990). Crustal extension in the Northern Apennines: the transition from compression to extension in the Alpi Apuane core complex. Tectonics, 9(6), 1275-1303.

Chiou, B. S. J., & Youngs, R. R. (2014). Update of the Chiou and Youngs NGA model for the average horizontal component of peak ground motion and response spectra. Earthquake Spectra, 30(3), 1117-1153. https://doi.org/10.1193/072813EQS219M

Comina, C., Vagnon, F., Arato, A., & Antonietti, A. (2020). Effective Vs and Vp characterization from Surface Waves streamer data along river embankments. Journal of Applied Geophysics, 183, 104221.

DPC, 2019. Dipartimento della Protezione Civile. Studi di microzonazione sismica in Italia. www.webms.it.

Forte, G., Chioccarelli, E., De Falco, M., Cito, P., Santo, A., & Iervolino, I. (2019). Seismic soil classification of Italy based on surface geology and shear-wave velocity measurements. Soil Dynamics and Earthquake Engineering, 122, 79-93. https://doi.org/10.1016/j.soildyn.2019.04.002

Horn, B. K. (1981). Hill shading and the reflectance map. Proceedings of the IEEE, 69(1), 14-47. https://doi.org/10.1109/PROC.1981.11918

Karimzadeh, S., Feizizadeh, B., & Matsuoka, M. (2019). DEM-based Vs30 map and terrain surface classification in nationwide scale—A case study in Iran. ISPRS International Journal of Geo-Information, 8(12), 537.

Kramer, S. L. (1996). Geotechnical earthquake engineering. Pearson Education India.

Lanzano, G., Luzi, L., Pacor, F., Felicetta, C., Puglia, R., Sgobba, S., & D'Amico, M. (2019). A Revised Ground-Motion Prediction Model for Shallow Crustal Earthquakes in Italy. Bulletin of the Seismological Society of America, 109(2), 525-540. https://doi.org/10.1785/0120180210

Luzi, L., Puglia, R., Russo, E., D'Amico, M., Felicetta, C., Pacor, F., Zare, M. (2016). The engineering strong-motion database: A platform to access Pan-European accelerometric data. Seismological Research Letters, 87(4), 987-997.

Luzi L., Lanzano G., Felicetta C., D'Amico M. C., Russo E., Sgobba S., Pacor, F., & ORFEUS Working Group 5 (2020). Engineering Strong Motion Database (ESM) (Version 2.0). Istituto Nazionale di Geofisica e Vulcanologia (INGV). https://doi.org/10.13127/ESM.2

Malinverno, A., & Ryan, W. B. (1986). Extension in the Tyrrhenian Sea and shortening in the Apennines as result of arc migration driven by sinking of the lithosphere. Tectonics, 5(2), 227-245.

Mazzoli, S., Deiana, G., Galdenzi, S., & Cello, G. (2002). Miocene fault-controlled sedimentation and thrust propagation in the previously faulted external zones of the Umbria-Marche Apennines, Italy. EGU Stephan Mueller Special Publication Series, 1, 195-209.

Mori, F., Mendicelli, A., Moscatelli, M., Romagnoli, G., Peronace, E., & Naso, G. (2020). A new Vs30 map for Italy based on the seismic microzonation dataset. Engineering Geology, 275, 105745. https://doi.org/10.1016/j.enggeo.2020.105745

NASA/METI/AIST/Japan Spacesystems and U.S./Japan ASTER Science Team (2019). ASTER Global Digital Elevation Model V003 [Data set]. NASA EOSDIS Land Processes Distributed Active Archive Center. Accessed 2024-02-06 from https://doi.org/10.5067/ASTER/ASTGTM.003

Parker, G. A., Harmon, J. A., Stewart, J. P., Hashash, Y. M., Kottke, A. R., Rathje, E. M., Campbell, K. W. (2017). Proxy-based VS 30 estimation in central and eastern North America. Bulletin of the Seismological Society of America, 107(1), 117-131. https://doi.org/10.1785/0120160101

Pierantoni, P., Deiana, G., & Galdenzi, S. (2013). Stratigraphic and structural features of the Sibillini mountains (Umbria-Marche Apennines, Italy). Italian Journal of Geosciences, 132(3), 497-520.

Stewart, J. P., Klimis, N., Savvaidis, A., Theodoulidis, N., Zargli, E., Athanasopoulos, G., Margaris, B. (2014). Compilation of a local VS profile database and its application for inference of VS 30 from geologic-and terrain-based proxies. Bulletin of the Seismological Society of America, 104(6), 2827-2841.

Wald, D. J., & Allen, T. I. (2007). Topographic slope as a proxy for seismic site conditions and amplification. Bulletin of the Seismological Society of America, 97(5), 1379-1395. https://doi.org/10.1785/0120060267

Wang, J. S., Hwang, J. H., Lu, C. C., & Deng, Y. C. (2022). Measurement uncertainty of shear wave velocity: A case study of thirteen alluvium test sites in Taipei Basin. Soil Dynamics and Earthquake Engineering, 155, 107195.

Wills, C. J., & Clahan, K. B. (2006). Developing a map of geologically defined site-condition categories for California. Bulletin of the Seismological Society of America, 96(4A), 1483-1501. https://doi.org/10.1785/0120050179

Wills, C. J., Gutierrez, C. I., Perez, F. G., & Branum, D. M. (2015). A Next Generation VS30 Map for California Based on Geology and TopographyA Next Generation VS30 Map for California Based on Geology and Topography. Bulletin of the Seismological Society of America, 105(6), 3083-3091. https://doi.org/10.1785/0120150105

Xia, J., Miller, R. D., Park, C. B., Hunter, J. A., Harris, J. B., & Ivanov, J. (2002). Comparing shear-wave velocity profiles inverted from multichannel surface wave with borehole measurements. Soil dynamics and earthquake engineering, 22(3), 181-190.

Yong, A., Hough, S. E., Iwahashi, J., & Braverman, A. (2012). A terrain-based site-conditions map of California with implications for the contiguous United States. Bulletin of the Seismological Society of America, 102(1), 114-128. https://doi.org/10.1785/012010026

CHAPTER 6

GROUND MOTION SIMULATION OF HISTORICAL EARTHQUAKES: THE CASE STUDY OF THE FABRIANO (1741, Mw = 6.1) AND CAMERINO (1799, Mw = 6.1) EARTHQUAKES IN CENTRAL ITALY

This Chapter presents the methodology for determining the 3D seismogenic sources of two historical earthquakes occurred in the Marche Region (Central Italy): the Fabriano event 1741 (Imax 9 MCS; Mw 6.17) and the Camerino event 1799 (Imax 9-10 MCS; Mw 6.18) and generating shaking scenarios. The ground motion has been calculated as Peak Ground Acceleration (PGA) and Peak Ground Velocity (PGV) using the recent GMM for Italy (ITA18, Lanzano et al., 2019). The 3D geometry of the sources has been discriminated through the residual analysis between observed and predicted macroseismic intensities that have been obtained by the conversion of the PGV into macroseismic intensity using conversion relations provided by Gomez Capera et al. (2020). Finally, the site effect has been included in the shaking scenarios through a Vs,30 map of the Umbria-Marche Regions developed with the methodology presented in Chapter 5.

The present article has been published in Bulletin of Earthquake Engineering (Springer). DOI: 10.1007/s10518-023-01759-y.

6. Ground motion simulations of historical earthquakes: The case study of the Fabriano (1741, Mw = 6.1) and Camerino (1799, Mw = 6.1) earthquakes in Central Italy

Veronica Gironelli [1,2], Tiziano Volatili [1], Lucia Luzi [3], Giulio Brunelli [1,3], Miller Zambrano [1], Emanuele Tondi [1,2]

[1]*School of Science and Technology – Geology Division, University of Camerino, Italy*

[2]*National Institute of Geophysics and Volcanology, Seismology and Tectonophysics Division, Camerino, Italy*

[3]*National Institute of Geophysics and Volcanology, Milan, Italy*

Abstract

The determination of ground motion is crucial to plan the appropriate emergency activities, especially in areas characterised by an intense seismic history like the Italian peninsula. Ground motion assessment is generally based on the seismological parameters reported in the instrumental and parametric seismic catalogues. Therefore, the computation of shaking scenarios of historical earthquakes is very challenging, due to the poorly constrained variables (i.e., magnitudes, epicentral location, seismogenic sources), derived from the macroseismic intensity. In this study, we propose a novel approach to investigate the location and parametrization of the seismogenic sources of historical earthquakes and derive shaking scenarios. To this aim, the ground motion of two historical events, the Fabriano (1741, Mw = 6.1, Imax IX MCS) and Camerino (1799, Mw = 6.1, Imax IX–X MCS) earthquakes is simulated. In order to include the site response, a Vs,30 map of the Umbria and Marche regions is created from near-surface data. Different causative faults solutions are tested, finally discussing the ideal seismogenic source based on the residual analysis between observed and simulated macroseismic intensities. The resultant shaking scenarios of the two events are obtained by integrating observed intensities and simulations.

Keywords: *Historical earthquake; Macroseismic intensity; Ground motion simulation; Seismogenic source.*

6.1. Introduction

The Italian Peninsula is a high seismic hazard region, characterised by a well-documented historical and instrumental seismicity reported in the Parametric Catalogue of the Italian Earthquakes (*Catalogo Parametrico dei Terremoti Italiani - CPTI15 v4.0; Rovida et al. 2022).* Over the last seven centuries, 44 moderate-to-strong earthquakes (Mw ≥ 5.5) affected the central Apennines, according to the CPTI15. The last three destructive seismic sequences occurred in 1997 (Mw = 6.0) Colfiorito, in 2009 (Mw = 6.3) L'Aquila, and in 2016 (Mw = 6.5) Amatrice-Visso-Norcia.

After the 1997 seismic events, the Umbria-Marche Apennines (central Italy) has become a subject of great scientific interest and many studies have been carried out on the seismic hazard of the area (e.g., Boncio et al. 2004; Pizzi et al. 2002, 2017; Pantosti et al. 2012; Tondi 2000; Tondi et al. 2009), as well as on the main causative faults, and the evolution of the three main seismic sequences (Amato et al. 1998; Chiarabba et al, 2009; Chiaraluce et al. 2017). Historically, the portion of the Marche Region immediately north of the area hit by the aforementioned seismic sequences was the epicentral area of strong earthquakes. The CPTI15 catalogue lists two highly damaging events with Mw ≥ 5.5 that occurred on April 24th, 1741 "Fabrianese earthquake" (Imax IX MCS) and on July 28th, 1799 "Appennino Marchigiano earthquake" (Imax IX-X MCS). These earthquakes heavily affected the cities of Fabriano and Camerino causing the highest macroseismic intensities in these areas, hereinafter called "Fabriano" and "Camerino" earthquakes, respectively (See locations in Fig. 6.1).

The study of moderate-to-large historical earthquakes is challenging in active continental regions like Italy. Specifically, the computation of the ground motion of earthquakes that have return periods significantly larger than the timespan of instrumental network coverage is of paramount importance to consider the impact they could have on today's urban setting. Pre-instrumental earthquakes are only characterised by macroseismic intensity, which is a measure of the effects of earthquakes on both people and buildings, and it shows a good correlation with ground motion measures (Wald et al. 1999; Kaka and Atkinson, 2004; Atkinson and Kaka, 2007; Worden et al. 2012; Caprio et al. 2015). In order to compute a shaking scenario of large historical events in terms of peak values or response spectra ordinates from historical data we need i) the information on the seismic source geometry, ii) models to predict ground

shaking or macroseismic intensity in function of the event size and the source-to-site distance and, possibly, the site amplification; iii) tools to convert macroseismic intensity into ground motion and vice versa.

Intensity Prediction Equations (IPEs) and Ground Motion Models (GMMs) are robust empirical models to predict macroseismic intensity or peak parameters (e.g., Peak Ground Acceleration, Peak Ground Velocity) and spectral amplitudes. IPEs predict macroseismic intensities in function of magnitude (or epicentral intensity) and source-to-site distance; while GMMs predict ground motion parameters in function of some explanatory variables such as magnitude, source-to-site distance, and proxies of site effects. IPEs and GMMs are derived by regressions conducted on data from recorded earthquakes (e.g., Bozorgnia et al. 2014; Gomez Capera et al. 2019). Peak parameters and spectral amplitudes can be converted into macroseismic intensities or vice versa to analyse and simulate the ground motion of past events using the Ground Motion Intensity Conversion Equation (GMICE; e.g., Caprio et al. 2015; Gomez Capera et al. 2020; Oliveti et al. 2022).

We individuate two possible approaches (i.e., IPE- and GMM-based methods) that could be followed to calculate the shaking scenarios of past earthquakes using the aforementioned empirical models:

The IPE-based methods consist of the computation of residuals between observed and predicted macroseismic intensities. The mean of the residuals (between-event error) is added to the predicted intensities in order to enhance the computation of the scenario and, finally, observations and predictions are interpolated to obtain a realistic representation of the ground shaking in terms of macroseismic intensity. The disadvantage of using IPEs is that the source-to-site distance is either the epicentral distance (i.e., the distance from the earthquake epicentre, Gomez Capera, 2006) or an hypocentral distance which is approximated with a pseudo depth obtained by regression, and therefore it is a not representative measure in case of events with $Mw \geq 5.5$. Moreover, IPEs do not consider site effects. An additional disadvantage is that macroseismic intensities are integer values, or can be approximated to the nearest half unit, which determines the representation of the shaking scenario as intensity classes instead of a continuous distribution.

The GMM-based approach consists of the prediction of peak values or spectral ordinates in function of magnitude and distance from the fault plane allowing to exploit of the 3D source geometry information, which is fundamental for earthquakes with magnitude Mw ≥ 5.5 and because the fault dimension affects the measure of the distance from the fault to the site of interest. Moreover, the site amplifications can be quantified through site amplification proxies (e.g., averaged shear-wave velocity in the uppermost 30 m-Vs,30; soil classes). The residuals between the predictions (ground motion measures converted into macroseismic intensities) and observations at the same sites can be used to select the 3D fault geometry that minimised the residuals. After the best fault solution has been identified, the GMM predictions and the macroseismic observations (converted into ground motion measures) can be interpolated to obtain a shaking scenario expressed as continuous values.

Similarly, a GMM-based approach could be handled by the software ShakeMap® developed by the U. S. Geological Survey Earthquake Hazards Program (Wald et al. 2005), to compute shaking maps by combining ground-truth observations (ground motion or macroseismic intensity) and GMMs. In alternative to the USGS Shakemap, we create a customised procedure, since the limitation of the Shakemap tool is that the Vs,30 values are interpolated to fit a predefined map grid that modifies the original values (https://usgs.github.io/shakemap/, last access 7 March 2023), whereas our aim is to use a customised Vs,30 grid.

The GMM-based approach is used to simulate the scenarios of the 1741 Fabriano and 1799 Camerino seismic events. Several studies have focused on the macroseismic effects and the possible seismogenic sources of these earthquakes (Pergalani et al. 1986; Monachesi 1987; Boschi et al. 1995, 1998; Castelli et al. 1997; Marcellini and Tiberi, 2000; Castelli and Monachesi, 2001), although the causative faults are still uncertain since there is no direct surface evidence of active tectonics. Therefore, a large effort is spent in this study investigating the 3D causative faults of the two earthquakes through residual analysis between simulated and observed macroseismic intensities. The macroseismic data of the seismic events are obtained from the Italian Macroseismic Database (*Database Macrosismico Italiano* - DBMI15 v4.0, Locati et al. 2022), while the seismogenic sources are proposed in the Italian Database of Individual Seismogenic Sources (DISS; DISS Working Group, 2021; Basili et al. 2008). We make use of the

most recent GMM for Italy (Lanzano et al. 2019) to predict the ground motion and the Ground Motion Intensity Conversion Equation (GMICE) by Gomez Capera et al. (2020) to convert the ground motion parameters into macroseismic intensities and vice versa.

The presented workflow is highly adaptable to different localities and geological conditions. This contribution improves the analysis of historical seismicity and allows the identification of the 3D geometry of poorly constrained causative faults to derive shaking scenarios of historical earthquakes, contributing to seismic hazard analysis.

6.2. Seismotectonic Setting and Seismicity

The central Apennines are part of the Neogene peri-Mediterranean fold-and-thrust belt dominated by carbonate and terrigenous sequences and controlled by the subduction of the Adriatic plate to the east and the back-arc Tyrrhenian Sea to the west (Cipollari and Cosentino, 1996; Galadini, 1999; Centamore et al. 2009; Cosentino et al. 2010). From a structural point of view, the central Apennines are characterised by the coexistence of both extensional and compressive structures NW-SE oriented (Lavecchia et al. 1994, Mazzoli et al. 2002; Materazzi et al. 2022), as shown in Fig. 6.1. The seismicity of the study area well reflects the different structural framework of the central Apennines. According to the focal mechanisms reported by Monachesi et al. (2021), the minor seismicity influencing the Adriatic coastal sector is characterised by compressive and transpressive focal mechanisms (Mazzoli et al. 2015). Conversely, most of the earthquakes which occur along the Apennines chain are mainly crustal events (i.e., hypocentral depths lower than 20 km) (Collettini, 2002; Collettini et al. 2003; Lavecchia et al. 2004), characterised by focal mechanisms with a clearly extensional component. The main active faults are of extensional type, arranged close to the axis of the Apennines chain and are mainly related to the Plio-Quaternary extension associated with the evolution of the Apennines (Patacca et al. 1990; Cinque et al. 1993; Pantosti et al. 1993). This sector of the Apennine chain is tectonically active and is affected by intense seismicity as attested by the occurrence of relatively frequent earthquakes in the Mw 5.5-6.5 range from the CPTI15 catalogue (Rovida et al. 2022).

A total of 44 historical and instrumental earthquakes strong enough to cause severe damage and surface effects occurred in the area. Based on field data, mainly geophysics and paleoseismology, most events have been associated with a specific seismogenic fault (DISS Working Group, 2021, and references therein), whereas the characteristics of the capable faults are summarised in the ITHACA database (ITaly HAzard from CApable faults; ITHACA Working Group, 2019).

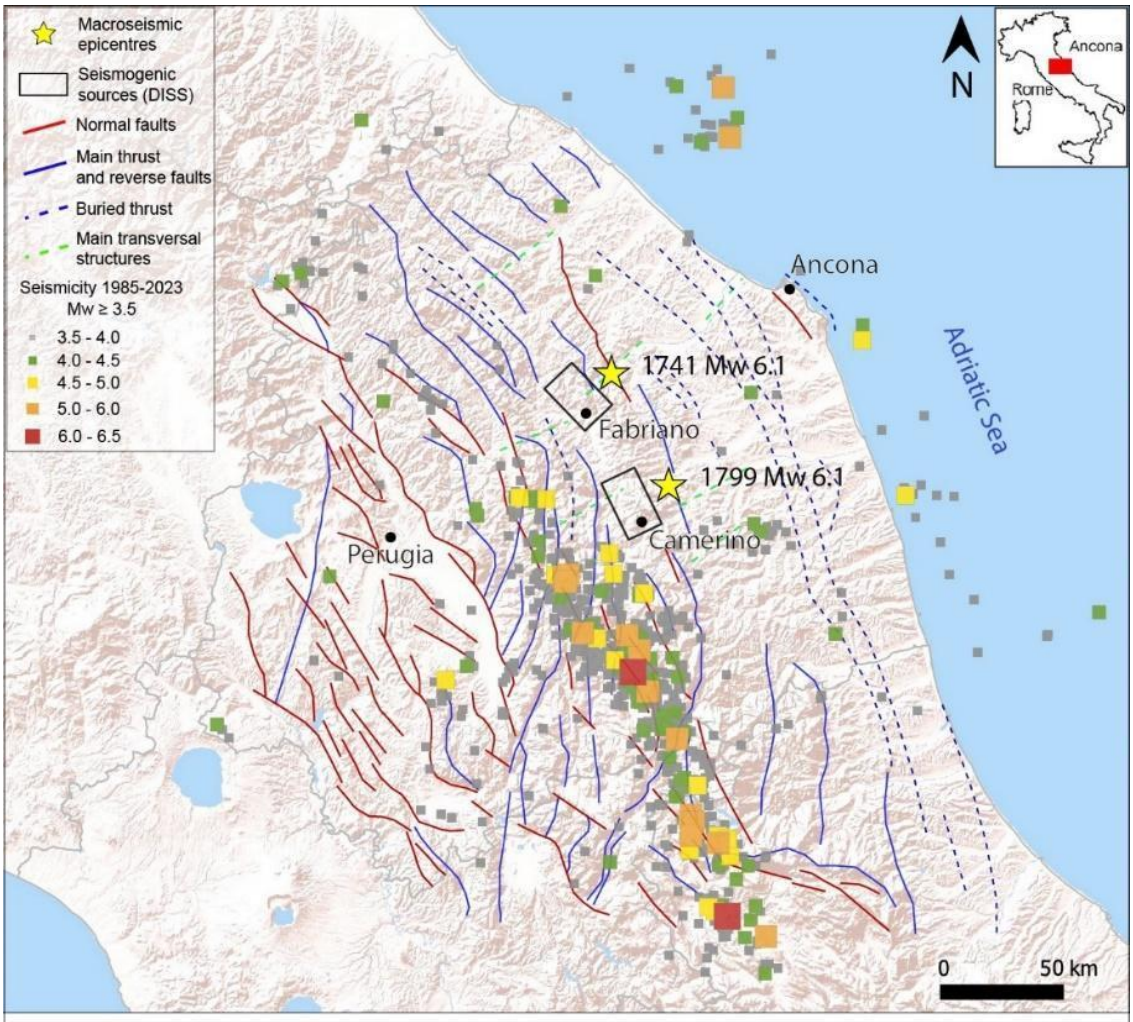

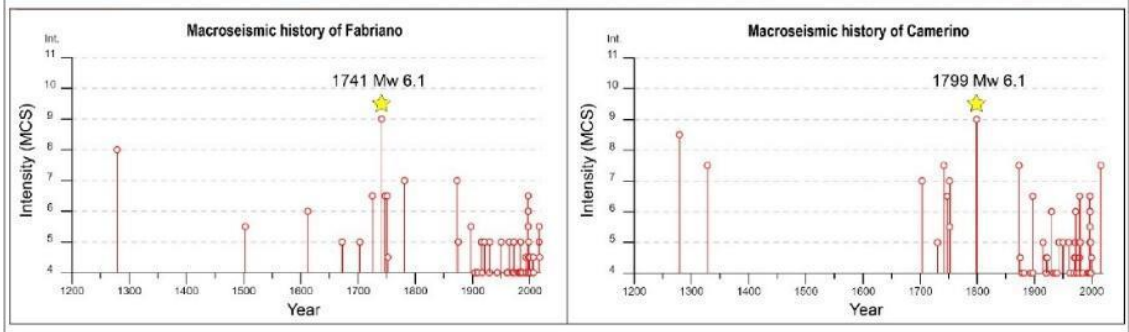

Seismogenic Sources Parameters from DISS

Event	ID_DISS	Strike (°)	Dip (°)	Length (km)	Width (km)	Min depth (km)	Max depth (km)
1741 Fabriano	ITIS048	135	20	13	9	14	17
1799 Camerino	ITIS049	153	30	14	9.5	3	7.8

Figure 6.1. Main tectonic structures of the study area, modified after Mazzoli et al. (2002) and Materazzi et al. (2022). The yellow stars show the location of the macroseismic epicentres of the 1741 Fabriano and 1799 Camerino earthquakes from CPTI15 (Rovida et al. 2022). Bottom panels: macroseismic history of

the Fabriano and Camerino municipalities from DBMI15 (Locati et al. 2022); geometric parameters of the seismogenic sources; Min depth and Max depth indicate the upper and bottom depth of the fault plane, respectively, from DISS (DISS Working Group, 2021).

Differently, the Foothill zone which is located between the extensional tectonic regime of the Apennines belt and the eastward compressive regime of the Adriatic coast (Scandone et al. 1996, Lavecchia et al. 2003) is characterised by a few historical events and the recent background seismicity comprises both shallow (< 10 km) and relatively deep (15-30 km) instrumental earthquakes (Mw < 5.5) with mixed kinematics (normal, strike-slip or reverse).

During the XVIII century, two significant seismic events occurred in that area: the 1741 Fabriano earthquake with an epicentral intensity of IX MCS (Stucchi et al. 1991; Monachesi and Stucchi, 1997) and the 1799 Camerino earthquake with an epicentral intensity of IX-X MCS (Monachesi et al. 2016). These two events have been felt over a large area in the Umbria-Marche region as reported by the abundant historical documents (Stucchi et al. 1991, Monachesi et al. 2016) and attested by the number of macroseismic observations (NMO) in the DBMI15, consisting of 135 intensity data points for the 1741 earthquake and 70 for the 1799 earthquake, respectively. The Fabriano earthquake caused severe damage in the hinterland of Ancona province, including Fabriano, Serra San Quirico and the villages of Sasso and Mergo (Castelli and Monachesi, 2001). The 1799 earthquake instead caused extensive damage in Camerino, Cessapalombo, San Ginesio and Sarnano, and a huge number of casualties. Consequently, the 1741 earthquake is currently assigned an intensity-based moment magnitude (Mw) of 6.1, while the 1799 earthquake is associated with an Mw of 6.1 in the CPTI15 (Rovida et al. 2022). The epicentres of the 1741 and 1799 earthquakes obtained from the macroseismic intensity distribution are located at about 8 km NE from Fabriano and at about 6 km NE from Camerino, respectively.

Unfortunately, the origin of these events is still largely discussed due to the absence of geological and paleo-seismological data, and evidence at the surface about the causative faults. Additionally, the lack of significant seismic activity in these areas makes the identification of the seismogenic sources of these earthquakes difficult. Nevertheless, some interpretations have been proposed based on dated low-resolution scale seismic sections (Barchi et al. 1998; Finetti et al. 2001; Carminati et al. 2004).

For the 1741 Fabriano earthquake, there are two main hypotheses: the DISS database (Basili et al. 2008 and references therein) proposes an NW-SE dipping SW low-angle (20°) reverse fault, labelled ITIS048; other authors (Cello et al. 1997; Materazzi et al. 2022) suggest a NE-SW strike-slip mechanism, sub-perpendicular to the Apennine axis. On the other hand, there is a univocal interpretation of the causative fault of the 1799 Camerino earthquake, which is identified as an NW-SE structure, labelled ITIS049, with the typical normal mechanism of the Apennine faults (Barchi et al. 1998; Finetti et al. 2001; Lavecchia et al. 2004). The geometrical parameters for the seismogenic sources proposed by the DISS database are summarised in Fig. 6.1.

6.3. Data and Methods

The proposed workflow can be divided into two main parts: the first is dedicated to the creation of a Vs,30 map for the Umbria-Marche region as a proxy of site effects, whereas the second part deals with the earthquake ground motion scenarios and residual analysis.

6.3.1. Calibration of a Vs,30 map

The observed macroseismic intensity includes the effect of site amplification, the ground motion should be simulated at the site, and the site amplification is evaluated through proxies (e.g., Vs,30, soil classes). Recently, many studies focused on site condition mapping based on soil type, stratigraphic age and Vs,30 measurements (Tinsley and Fumal; 1985) and on the correlation between Vs,30 measurements, topography, and geological units (e.g., Wald and Allen, 2007; Allen and Wald; 2009; Iwahashi et al. 2010; Willis et al. 2015, Forte et al. 2019). Other contributions have focused on geological units, topographic data, and geophysical and geotechnical measurements (Hassanzadeh et al. 2013; Karimzadeh et al. 2014; Mori et al. 2020).
We created a Vs,30 map for the Umbria-Marche region following the approaches presented by Forte et al. (2019) and Mori et al. (2020).

Firstly, we collected data from the Italian seismic microzonation dataset (e.g., https://sisma2016data.it/microzonazione/, last access February 2023; qmap-protciv.regione.marche.it, last access February 2023), consisting of a total of 4115

shear-wave velocity (Vs) profiles obtained by different geophysical tests: borehole methods (Down-Hole, Cross-Hole) and seismic refraction and surface-waves surveys (Multichannel Analysis of Surface Waves, MASW; Spectral Analysis of Surface Waves, SAWS; and REfraction MIcrotremors, REMI). The shear-wave velocity profiles are validated and processed to eliminate unreliable values and finally calculate the Vs,30 values. The geologic information is obtained from the 1:100.000 geo-lithological map of Italy (courtesy of the Italian Institute for Environmental Protection and Research, ISPRA – Italian Geological Survey; Servizio Geologico d'Italia, 2004).

To harmonise the 28 original lithologic categories, we (i) differentiate between surface deposits (Quaternary) and bedrock formations (Jurassic to Pleistocene) and (ii) merge the geological formations with similar expected geotechnical behaviour (Fig. 6.2).

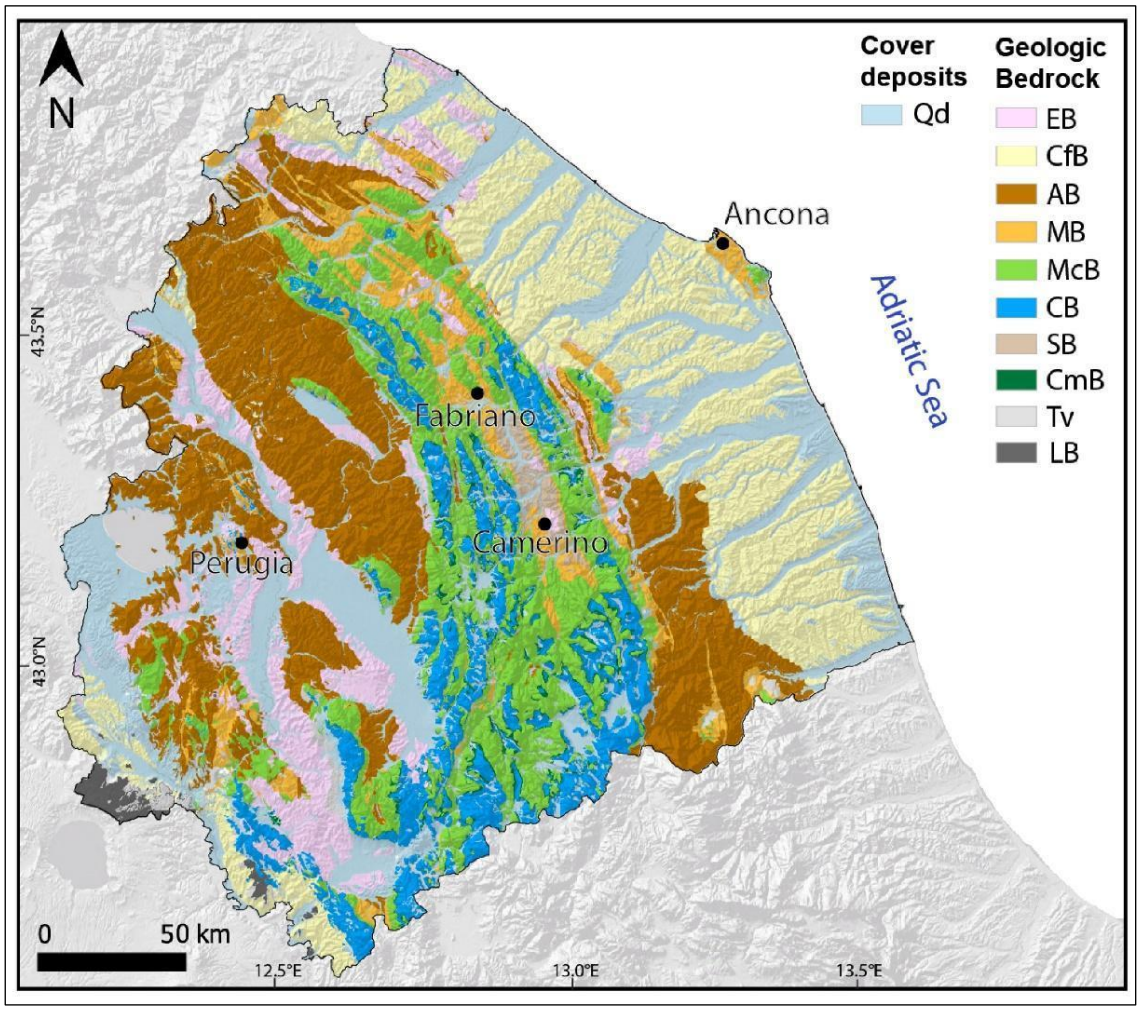

Figure 6.2. Map of Umbria-Marche region showing the identified geo-lithological complexes (lithological codes are listed in Table 6.1).

Table 6.1. The geo-lithological complexes identified in the study area.

Name of the complex	ID	Description
Cover deposits		
Quaternary deposits	Qd	Alluvial and terraced deposits, colluvium, alluvial fan
Geologic Bedrock		
Evaporites	EB	Evaporitic rocks, gypsum, diatomite
Clay	CfB	Clay, clayey sands
Arenaceous	AB	Arenaceous rocks
Marl	MB	Marl, clayey marls
Marly limestone	McB	Marly, calcareous and siliceous succession
Carbonate	CB	Limestones and dolostones
Sand	SB	Sands and sandstone bedrocks
Calcareous marl	CmB	Marlstones
Travertine	Tv	Travertine and soft limestone
Lava	LB	Volcanic materials, lava, tuffs, ignimbrites

The ANOVA test is performed to verify whether the geo-lithological complexes listed in Table 6.1 are significantly different from each other in terms of measured Vs,30 values. The distribution of Vs,30 values are shown in Fig. 6.3 as box plots. Here, the first quartile, the median value, and the third quartile are reported together with the minimum and maximum values of the distribution, and the outliers. The ANOVA uses the statistic-F (F) to compare the between- and within-group variances and the statistical significance is determined through the significance probability value (P-value). The statistical analysis results revealed a statistically significant difference in Vs,30 between the eleven geo-lithological complexes (F = 29.7) and the small P-value of $7.56e\text{-}^{53}$ indicates that the means of the geo-lithological complexes are correctly differentiated.

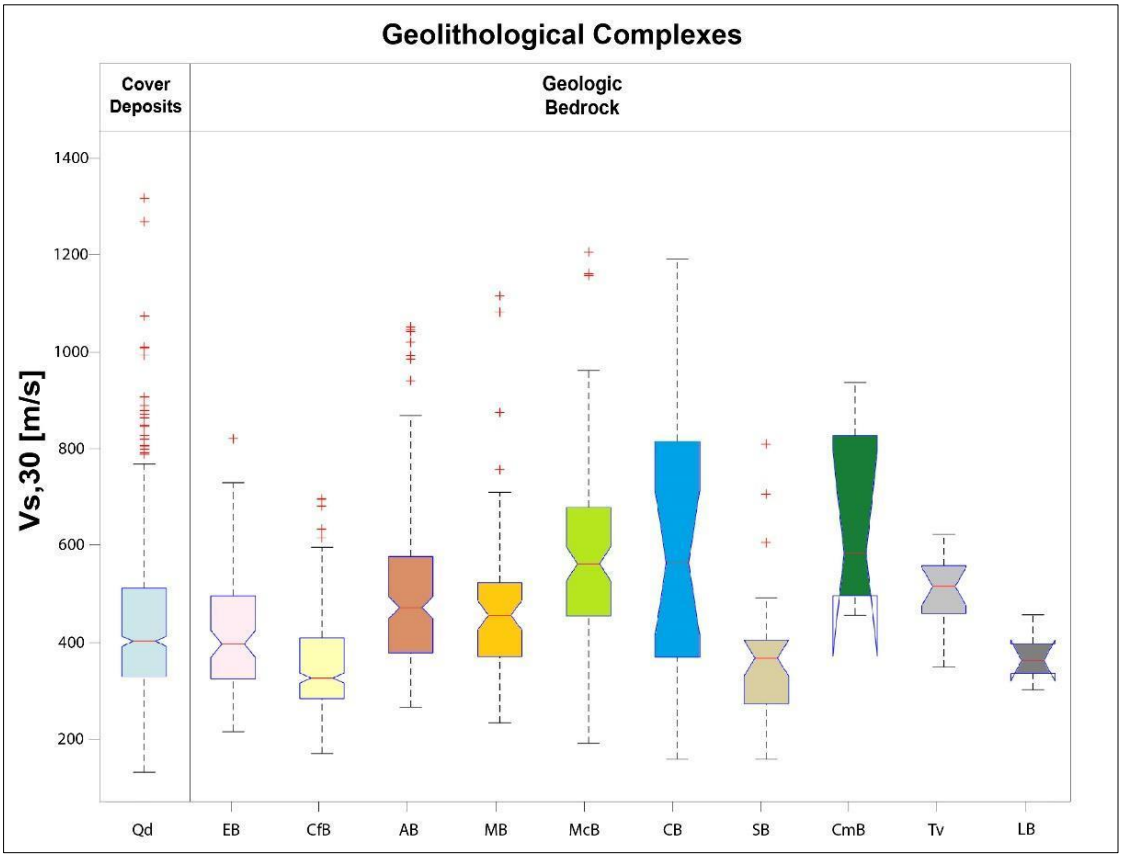

Figure 6.3. Box plots showing the distributions of Vs,30 for the geo-lithological complexes listed in Table 6.1.

From Fig. 6.3, the complexes consisting of mainly calcareous formations (CB, CmB and McB) show an overall wide Vs,30 velocity range (390-800 m/s) with a median value of 590 m/s. The complexes composed of marly-arenaceous formations (MB and AB) are characterised by Vs,30 values in the range of 390-590 m/s, with a median Vs,30 of about 480 m/s. Conversely, the shear-waves velocity ranges are comparable for the complexes composed of mainly sandy-clayish formations and characterised by lower Vs,30 values. The median Vs,30 values for SB and CfB are 380 m/s and 320 m/s, respectively. The other geo-lithological complexes show median Vs,30 values of 400 m/s and 520 m/s.

Wald et al. (1999, 2007) found a good correlation between the topographic data and the Vs,30 measurements in tectonically active areas by using a global 30 arc sec topographic dataset. In this study, we use an ASTER Global Digital Elevation Model (GDEM) with a spatial resolution of 30 m. The topographic slopes are calculated using

the “Slope” tool provided by ArcGIS, an algorithm that uses a weighted average of three central differences, which includes the eight neighbouring pixels associated with a weighting matrix (Horn, 1981).

A regression is performed to predict the Vs,30 values as a function of lithology and topographic slope. The adopted regression procedure employs the mixed-effects model (Abrahamson and Youngs 1992) embedded the *lme* function in MATLAB. The fixed effect is the lithology, while the random effect is for slope grouped by lithology.

The resulting empirical equation used to predict Vs,30 values is the following:

$$Vs,30 = a_0 + S_{Ln} * \beta + L_n \qquad (6.1)$$

where a_0 is a constant and S_{Ln} and L_n are the slope coefficients for each lithology and the lithology coefficients, respectively; β is the topographic slope and n is the number of lithology classes (Table 6.2).

Table 6.2. Coefficients of eq. 1 for the lithology and the coefficients of slope for each lithology class.

Geo-lithological Complexes	**L_n**	**S_{Ln}**
Qd	-108.74	4.0703
EB	-114.75	2.4458
CfB	-170.78	1.5291
AB	-15.085	0.4295
MB	-54.32	1.7018
McB	154.46	-3.5051
CB	127.71	-1.8367
SB	-160.62	3.0205
CmB	85.17	-0.3886
Tv	-3.41	0.0160
LB	-170.99	2.0221

The resulting map is created by using the ArcGis Map Algebra and is shown in Fig. 6.4. From this map, three zones with different shear-wave velocities can be distinguished. The first zone is characterised by Vs,30 in the range 600-800 m/s (high velocity) and it is recognised in correspondence with the Umbria-Marche ridge, dominated by calcareous lithologies (stiff rocks). The second zone is characterised by intermediate shear-wave velocity, ranging from 400 to 600 m/s, and it is associated with marly-arenaceous lithologies. The third zone is characterised by the lowest Vs,30 values, ranging from 300-400 m/s, and it corresponds to the geological formations dominated by "soft" lithologies such as sandy/clayish sediments and quaternary deposits which are mainly representative of the foreland and alluvial valleys. The Vs,30 map has a resolution of 30 m, consistently with resolution of the DEM used. Finally, to the scope of the shaking scenarios, due to computational limitations, the map is resampled with a resolution of 250 m, nevertheless consistent with the small dimension of most settlements with assigned macroseismic intensities. Therefore, we do not expect a large variability of Vs,30 inside each settlement.

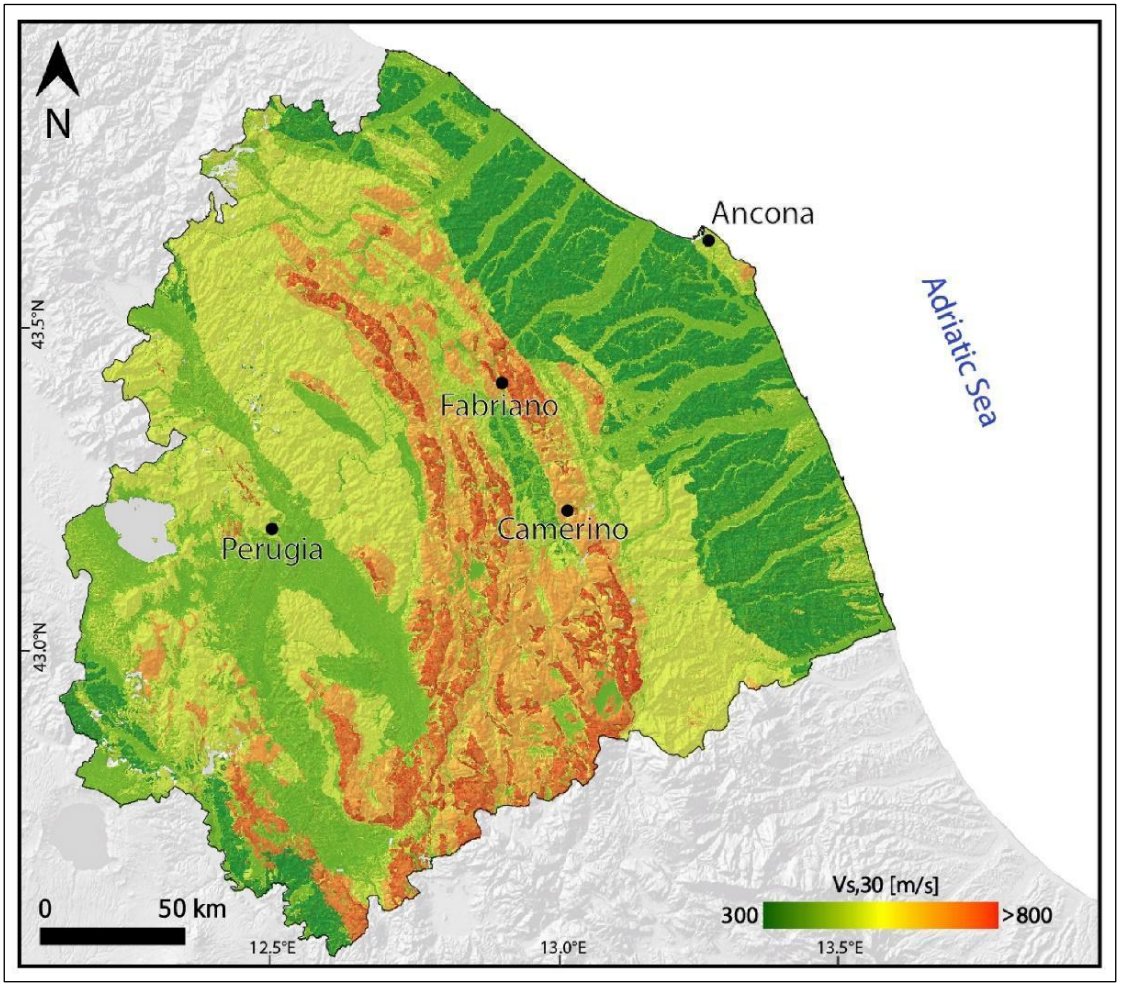

Figure 6.4. Umbria -Marche Vs,30 map. The colours correspond to the Vs,30-mean from Eq.1.

6.3.2. Workflow to generate ground motion scenarios of historical earthquakes

In order to generate a shaking scenario of historical earthquakes, exploiting the information of macroseismic intensity, we adopt the GMM-based approach and identify the best earthquake causative fault as follows: (i) identification of the potential seismogenic sources in terms of geometrical parameters (i.e., length, width), orientation (i.e., strike, and dip) and hypocentral depth; (ii) computation of the peak-ground acceleration (PGA) and peak ground velocity (PGV) at the geographic locations where the observed macroseismic intensities are available; (iii) conversion of the computed PGAs and PGVs into macroseismic intensities and calculation of the residuals between observed and predicted I_{MCS}; the distribution in space, the mean (between-event error)

and the root mean square error (RMSE) of the residuals are used to choose the best-fitting source.

The potential causative faults are initially selected from the DISS database: the "ITIS048" source for the Mw 6.1, 1741 Fabriano earthquake and "ITIS049" for the Mw 6.1, 1799 Camerino earthquake. The characteristics of the two sources are in Fig. 6.1. An alternative source, for the 1741 Fabriano earthquake is a NE-SW oriented strike-slip fault by Materazzi et al. (2022), who found geomorphological evidence of an earthquake affecting a sector of the "Fossato di Vico-Valle dell' Esino line" (FV-VE), a major transverse lineament in the outskirts of Fabriano. Based on the radiocarbon dating of the Santa Maria Bench alluvial deposits, they found it coherent with the 1741 earthquake. The strike-slip fault geometry is modelled with a length L = 18 km, a width W = 8 km and a dip angle of 78 degrees that are derived via the Wells and Coppersmith (1994) relationships.

To predict the peak values, we decided to use an existing GMM. Although a wide number of global and regional models are available in the literature (e.g., Abrahamson et al. 2008; Cauzzi and Faccioli 2008; Akkar and Bommer 2010; Bindi et al. 2011, 2014) we select a model specifically calibrated for Italy (Lanzano et al. 2019; hereinafter ITA18), since it is the most recent model and it takes into account the closest distance from the rupture plane of the fault (Rrup) allowing to consider the 3D geometry of the seismogenic source. A sensitivity analysis of fault depth (Fig. 6.5) is performed by varying the hypocentral depth, and therefore the Rrup. The analysed fault geometries are translated in depth by assuming the hypocentre located at 2/3 along-dip of the fault plane. Moreover, the site amplification is evaluated by the average shear-wave velocity in the uppermost 30 m (Vs,30). Peak ground acceleration (PGA) and peak ground velocity (PGV) can be converted into macroseismic intensity using the following intensity conversion equation by Gomez - Capera et al. (2020) and are approximated to the nearest half unit.

$$I_{MCS} = a\, e^{(b\, LogGMP)} \qquad (6.2)$$

The inverse relation by Gomez Capera et al. 2020 can be used to convert the observed macroseismic intensity data into ground motion parameters to process the shaking scenarios in peak values.

$$LogGMP = a' + b' \, Log(I_{MCS}) \qquad (6.3)$$

where a and b, and a' and b' are the regression coefficients.

For the residual analysis, we used the PGV converted into macroseismic intensity with Eq. 2, since PGV was demonstrated to be the best ground motion parameter to assess the damage to structures (Bommer and Alarcon, 2006; Gomez Capera et al. 2020). Moreover, the PGV-derived intensities simulate the observed macroseismic intensities significantly better than PGAs (Wald et al. 1999; Yih-Mun et al. 2003; Gomez Capera et al. 2007).

After the best-fitting seismogenic source is identified, the calculation of shaking scenarios in terms of peak values (i.e., PGA and PGV) and macroseismic intensities is performed through the workflow shown in Fig. 6.6.

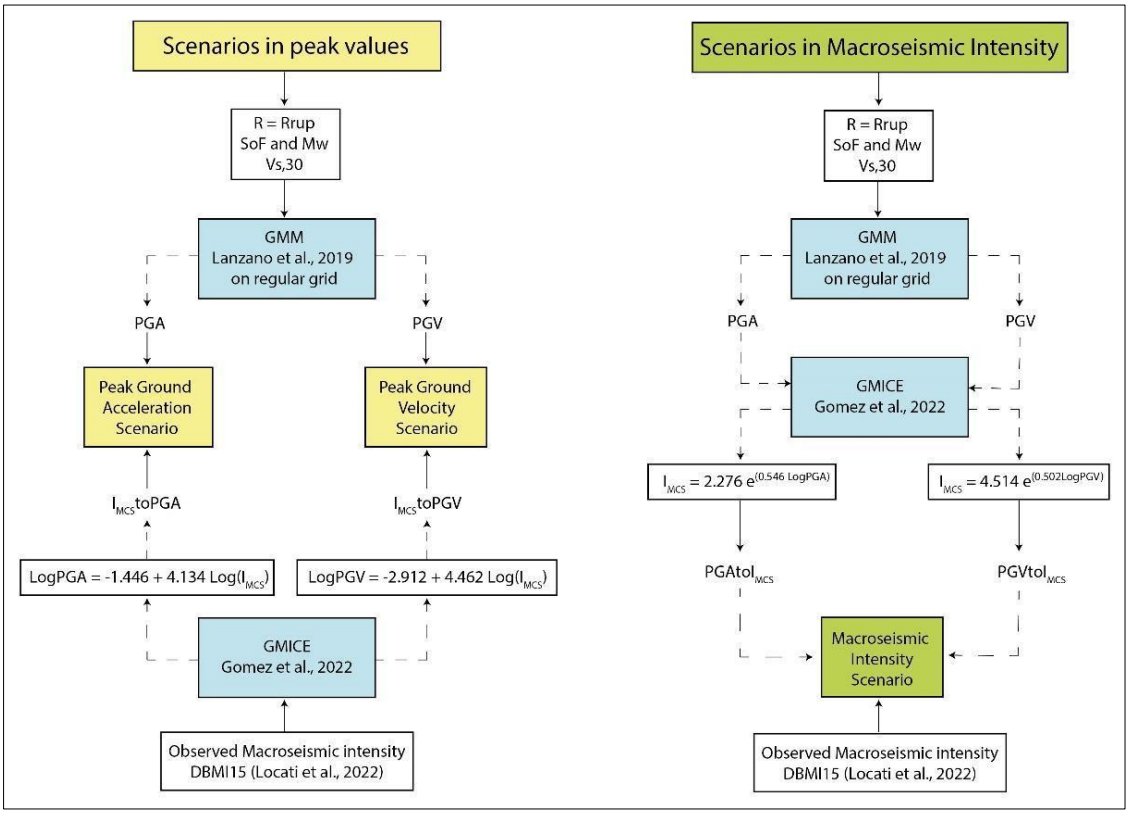

Figure 6.6. Flow charts indicating the steps for computing shaking scenarios in terms of peak values and macroseismic intensity.

6.4. Ground Motion Simulations

6.4.1. Fabriano 1741 (Mw = 6.1) earthquake scenarios

The earthquake scenarios for the 1741 Fabriano earthquake are calibrated using the seismogenic source "ITIS048" (DISS Working Group, 2021; Basili et al. 2008) corresponding to a NW-SE oriented reverse fault.

We tested different fault geometries varying the hypocentral depth and we chose the one that minimises the between-event error (Fig. 6.5a). The geometry proposed by the DISS database (Fig. 6.1) is consistent with the hypocentral depth of 16 km. Whereas, the fault geometry that minimises the residuals is associated with a hypocentral depth of 10 km. The resulting values are reported in Fig. 6.7a-b and presented together with the spatial distribution of the macroseismic intensities residuals obtained for the two fault geometries. Positive residuals, marked by blue circles, indicate an underestimation of the predicted macroseismic intensities compared to the observations, while negative residuals in red, indicate an overestimation of the predicted intensities. The mean of the residuals (between-event error) and the RMSE in the case of a nucleation point at 16 km are 0.34 and 0.94, respectively, whereas, in the case of a nucleation point at 10 km, the two values are equal to 0.05 and 0.97, therefore, we suppose that the latter is the best seismogenic source candidate.

Hence, we calculate the shaking scenarios for the best-fitting seismogenic source expressed in terms of PGA, PGV and macroseismic intensity, by interpolating predictions and observations, according with the workflow of Fig. 6.6. The PGA values of 120–190 cm/s^2 are predicted at epicentral distances of about 12 km, whereas the predicted PGVs are in the range of 8-15 cm/s (Fig. 6.7 c-d). These values are similar to those observed for October 26th, 2016, Visso earthquake (Mw = 5.9). Furthermore, at comparable epicentral distances from the source, a rapid westward attenuation of PGA and PGV values is observed with respect to the Adriatic coast side. This could be related to the presence of sandy-clayish lithologies to the east, that tend to amplify the shaking. The scenario in terms of macroseismic intensity in Fig. 6.7e, obtained from the interpolation of simulated intensities derived from the PGVs conversion and the observed macroseismic intensities (DBMI15), shows that the maximum intensity in the proximity of the source is equal to VIII-IX, which agrees to the intensity value assigned by the CPTI15 catalogue. Concerning the site effects introduced through the Vs,30 map,

a ground motion amplification is predicted in correspondence with the main sedimentary basins located in the study area (e.g., Gubbio and Camerino).

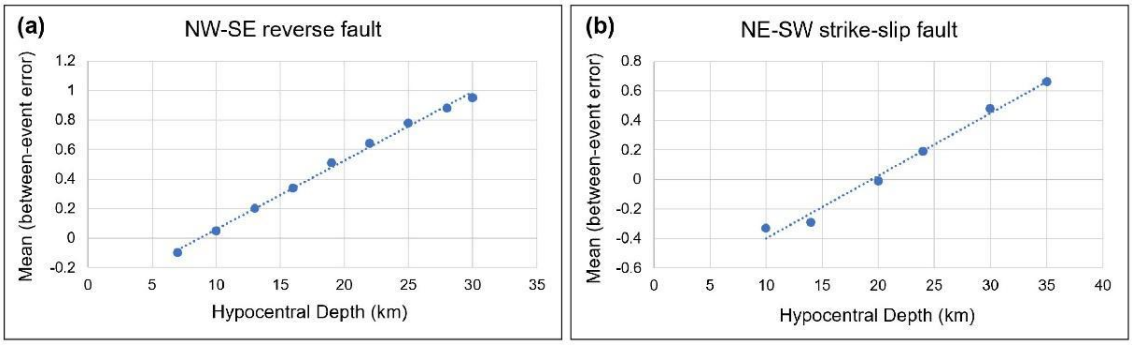

Figure 6.5. Mean (between-event error) of the residuals for the different hypocentral depths for the NW-SE reverse fault (a) and the NE-SW strike-slip fault (b) used for the 1741 Fabriano earthquake. The blue points correspond to the residuals' mean obtained from the difference between the observed and the predicted macroseismic intensity.

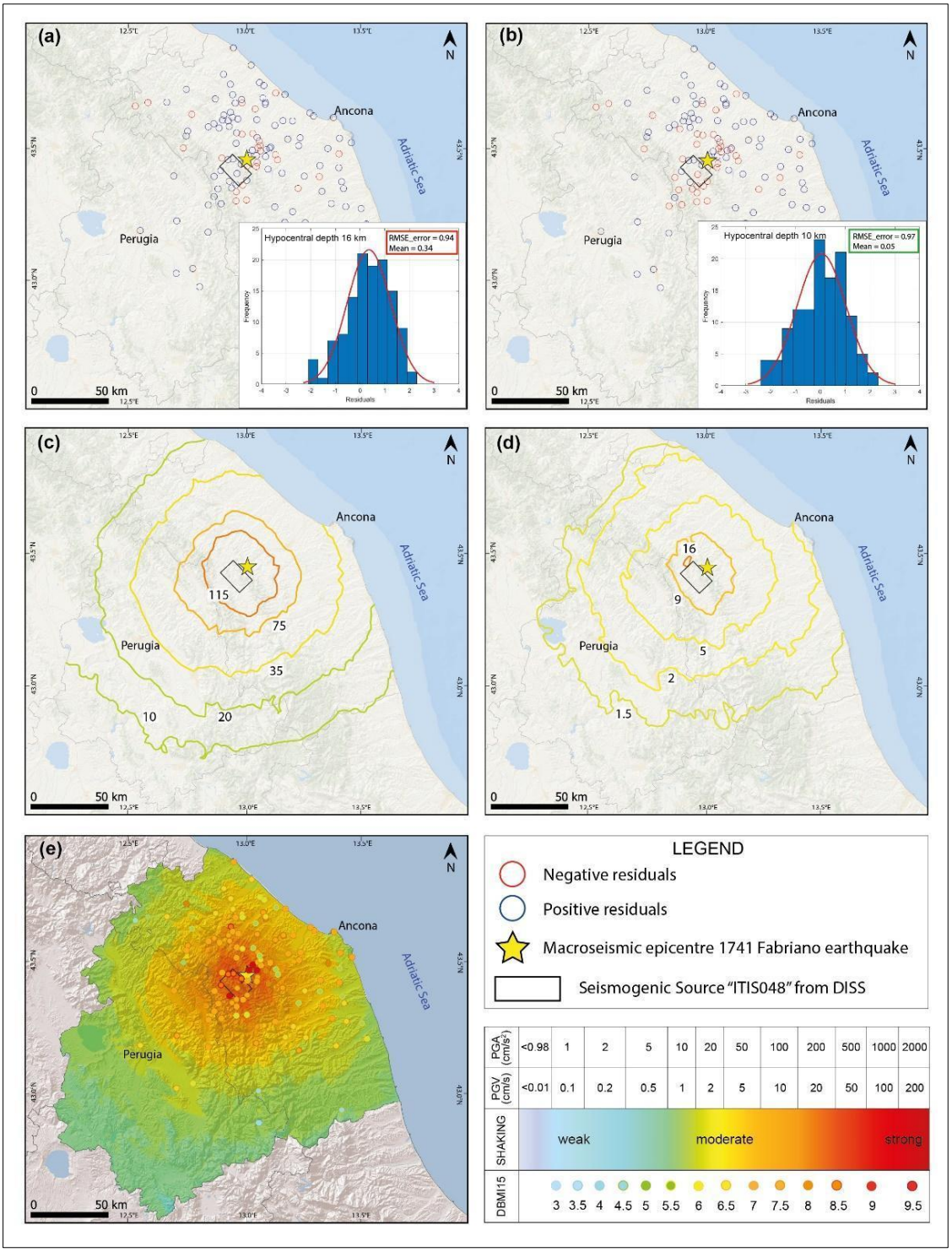

Figure 6.7. Spatial distribution of the macroseismic intensity residuals for the seismogenic source "ITIS048" with hypocentral depth at 16 km (a) and at 10 km (b). The bottom right inserts show the histogram of the residuals, the RMSE and the mean (between-event error) of residuals. The shaking scenarios relative to the best-fitting seismogenic source in (b) are presented in terms of (c) Peak Ground Acceleration (PGA in cm/s2), and (d) Peak Ground Velocity (PGV in cm/s) maps, and (e) Macroseismic intensity expressed in the Mercalli-Cancani-Sieberg (MCS) scale by following the workflow presented in Fig. 6.6.

Additionally, for the 1741 Fabriano earthquake, we calculate the shaking scenario relative to the alternative NE-SW oriented strike-slip fault, suggested as a source hypothesis in Materazzi et al. (2022). The causative fault is modelled using a length L = 18 km and width W = 8 km and the dip has been set equal to 78 degrees.

We calculated the scenarios assuming different hypocentral depths ranging from 10 to 35. This range of depths is coherent with most of the strike-slip earthquakes of the study area. For each fault geometry, the mean of the residuals (between-event error) is determined. The results of the complete set of simulations are presented in Fig. 6.5b. We then report in Fig. 6.8a-b the scenario with the transversal fault simulated assuming a hypocentral depth of 10 km, which has represented the better depth hypothesis for the case of a NW-SE reverse fault. In contrast, the second one represents the scenario that minimises the between-event error obtained by adopting a deeper hypocentral depth, equal to 20 km.

The distribution of residuals shown in Fig. 6.8a indicates an overestimation of the macroseismic intensity in the near-source when a hypocentral depth of 10 km is considered. Whereas the spatial pattern of residuals (Fig. 6.8b), for the rupture enucleated at 20 km, shows comparable simulated and observed macroseismic intensities. The values of RMSE and mean residual values for a nucleation point at 10 km are 1.25 and -0.33, respectively. The results for a nucleation point at 20 km show a lower RMSE, equal to 1, and a mean residual value of -0.01. Thus, the latter scenario represents the best fault geometry candidate. The shaking scenarios in terms of PGA, PGV and macroseismic intensities are shown in Fig. 6.8c-d-e. The maximum PGA values computed for the 1741 earthquake scenario by assuming the proposed alternative seismogenic source are in the range of 190-220 cm/s^2, whereas the PGVs are in the range of 10-14 cm/s at distances of about 12 km from the source. The macroseismic intensity scenario shows that the maximum intensity reached in the proximity of the source corresponds to an I_{MCS} of VIII-IX which is comparable with the intensity value assigned by the CPTI15 catalogue.

The origin of the 1741 Fabriano earthquake is largely debated due to the absence of significant aftershocks and geological and paleo-seismological data about the causative fault. Since the results are similar both source hypotheses could be possible. The seismogenic source proposed in the DISS database is consistent with a shallower

hypocentral depth (10 km), whereas the NE-SW strike-slip fault hypothesis with a deeper hypocentral depth of 20 km. However, macroseismic studies in the literature (Pergalani et al. 1986; Stucchi et al. 1991; Boschi et al. 1995, 1997) associated this event with a rupture generated by a deep source according to the large damaging level observed along the Italian Peninsula, although the event depth is not quantified. Monachesi et al. (2000), hypothesised that the 1741 event originated at an even greater depth (between 30 and 60 km) because of the very wide macroseismic intensity distribution. Sbarra et al. (2019) proposed a method to determine the hypocentral depth of historical earthquakes based on macroseismic intensity data and they inferred a depth of 35 km for the 1741 Fabriano earthquake by computing the "steepness" of the line that better approximates the macroseismic intensity attenuation curve of the event within 50 km from the source. The trend of the highest observed macroseismic intensities indicates an evident NE-SW direction (Monachesi 1987), that is in good agreement with the adopted transversal fault geometry. Furthermore, the site effects depicted in Fig. 6.8e well reproduce the areal distribution of the observed data reported in the DBMI15, since ground shaking attenuates more slowly in the case of a deep source. However, the mean of the residuals (between-event error) is higher for these larger hypocentral depths (Fig. 6.5). Therefore, we consider the NE-SW strike-slip fault enucleated at 20 km the most likely source of the 1741 Fabriano earthquake.

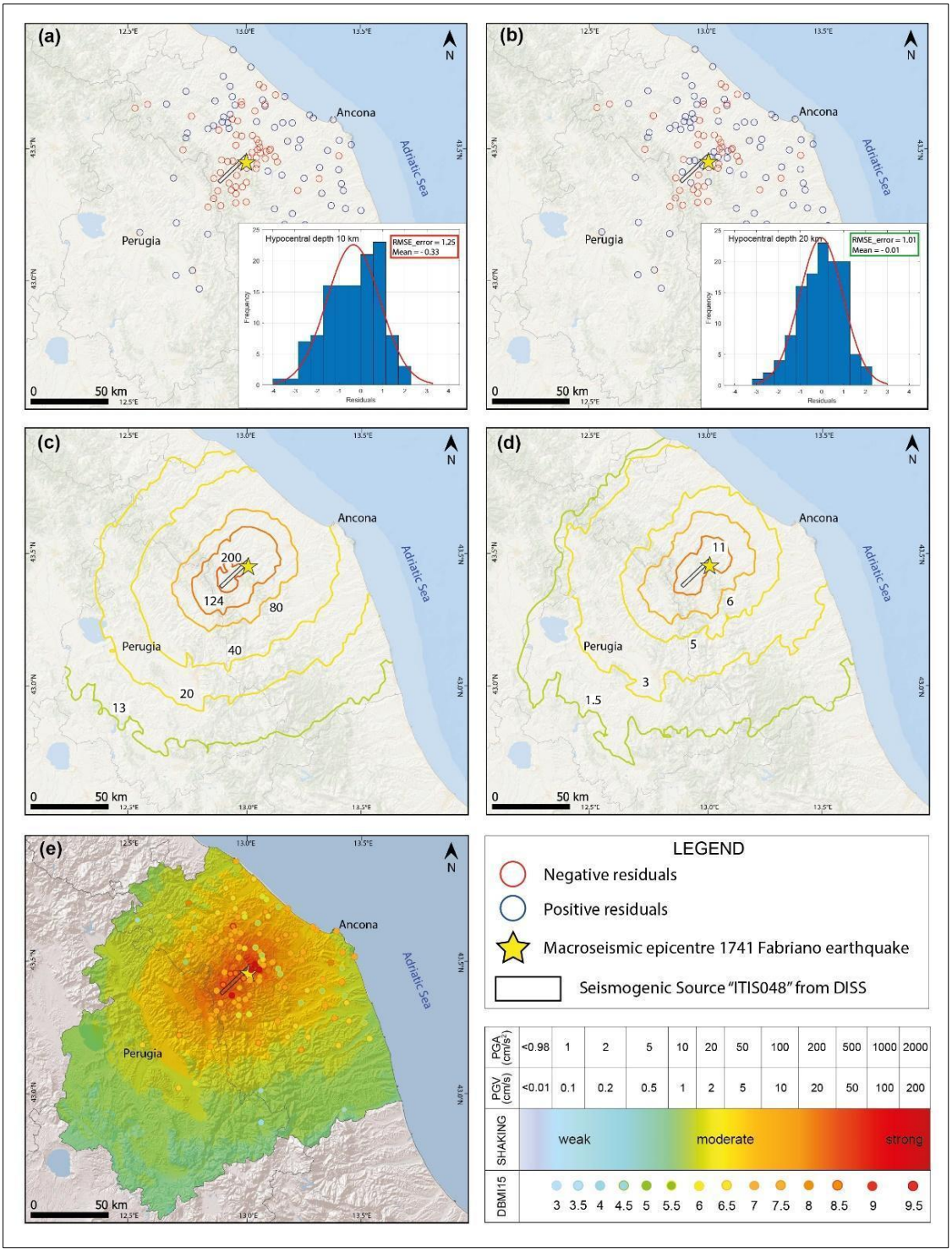

Figure 6.8. Spatial distribution of the macroseismic intensity residuals for the NE-SW strike-slip fault with hypocentral depth at 10 km (a) and at 20 km (b). The bottom right inserts show the histogram of the residuals, the RMSE and the mean (between-event error) of residuals. The final shaking scenarios relative to the best-fitting seismogenic source in (b) are presented in terms of (c) Peak Ground Acceleration (PGA in cm/s2), and (d) Peak Ground Velocity (PGV in cm/s) maps, and (e) Macroseismic intensity expressed in the Mercalli-Cancani-Sieberg (MCS) scale by following the workflow presented in Fig. 6.6.

6.4.2. Camerino 1799 (Mw = 6.1) earthquake scenarios

The origin of the 1799 earthquake has been associated with a shallow crustal extensional fault (DISS Working Group, 2021 and references therein). The DISS database (Basili et al. 2008) hypothesises a shallow source, labelled "ITIS049" (Fig.6.1), that is an NW-SE normal fault with enucleation in a depth range of 3-7.8 km. Sbarra et al. (2019), in agreement with DISS, calculated an expected depth of about 6 km for this earthquake. Conversely, Monachesi (2016) attributed to this event a crustal rupture at a depth ranging between 9-15 km, based on macroseismic evidence. Therefore, two alternative scenarios have been computed by assuming two nucleation depths at 6 km and 14 km, respectively.

The DISS hypothesis compatible with a rupture enucleated at 6 km gives negative residuals (red circles, in Fig. 6.9a), observed especially in the near-source with a between-event equal to -0.85 and an RMSE of 1.32, indicating a poor fit. In the second case we shift the DISS source in order to have a rupture plane enucleating at 14 km (Fig. 6.9b), and we observe a much better fit since the between-event is slightly positive and equal to 0.06 and the RMSE is substantially lower and equal to 0.89. Therefore, the final shaking scenario is relative to the source at 14 km, in agreement with the hypothesis supported by Monachesi (2016) based on the distribution of macroseismic intensity data points.

The PGA values obtained by interpolating the predictions and the observations range from 170-220 cm/s^2 at epicentral distances of about 12 km, whereas the PGVs are in the range of 8-12 cm/s (Fig. 6.9c-d). The resulting peak values are rather comparable with those registered after the October 26th, 2016, Visso earthquake (Mw = 5.9) at similar distances from the source. Additionally, the site effects and the associated amplification are mainly distributed close to the seismogenic source and are mainly associated with the lithological characteristics of the Camerino basin and with the presence of geological structures bordering the basin itself. The simulated macroseismic intensity scenario is shown in (Fig. 6.9e) together with the observed macroseismic intensity data points. The low difference between observed and predicted intensities confirms the reliability of the adopted approach.

Finally, to further support the choice of the best-fitting sources for the 1741 Fabriano and 1799 Camerino earthquakes, we decided to perform the residual analysis

considering only the intensity data points, both observed and predicted, within 50 km from the source. With a negligible outcomes difference, this cross-check confirmed the best seismogenic sources previously identified.

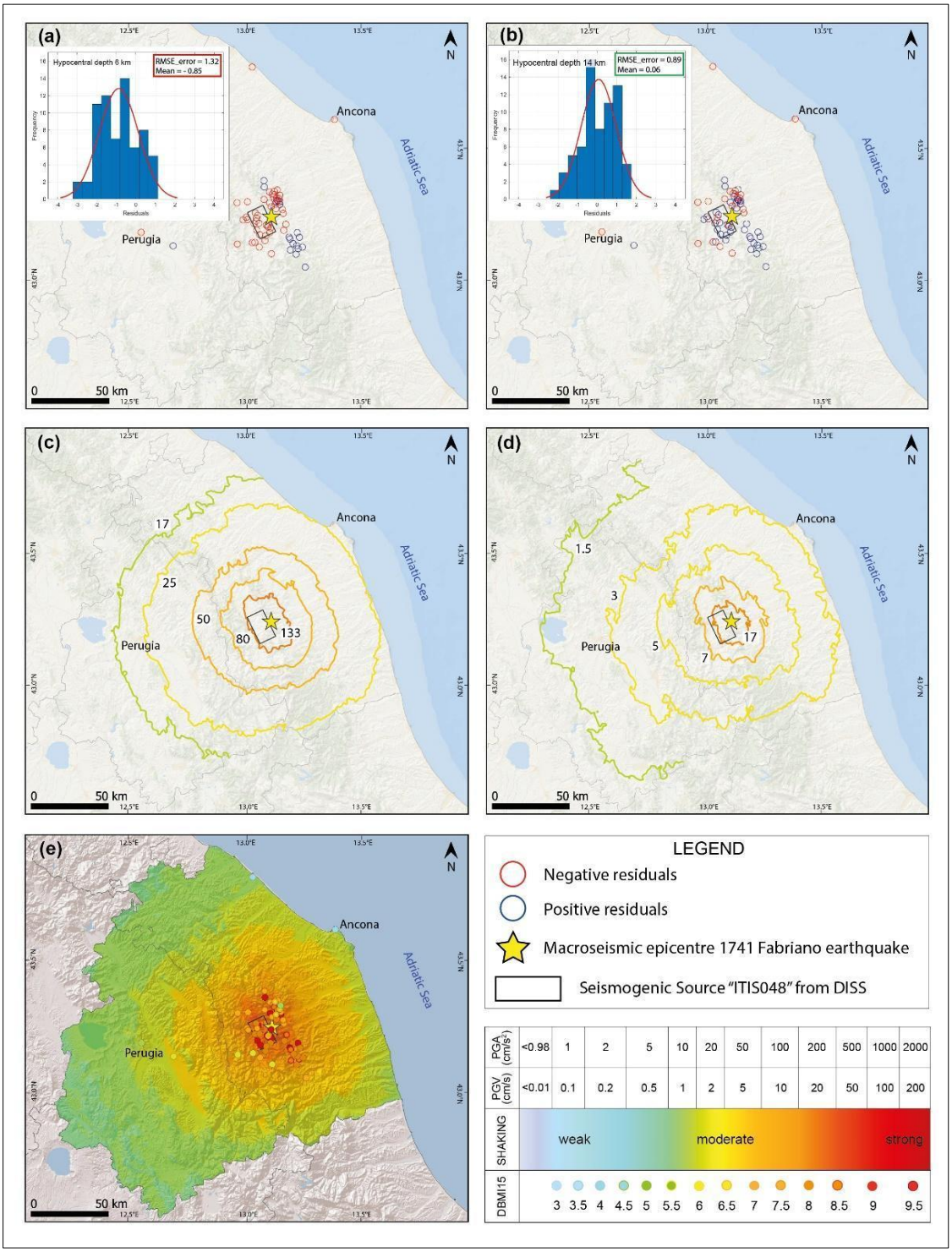

Figure 6.9. Spatial distribution of the macroseismic intensity residuals for the NE-SW strike-slip fault with hypocentral depth at 6 km (a) and at 14 km (b). The bottom right inserts show the histogram of the

residuals, the RMSE and the mean (between-event error) of residuals. The final shaking scenarios relative to the best-fitting seismogenic source in (b) are presented in terms of (c) Peak Ground Acceleration (PGA in cm/s2), and (d) Peak Ground Velocity (PGV in cm/s) maps, and (e) Macroseismic intensity expressed in the Mercalli-Cancani-Sieberg (MCS) scale by following the workflow presented in Fig. 6.6.

6.5. Conclusions

The aim of this study is to calculate shaking scenarios of earthquakes that occurred during the pre-instrumental era (i.e., 1741 Fabriano and 1799 Camerino) integrating the macroseismic intensity observations, the available ground motion models and the empirical conversion between macroseismic intensity and ground motion parameters and vice versa. The workflow proposed for the calculation of historical earthquake scenarios consists of two main parts: (i) identification of the potential seismogenic sources using the residual analysis; (ii) calculation of the shaking scenarios in terms of peak values and macroseismic intensity using both predictions and observations.

The macroseismic data are obtained from the Italian Macroseismic Database (DBMI15; Locati et al. 2022), while the seismogenic sources are proposed in the Italian Database of Individual Seismogenic Sources (DISS; Working Group, 2021, Basili et al. 2008). We use the most recent GMM for Italy (Lanzano et al. 2019) to simulate the ground motion and the Ground Motion Intensity Conversion Equation (GMICE) by Gomez Capera et al. (2020) to convert the ground motion parameters into macroseismic intensities and vice versa. In our application we have created the Umbria-Marche Vs,30 map to account for site amplifications.

The results of this study are reliable shaking scenarios for the 1741 Fabriano and 1799 Camerino earthquakes, coherent with macroseismic observations and accounting for the 3D geometry of seismic sources and site effects.

The shaking scenario for the 1741 Fabriano earthquake is associated with a NE-SW oriented strike-slip fault and a focal depth of 20 km. This result confirms the conclusions by Materazzi et al. (2022) and is also in agreement with the literature since this earthquake has been associated with a rupture generated by a deep source, because of the large damage observed along the Italian Peninsula (Pergalani et al. 1986; Stucchi et al. 1991; Boschi et al. 1995, 1997).

The best scenario of the 1799 Camerino earthquake is associated with a normal fault with an enucleation point at a depth of 14 km, in agreement with the narrower

distribution of the macroseismic intensity. This source supports the hypothesis of Monachesi (2014) who suggested that it was generated at a lower depth with respect to the 1741 Fabriano earthquake, based on macroseismic evidence.

Based on the results described in the present study, we conclude that this method allows individuating the 3D geometry of seismogenic sources of historical earthquakes and the calibration of realistic shaking scenarios, based on the integration of predictions and observations. The workflow described in the present study can be highly adaptable to different localities and geological conditions.

Moreover, this method can be applied to evaluate the history of ground motion shaking at any site, even if macroseismic observations are not available. This contribution could be relevant for defining the seismic input in the context of seismic hazard assessment and risk mitigation and emergency planning activities.

References

Abrahamson, N. A., and Youngs, R. R. (1992). A stable algorithm for regression analyses using the random effects model. Bulletin of the Seismological Society of America, 82(1), 505-510. https://doi.org/10.1785/BSSA0820010505

Abrahamson, N., Atkinson, G., Boore, D., Bozorgnia, Y., Campbell, K., Chiou, B., ... and Youngs, R. (2008). Comparisons of the NGA ground-motion relations. Earthquake Spectra, 24(1), 45-66. https://doi.org/10.1193/1.2924363

Abrahamson, N. A., Silva, W. J., and Kamai, R. (2014). Summary of the ASK14 ground motion relation for active crustal regions. Earthquake Spectra, 30(3), 1025-1055. https://doi.org/10.1193/070913EQS198M

Allen, T. I., and Wald, D. J. (2009). On the use of high-resolution topographic data as a proxy for seismic site conditions (VS 30). Bulletin of the Seismological Society of America, 99(2A), 935-943. https://doi.org/10.1785/0120080255

Akkar, S., and Bommer, J. J. (2010). Empirical equations for the prediction of PGA, PGV, and spectral accelerations in Europe, the Mediterranean region, and the Middle East. Seismological Research Letters, 81(2), 195-206. https://doi.org/10.1785/gssrl.81.2.195

Amato, A., Azzara, R., Chiarabba, C., Cimini, G. B., Cocco, M., Di Bona, M., ... and Ripepe, M. (1998). The 1997 Umbria-Marche, Italy, earthquake sequence: A first look at the main shocks and aftershocks. Geophysical Research Letters, 25(15), 2861-2864. https://doi.org/10.1029/98GL51842

Ambraseys, N. (1985). Intensity-attenuation and magnitude-intensity relationships for northwest European earthquakes. Earthquake engineering and structural dynamics, 13(6), 733-778. https://doi.org/10.1002/eqe.4290130604

Atkinson, G. M., and Boore, D. M. (1995). Ground-motion relations for eastern North America. Bulletin of the Seismological Society of America, 85(1), 17-30. https://doi.org/10.1785/BSSA0850010017

Atkinson, G. M., and Kaka, S. I. (2007). Relationships between felt intensity and instrumental ground motion in the central United States and California. Bulletin of the Seismological Society of America, 97(2), 497-510. https://doi.org/10.1785/0120060154

Bakun, W. U., and Wentworth, C. M. (1997). Estimating earthquake location and magnitude from seismic intensity data. Bulletin of the Seismological Society of America, 87(6), 1502-1521. https://doi.org/10.1785/BSSA0870061502

Barchi, M. R., A. De Feyter, M. B. Magnani, G. Minelli, G. Pialli and M. Sotera (1998), Structural style of the Umbria-Marche fold and thrust belt. Mem. Soc. Geol. It., 52, 557-578.

Basili, R., Valensise, G., Vannoli, P., Burrato, P., Fracassi, U., Mariano, S., ... and Boschi, E. (2008). The Database of Individual Seismogenic Sources (DISS), version 3: summarizing 20 years of research on Italy's earthquake geology. Tectonophysics, 453(1-4), 20-43. https://doi.org/10.1016/j.tecto.2007.04.014

Bindi, D., Pacor, F., Luzi, L., Puglia, R., Massa, M., Ameri, G., and Paolucci, R. (2011). Ground motion prediction equations derived from the Italian strong motion database. Bulletin of Earthquake Engineering, 9, 1899-1920.

Bindi, D., Massa, M., Luzi, L., Ameri, G., Pacor, F., Puglia, R., and Augliera, P. (2014). Pan-European ground-motion prediction equations for the average horizontal component of PGA, PGV, and 5%-damped PSA at spectral periods up to 3.0 s using the RESORCE dataset. Bulletin of Earthquake Engineering, 12, 391-430.

Bommer, J. J., and Alarcon, J. E. (2006). The prediction and use of peak ground velocity. Journal of Earthquake Engineering, 10(01), 1-31.

Boncio, P., Lavecchia, G., Milana, G., and Rozzi, B. (2004). Seismogenesis in Central Apennines, Italy: an integrated analysis of minor earthquake sequences and structural data in the Amatrice-Campotosto area. Annals of Geophysics.

Boncio, P., Lavecchia, G., and Pace, B. (2004). Defining a model of 3D seismogenic sources for Seismic Hazard Assessment applications: the case of central Apennines (Italy). Journal of Seismology, 8(3), 407-425.

Boore, D. M. (1983). Stochastic simulation of high-frequency ground motions based on seismological models of the radiated spectra. Bulletin of the Seismological Society of America, 73(6A), 1865-1894. https://doi.org/10.1785/BSSA07306A1865

Boore, D. M., Stewart, J. P., Seyhan, E., and Atkinson, G. M. (2014). NGA-West2 equations for predicting PGA, PGV, and 5% damped PSA for shallow crustal earthquakes. Earthquake Spectra, 30(3), 1057-1085. https://doi.org/10.1193/070113EQS184M

Boschi E, Ferrari G, Gasperini P, Guidoboni E, Smeriglio G, Valensise G (eds) (1995) Catalogo dei forti terremoti in Italia dal 461 a.C. al 1980. ING-SGA, Bologna, pp 970.

Boschi E, Guidoboni E, Ferrari G, Valensise G, Gasperini P (Eds.) (1997) Catalogo dei forti terremoti in Italia dal 461 a.C. al 1990, vol 2. ING-SGA, Bologna, pp 644.

Bozorgnia, Y., N. A. Abrahamson, L. Al-Atik, T. D. Ancheta, G. M. Atkinson, J. W. Baker, A. Baltay, D. M. Boore, K. W. Campbell, B. S.-J. Chiou, et al. (2014). NGA-West2 research project, Earthq. Spectra 30, no. 3, 973–987. https://doi.org/10.1193/072113EQS209M

Caprio, M., Tarigan, B., Worden, C. B., Wiemer, S., and Wald, D. J. (2015). Ground motion to intensity conversion equations (GMICEs): A global relationship and evaluation of regional dependency. Bulletin of the Seismological Society of America, 105(3), 1476-1490. https://doi.org/10.1785/0120140286

Carminati, E., Doglioni, C., and Barba, S. (2004). Reverse migration of seismicity on thrusts and normal faults. Earth-Science Reviews, 65(3-4), 195-222. https://doi.org/10.1016/S0012-8252(03)00083-7

Castelli, V., and Monachesi, G. (2001). Seismic history and historical earthquake scenario for the town of Fabriano (Central Italy). Italian Geotechnical Journal, 35(2), 36-46.

Cauzzi, C., and Faccioli, E. (2008). Broadband (0.05 to 20 s) prediction of displacement response spectra based on worldwide digital records. Journal of Seismology, 12, 453-475.

Cello, G., Mazzoli, S., Tondi, E., and Turco, E. (1997). Active tectonics in the central Apennines and possible implications for seismic hazard analysis in peninsular Italy. Tectonophysics, 272(1), 43-68. https://doi.org/10.1016/S0040-1951(96)00275-2

Centamore, E., and Rossi, D. (2009). Neogene-Quaternary tectonics and sedimentation in the Central Apennines. Italian Journal of Geosciences, 128(1), 73-88.

Chiarabba, C., Amato, A., Anselmi, M., Baccheschi, P., Bianchi, I., Cattaneo, M., ... and Valoroso, L. (2009). The 2009 L'Aquila (central Italy) MW 6.3 earthquake: Main shock and aftershocks. Geophysical Research Letters, 36(18). https://doi.org/10.1029/2009GL039627

Chiaraluce, L., Di Stefano, R., Tinti, E., Scognamiglio, L., Michele, M., Casarotti, E., ... and Marzorati, S. (2017). The 2016 central Italy seismic sequence: A first look at the mainshocks, aftershocks, and source models. Seismological Research Letters, 88(3), 757-771. https://doi.org/10.1785/0220160221

Chiou, B. S. J., and Youngs, R. R. (2014). Update of the Chiou and Youngs NGA model for the average horizontal component of peak ground motion and response spectra. Earthquake Spectra, 30(3), 1117-1153. https://doi.org/10.1193/072813EQS219M

Cinque, A., Patacca, E., Scandone, P., and Tozzi, M. (1993). Quaternary kinematic evolution of the Southern Appennines. Relationships between surface geological features and deep lithospheric structures.

Cipollari, P., and Cosentino, D. (1996). Miocene tectono-sedimentary events and geodynamic evolution of the central Apennines (Italy). Notes et Mem. Serv. Geol. Maroc, 387, 163-176.

Collettini, C., and Barchi, M. R. (2002). A low-angle normal fault in the Umbria region (Central Italy): a mechanical model for the related microseismicity. Tectonophysics, 359(1-2), 97-115. https://doi.org/10.1016/S0040-1951(02)00441-9

Collettini, C., Barchi, M. R., Chiaraluce, L., Mirabella, F., and Pucci, S. (2003). The Gubbio fault: can different methods give pictures of the same object. Journal of Geodynamics, 36(1-2), 51-66. https://doi.org/10.1016/S0264-3707(03)00038-3

Cosentino, D., Cipollari, P., Marsili, P., and Scrocca, D. (2010). Geology of the central Apennines: a regional review. Journal of the virtual explorer, 36(11), 1-37.

DISS Working Group (2021). Database of Individual Seismogenic Sources (DISS), Version 3.3.0: A compilation of potential sources for earthquakes larger than M 5.5 in Italy and surrounding areas. Istituto Nazionale di Geofisica e Vulcanologia (INGV). https://doi.org/10.13127/diss3.3.0

Evernden, J. F. (1975). Seismic intensities, "size" of earthquakes and related parameters. Bulletin of the Seismological Society of America, 65(5), 1287-1313. https://doi.org/10.1785/BSSA0650051287

Faccioli, E., and Cauzzi, C. (2006, September). Macroseismic intensities for seismic scenarios estimated from instrumentally based correlations. In Proc. First European Conference on Earthquake Engineering and Seismology, paper (No. 569).

Finetti, I. R., Boccaletti, M., Bonini, M., Del Ben, A., Geletti, R., Pipan, M., and Sani, F. (2001). Crustal section based on CROP seismic data across the North Tyrrhenian–Northern Apennines–Adriatic Sea. Tectonophysics, 343(3-4), 135-163. https://doi.org/10.1016/S0040-1951(01)00141-X

Forte, G., Chioccarelli, E., De Falco, M., Cito, P., Santo, A., and Iervolino, I. (2019). Seismic soil classification of Italy based on surface geology and shear-wave velocity measurements. Soil Dynamics and Earthquake Engineering, 122, 79-93. https://doi.org/10.1016/j.soildyn.2019.04.002

Galadini, F. (1999). Pleistocene changes in the central Apennine fault kinematics: a key to decipher active tectonics in central Italy. Tectonics, 18(5), 877-894. https://doi.org/10.1029/1999TC900020

Gasperini, P., Bernardini, F., Valensise, G., and Boschi, E. (1999). Defining seismogenic sources from historical earthquake felt reports. Bulletin of the Seismological Society of America, 89(1), 94-110. https://doi.org/10.1785/BSSA0890010094

Gasperini, P., and Ferrari, G. (2000). Deriving numerical estimates from descriptive information: the computation of earthquake parameters.

Gasperini, P., Vannucci, G., Tripone, D., and Boschi, E. (2010). The location and sizing of historical earthquakes using the attenuation of macroseismic intensity with distance location and sizing of historical earthquakes using attenuation of macroseismic intensity. Bulletin of the Seismological Society of America, 100(5A), 2035-2066. https://doi.org/10.1785/0120090330

Gómez, C., and Augusto, A. (2006). Seismic hazard map for the Italian territory using macroseismic data. Earth Sciences Research Journal, 10(2), 67-90.

Gómez-Capera, A. A., Santulin, M., Massa, M., Locati, M., and Puglia, R. (2019). Conversione tra parametri del moto del suolo e intensità macrosismica.

Gomez-Capera, A. A., D'Amico, M., Lanzano, G., Locati, M., and Santulin, M. (2020). Relationships between ground motion parameters and macroseismic intensity for Italy. Bulletin of Earthquake Engineering, 18, 5143-5164.

Guidoboni, E., Ferrari, G., Tarabusi, G., Sgattoni, G., Comastri, A., Mariotti, D., ... and Valensise, G. (2019). CFTI5Med, the new release of the catalogue of strong earthquakes in Italy and in the Mediterranean area. Scientific data, 6(1), 1-15.

Gutenberg, B., and Richter, C. F. (1956). Earthquake magnitude, intensity, energy, and acceleration: (Second paper). Bulletin of the seismological society of America, 46(2), 105-145. https://doi.org/10.1785/BSSA0460020105

Hassanzadeh, R., Nedović-Budić, Z., Razavi, A. A., Norouzzadeh, M., and Hodhodkian, H. (2013). Interactive approach for GIS-based earthquake scenario development and resource estimation (Karmania hazard model). Computers and geosciences, 51, 324-338. https://doi.org/10.1016/j.cageo.2012.08.016

Horn, B. K. (1981). Hill shading and the reflectance map. Proceedings of the IEEE, 69(1), 14-47.

ISIDe Working Group. (2007). Italian Seismological Instrumental and Parametric Database (ISIDe). Istituto Nazionale di Geofisica e Vulcanologia (INGV). https://doi.org/10.13127/ISIDE

ITHACA Working Group (2019). ITHACA (ITaly HAzard from CApable faulting), A database of active capable faults of the Italian territory. Version December 2019. ISPRA Geological Survey of Italy. Web Portal http://sgi2.isprambiente.it/ithacaweb/Mappatura.aspx

Iwahashi, J., Kamiya, I., and Matsuoka, M. (2010). Regression analysis of Vs30 using topographic attributes from a 50-m DEM. Geomorphology, 117(1-2), 202-205. https://doi.org/10.1016/j.geomorph.2009.11.004

Joyner, W. B., and Boore, D. M. (1981). Peak horizontal acceleration and velocity from strong-motion records including records from the 1979 Imperial Valley, California, earthquake. Bulletin of the seismological Society of America, 71(6), 2011-2038. https://doi.org/10.1785/BSSA0710062011

Joyner, W. B., Warrick, R. E., and Fumal, T. E. (1981). The effect of Quaternary alluvium on strong ground motion in the Coyote Lake, California, earthquake of 1979. Bulletin of the Seismological Society of America, 71(4), 1333-1349. https://doi.org/10.1785/BSSA0710041333

Karimzadeh, S., Miyajima, M., Hassanzadeh, R., Amiraslanzadeh, R., and Kamel, B. (2014). A GIS-based seismic hazard, building vulnerability and human loss assessment for the earthquake scenario in Tabriz. Soil Dynamics and Earthquake Engineering, 66, 263-280. https://doi.org/10.1016/j.soildyn.2014.06.026

Kaka, S. I., and Atkinson, G. M. (2004). Relationships between instrumental ground-motion parameters and modified Mercalli intensity in eastern North America. Bulletin

of the Seismological Society of America, 94(5), 1728-1736. https://doi.org/10.1785/012003228

Karimzadeh, S., Feizizadeh, B., and Matsuoka, M. (2017). From a GIS-based hybrid site condition map to an earthquake damage assessment in Iran: Methods and trends. International journal of disaster risk reduction, 22, 23-36. https://doi.org/10.1016/j.ijdrr.2017.02.016

Lanzano, G., Luzi, L., Pacor, F., Felicetta, C., Puglia, R., Sgobba, S., and D'Amico, M. (2019). A Revised Ground-Motion Prediction Model for Shallow Crustal Earthquakes in Italy. Bulletin of the Seismological Society of America, 109(2), 525-540. https://doi.org/10.1785/0120180210

Lavecchia, G., Brozzetti, F., Barchi, M., Menichetti, M., and Keller, J. V. (1994). Seismotectonic zoning in east-central Italy deduced from an analysis of the Neogene to present deformations and related stress fields. GSA Bulletin, 106(9), 1107-1120. https://doi.org/10.1130/0016-7606(1994)106<1107:SZIECI>2.3.CO;2

Lavecchia, G., Boncio, P., Creati, N., and Brozzetti, F. (2004). Stile strutturale, stato termo-meccanico e significato sismogenetico del thrust Adriatico; dati e spunti da una revisione del profilo CROP 03 integrata con l'analisi di dati sismologici. Bollettino della Società geologica italiana, 123(2), 111-125.

Locati M., Camassi R., Rovida A., Ercolani E., Bernardini F., Castelli V., Caracciolo C.H., Tertulliani A., Rossi A., Azzaro R., D'Amico S., Conte S., Rocchetti E., Antonucci A. (2022). Database Macrosismico Italiano (DBMI15), versione 4.0. Istituto Nazionale di Geofisica e Vulcanologia (INGV). https://doi.org/10.13127/dbmi/dbmi15.4

Lozos, J. C. (2016). A case for historic joint rupture of the San Andreas and San Jacinto faults. Science advances, 2(3), e1500621. DOI: 10.1126/sciadv.1500621

Marcellini A, Tiberi P (eds) (2000) La microzonazione sismica di Fabriano. C.N.R., G.N.D.T., Regione Marche., Biemmegraf s.r.l., Macerata, pp 291.

Materazzi, M., Bufalini, M., Dramis, F., Pambianchi, G., Gentili, B., and Di Leo, M. (2022). Active tectonics and paleoseismicity of a transverse lineament in the Fabriano valley, Umbria-Marche Apennine (central Italy). International Journal of Earth Sciences, 111(5), 1539-1549.

Mazzoli, S., Deiana, G., Galdenzi, S., and Cello, G. (2002). Miocene fault-controlled sedimentation and thrust propagation in the previously faulted external zones of the Umbria-Marche Apennines, Italy. EGU Stephan Mueller Special Publication Series, 1, 195-209.

Mazzoli, S., Santini, S., Macchiavelli, C., and Ascione, A. (2015). Active tectonics of the outer northern Apennines: Adriatic vs. Po Plain seismicity and stress fields. Journal of Geodynamics, 84, 62-76. https://doi.org/10.1016/j.jog.2014.10.002

Michelini, A., Faenza, L., Lauciani, V., and Malagnini, L. (2008). ShakeMap Implementation in Italy. SRL 79 (5): 688–697.

Monachesi G (ed) (1987) Revisione della sismicità di riferimento per i comuni di Cerreto d'Esi (AN), Esanatoglia (MC), Serra San Quirico (AN). In: Osservatorio Geofisico Sperimentale, Macerata, Internal Report, pp 240.

Monachesi, G., Stucchi, M., Coppari, H., Meloni, F., Molin, D., Zerga, A., ... and Rinaldi, G. R. (1997). DOM4. 1, un database di osservazioni macrosismiche.

Monachesi, G., Castelli, V., Coppari, H., Stucchi, M., Peruzza, L., Franceschina, G. L., ... and Priolo, E. (2000). Sismicita'di riferimento.

Monachesi, G., Castelli, V., and Camassi, R. (2016). Aggiornamento delle conoscenze sul terremoto del 28 luglio 1799 nel sub-Appennino maceratese. Quaderni di Geofisica (INGV).

Monachesi G., Ladina C., Calamita C., Pantaleo D., Cattaneo M., Marzorati S., Frapiccini M., D'Alema E., Carannante S. (2021). Beach Balls in central-eastern Italy [Data set]. Istituto Nazionale di Geofisica e Vulcanologia (INGV). https://doi.org/10.13127/bb2021

Mori, F., Mendicelli, A., Moscatelli, M., Romagnoli, G., Peronace, E., and Naso, G. (2020). A new Vs30 map for Italy based on the seismic microzonation dataset. Engineering Geology, 275, 105745. https://doi.org/10.1016/j.enggeo.2020.105745

Oliveti, I., Faenza, L., and Michelini, A. (2022). New reversible relationships between ground motion parameters and macroseismic intensity for Italy and their application in ShakeMap. Geophysical Journal International, 231(2), 1117-1137. https://doi.org/10.1093/gji/ggac245

Pantosti, D., and Boncio, P. (2012). Understanding the April 6th, 2009 L'Aquila earthquake-the geological contribution: an introductory note to the special issue. Italian Journal of Geosciences, 131(3), 303-308. https://doi.org/10.3301/IJG.2012.25

Patacca, E., Sartori, R., and Scandone, P. (1990). Tyrrhenian basin and Apenninic arcs: kinematic relations since late Tortonian times. Memorie della Società Geologica Italiana, 45, 425-451.

Pergalani F, Stucchi M, Polonara L (1986) Attività nel settore della difesa dai terremoti. In: Consiglio Nazionale delle Ricerche, Gruppo Nazionale per la Difesa dai Terremoti, Regione Marche, pp 36.

Pizzi, A., Calamita, F., Coltorti, M., and Pieruccini, P., (2002). Quaternary normal faults, intramontane basins and seismicity in the Umbria-Marche-Abruzzi Apennine Ridge (Italy): contribution of neotectonic analysis to seismic hazard assessment. Boll. Soc. Geol. It, 1, 923-929.

Pizzi, A., Di Domenica, A., Gallovič, F., Luzi, L., and Puglia, R. (2017). Fault segmentation as constraint to the occurrence of the main shocks of the 2016 Central

Italy seismic sequence. Tectonics, 36(11), 2370-2387. https://doi.org/10.1002/2017TC004652

Rovida A., Locati M., Camassi R., Lolli, B., Gasperini P., Antonucci A., 2022. Catalogo Parametrico dei Terremoti Italiani (CPTI15), versione 4.0. Istituto Nazionale di Geofisica e Vulcanologia (INGV). https://doi.org/10.13127/cpti/cpti15.4

Sbarra, P., Burrato, P., Tosi, P., Vannoli, P., De Rubeis, V., and Valensise, G. (2019). Inferring the depth of pre-instrumental earthquakes from macroseismic intensity data: a case-history from Northern Italy. Scientific reports, 9(1), 1-13.

Scandone, P., Patacca, E., Meletti, C., Bellatalla, M., Perilli, N., and Santini, U. (1990). Struttura geologica, evoluzione cinematica e schema sismotettonico della penisola italiana. Atti del Convegno GNDT, 1, 119-135.

Selvaggi, G., and Amato, A. (1992). Subcrustal earthquakes in the northern Apennines (Italy): evidence for a still active subduction. Geophysical Research Letters, 19(21), 2127-2130. https://doi.org/10.1029/92GL02503

Spudich, P. A., and S. H. Hartzell (1985). Predicting earthquake ground-motion time-histories, in Evaluating Earthquake Hazards in the Los Angeles Region, Professional Paper 1360, J. I. Ziony (Editor), 249–260.

Stucchi, M., Monachesi, G., and Mandrelli, F. M. (1991). Investigation of 18th century seismicity in central Italy in the light of the 1741 Fabriano earthquake. Tectonophysics, 193(1-3), 65-82. https://doi.org/10.1016/0040-1951(91)90189-Y

Stucchi, M., Meletti, C., Montaldo, V., Crowley, H., Calvi, G. M., and Boschi, E. (2011). Seismic hazard assessment (2003–2009) for the Italian building code. Bulletin of the Seismological Society of America, 101(4), 1885-1911. https://doi.org/10.1785/0120100130

Tinsley, J. C., Fumal, T. E., and Ziony, J. I. (1985). Mapping Quaternary sedimentary deposits for areal variations in shaking response. Evaluating Earthquake Hazards in the Los Angeles Region—An Earth Science Perspective, 1360, 101-126.

Tondi, E. (2000). Geological analysis and seismic hazard in the central Apennines (Italy). Journal of Geodynamics, 29(3-5), 517-533. https://doi.org/10.1016/S0264-3707(99)00048-4

Tondi, E., Chiaraluce, L., and Roberts, G. (2009). Ten years after the Umbria–Marche earthquake. Tectonophysics.

Wald, D. J., Quitoriano, V., Heaton, T. H., and Kanamori, H. (1999). Relationships between peak ground acceleration, peak ground velocity, and modified Mercalli intensity in California. Earthquake spectra, 15(3), 557-564. https://doi.org/10.1193/1.1586058

Wald, D. J., Worden, B. C., Quitoriano, V., and Pankow, K. L. (2005). ShakeMap manual: technical manual, user's guide, and software guide (No. 12-A1). https://doi.org/10.3133/tm12A1

Wald, D. J., and Allen, T. I. (2007). Topographic slope as a proxy for seismic site conditions and amplification. Bulletin of the Seismological Society of America, 97(5), 1379-1395. https://doi.org/10.1785/0120060267

Wells, D. L., and Coppersmith, K. J. (1994). New empirical relationships among magnitude, rupture length, rupture width, rupture area, and surface displacement. Bulletin of the seismological Society of America, 84(4), 974-1002. https://doi.org/10.1785/BSSA0840040974

Westaway, R. (1992). Seismic moment summation for historical earthquakes in Italy: tectonic implications. Journal of Geophysical Research: Solid Earth, 97(B11), 15437-15464. https://doi.org/10.1029/92JB00946

Wills, C. J., Gutierrez, C. I., Perez, F. G., and Branum, D. M. (2015). A Next Generation VS30 Map for California Based on Geology and Topography. A Next Generation VS30 Map for California Based on Geology and Topography. Bulletin of the Seismological Society of America, 105(6), 3083-3091. https://doi.org/10.1785/0120150105

Worden, C. B., Gerstenberger, M. C., Rhoades, D. A., and Wald, D. J. (2012). Probabilistic relationships between ground-motion parameters and modified Mercalli intensity in California. Bulletin of the Seismological Society of America, 102(1), 204-221. https://doi.org/10.1785/0120110156

Wu, Y. M., Teng, T. L., Shin, T. C., and Hsiao, N. C. (2003). Relationship between peak ground acceleration, peak ground velocity, and intensity in Taiwan. Bulletin of the Seismological Society of America, 93(1), 386-396. https://doi.org/10.1785/0120020097

CHAPTER 7

ELUSIVE SEISMOGENIC SOURCES OF HISTORICAL EARTHQUAKES: INSIGHTS FROM THE MW 6.8, 1706 MAIELLA EARTHQUAKE (CENTRAL ITALY)

This Chapter presents the application of the same methodology as Gironelli et al. (2023), described in Chapter 6, to find the seismogenic sources that best-fits the macroseismic intensity data of a historical earthquake occurred in the Abruzzi Region (central Italy): the Maiella event 1706 (Imax 10-11 MCS; Mw 6.84). Many seismogenic sources have been hypothesized in the literature for this event by several authors such as Galli and Pallone, (2019) and Bordoni et al. (2023), among others. In this work, the shaking scenarios have been calculated including the Vs,30 map, developed for Italy by Mori et al. (2020), to include the site effects.

The present article has been submitted in Bulletin of Earthquake Engineering.

7. Elusive seismogenic sources of historical earthquakes: Insights from the Mw 6.8, 1706 Maiella earthquake (Central Italy)

T. Volatili [1], V. Gironelli [1,5], L. Luzi [2], P. Galli [3], M. M. C. Carafa [4], E. Tondi [1,5]

[1] *School of Science and Technology – Geology Division, University of Camerino, Camerino, Italy*

[2] *National Institute of Geophysics and Volcanology, Milan, Italy*

[3]*Civil Protection Department, Presidency of the Council of Ministers, Rome, Italy*

[4]*National Institute of Geophysics and Volcanology, Seismology and Tectonophysics Division, L'Aquila, Italy*

[5]*National Institute of Geophysics and Volcanology, Seismology and Tectonophysics Division, Camerino, Italy*

Abstract

The central Apennines region is renowned for its active NW-SE striking and SW-dipping normal-fault systems responsible for significant seismic events. However, uncertainties persist in attributing seismogenic sources to some destructive earthquakes of the past. A notable example is the 1706 Maiella earthquake (Abruzzi region), whose epicenter and magnitude (Mw 6.8) derive from its macroseismic field, although its causative fault remains enigmatic. This study comprehensively assesses competing source hypotheses present in the literature and uses geological and geophysical data to constrain their fault geometry. Employing a 3D seismogenic source model approach, we rigorously analyze the earthquake-fault association, assessing the misfit between the simulated intensities and the observed macroseismic MCS values estimated from the historical accounts. Our findings highlight the complexities in determining the exact source of the 1706 earthquake. Finally, the best-fit source model was adopted to produce ground motion simulations in terms of PGA, PGV, and macroseismic intensity, including site effects, possibly unveiling the shaking scenario that occurred in the past and perhaps in the future. These results, shading light on one of the most relevant unknowns of the Apennine seismicity, offer valuable insights to better constrain the seismic hazard of this region, with implications for seismic risk mitigation strategies.

Keywords: *Seismogenic Source Modelling; Earthquake Scenarios; 1706 Maiella Earthquake; Central Apennines.*

7.1. Introduction

The central Apennines are characterized by two parallel sets of seismogenic NW-SE striking, SW-dipping normal-fault systems (e.g., Galadini and Galli, 1999, 2000; Boncio et al., 2004; Galli et al., 2008). These fault systems accommodate the dominant extensional processes affects the Apennine chain since the Middle Pleistocene and are thus associated with significant seismic events. This region has witnessed large historical earthquakes in 1461 (Mw = 6.5), 1703 (Mw = 6.7), 1706 (Mw = 6.7), and 1915 (Mw = 7.0), as reported in the Parametric Catalogue of Italian Earthquakes (Rovida et al., 2022).

The Abruzzi region is situated in the central Apennines and ranks among the highest Italian seismic hazard regions, as highlighted by Akinci et al. (2009), Petricca et al. (2015), and Meletti et al. (2021) among others. In this region, a well-known system of SW-dipping normal faults has been active historically and recently, as evidenced by moderate-to-large earthquakes (Mw $\geq$ 5.5). The most recent destructive event, the L'Aquila earthquake, occurred on April 6, 2009 (Mw = 6.3).

Following the events of 2009, there has been a growing interest in assessing the seismogenic potential of active faults in this region. Numerous studies have been conducted to identify active and potentially seismogenic structures based on the area's seismicity (Galadini and Galli, 2000; De Nardis et al., 2011; Romano et al., 2013; Puliti et al., 2021 among others). Uncertainties surround areas characterized by destructive historical earthquakes whose causative faults have yet to be determined. One such case is the Maiella Massif, located in the heart of the Abruzzi region. This area and its surroundings, characterized by destructive historical seismic events and a scarce instrumental seismicity (Fig. 7.1), could be one with the most alarming seismic gaps of the Italian territory. The two largest earthquakes occurred on November 3, 1706 (Mw6.8), and September 26, 1933 (Mw5.9), mainly affecting the Maiella Massif surroundings (CPTI15; Rovida et al., 2022; Fig. 7.1a). Although the earthquake of 1706 was approximately 30 times more energetic than that of 1933, the distribution of Macroseismic effects suggests a common seismogenic source (Fig. 7.1b). The 1706 earthquake destroyed 37 villages, resulting in an estimated casualty count of more than 2200 (Galli and Pallone, 2019). The 1933 earthquake was felt across an extensive area of approximately 17,700 km^2, and in Sulmona, the largest locality of the region, an

MCS intensity of 9-10 degree was estimated, as all buildings in the city experienced damage or complete collapse (Guidoboni et al., 2018). Damage concentrated in the northern and southeastern parts of the Maiella Massif, as indicated by the highest intensity data points (Is≥7). Despite being labelled as the Maiella earthquakes, the seismogenic structure responsible for these two events remains controversial. the epicentres of these earthquakes fall between the NW-SE active normal fault alignment and the N-S trending active thrust front, represented by the Abruzzo Citeriore Basal Thrust (ACBT, Fig. 7.1b). Consequently, some researchers have attributed these earthquakes to thrust faulting, while others have suggested upper-crust normal faulting. Lavecchia and De Nardis (2010) proposed that the southern portion of the ACBT could host the 1706 and 1933 earthquakes. They hypothesized an E-verging reverse fault beneath the Maiella Massif in agreement with the Composite Seismogenic Source ITCS078 of the DISS database (DISS Working Group, 2021).

Conversely, Patacca et al. (2008) disputed the existence of this basal thrust in their interpretation of the CROP 11 deep reflection seismic profile (Parotto et al., 2004); they suggested the presence of a blind E-dipping back-thrust that developed in the footwall of the Maiella anticline (MAFB, Fig. 7.1b). Following this interpretation, Galli and Pallone (2019), based on a revision of the distribution of macroseismic intensity data, propose the MAFB as the source of both the 1706 and 1933 events, excluding the possibility that they were generated by other well-known active normal faults. Indeed, the study area is dissected by primary extensional structures, with certain Quaternary activity, geographically consistent with the 1706 seismic event, like the Mt. Morrone fault (MOR, Fig. 7.1b), a normal fault with surface expression consistent with a maximum magnitude of 6.7±0.1 (Galli et al., 2015). However, paleo- and archaeo-seismological studies (i.e., Galadini and Galli, 2001; Ceccaroni et al., 2009; Galli et al., 2015) attributed the last activity of the Mt. Morrone fault to approximately 1.8 thousand years ago (II cent. CE); therefore, this fault is currently considered silent.

Many hypotheses exist as far as the causative fault of the 1706 Maiella earthquake is concerned. However, the current knowledge regarding the geometry and kinematics of these sources remains controversial. This study has the scope to analytically test these seismogenic source hypotheses based on the only parameter we can refer to for

historical earthquakes (i.e., the macroseismic intensity distribution). Our results, combined with the development of a shaking scenario, offer valuable insights to the research community and various stakeholders involved in decision-making processes related to seismic risk reduction in this area.

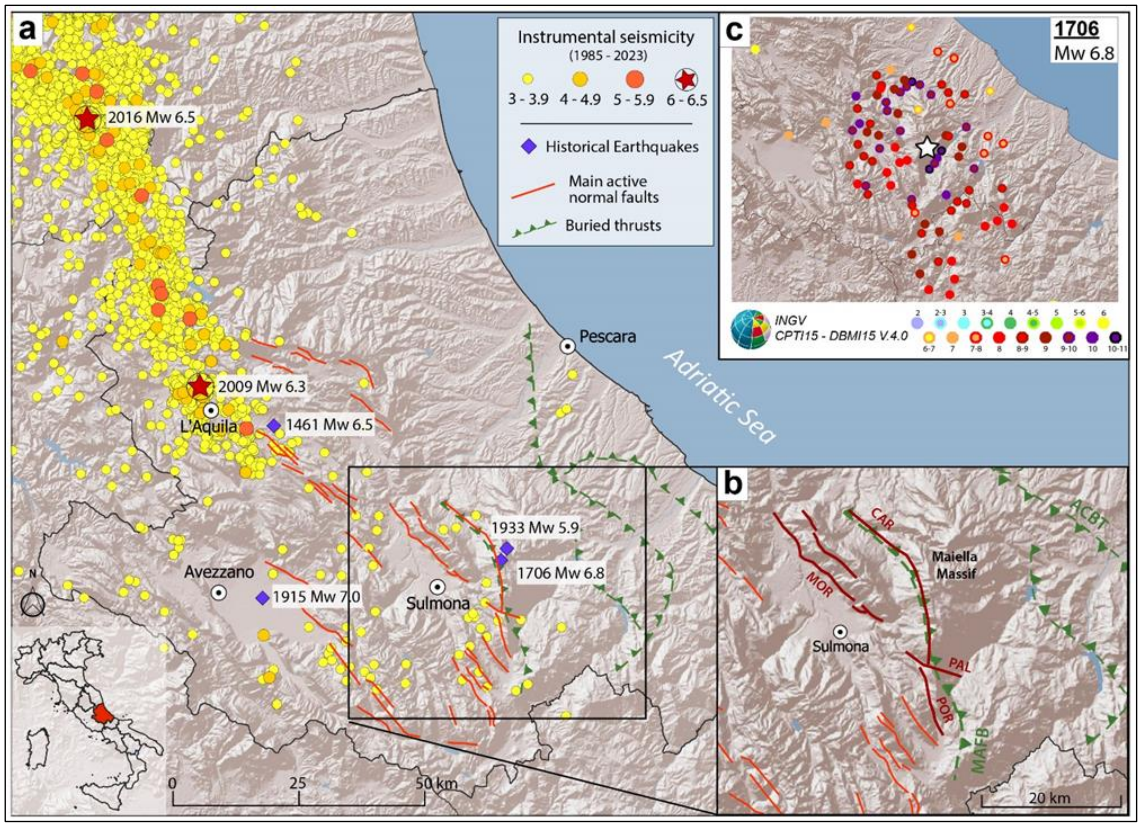

Figure 7.1. (a) Seismotectonic framework of the central Apennines with the major instrumental seismicity (Mw ≥ 3 from ISIDe Working Group, 2007) and the epicenters of the largest historical earthquakes that struck the region in the past millennium (purple diamonds, Mw ≥ 5.8 from CPTI15 - Rovida et al., 2022). Main active normal fault systems (red lines) and buried thrust (dashed green lines; modified after Galli and Pallone, 2019), and (b) related close-up of the study area with main structures details: MOR, Mt. Morrone fault; POR, Mt. Porrara fault; PAL, Palena fault; CAR, Caramanico fault; MAFB, Maiella anticline footwall back-thrust; ACBT, Abruzzo Citeriore Basal Thrust. (c) Observed macroseismic intensity field for the 1706 earthquake (DBMI15; Locati et al., 2022).

7.2. Seismogenic sources of the 1706 earthquake

This study provides a comprehensive review of the various seismogenic source hypotheses possibly related to the 1706 earthquake and applies the approach adopted by Gironelli et al., (2023) to analyse them. Before mentioning the modelled seismogenic source hypotheses, it is worth noting that Pomposo and Pizzi (2009) have hypothesized that the area east of the Morrone-Porrara fault alignment is undergoing active

compression, based on morphotectonic evidence of active anticline growth in the Orsogna area, suggesting a relationship with another strong event of the area (1881, Mw 5.4). This scenario would be consistent with the reactivation of a blind thrust beneath the Maiella Massif (Lavecchia et al., 2009; Lavecchia and De Nardis, 2010), however this scenario was not considered in the present study due to a lack of sufficient geological constrains to model the related seismogenic source.

Galli and Pallone (2019), who re-evaluated the macroseismic intensity distribution based on previously unknown historical sources, have suggested the activation of a blind back-thrust that developed during Early-Middle Pleistocene in the footwall of the Maiella anticline as the potential source for both the 1933 and 1706 earthquakes (labelled GALLI19 in Fig. 7.2). These authors also documented possible surface ruptures that occurred during the 1933 earthquake related to the Caramanico normal fault (labelled CARAMANICO in Fig. 7.2), a 26 km-long structure bounding westward the Maiella Massif. Although these surfaces evidence have been attributed to a likely passive motion of the Caramanico fault (Galli and Pallone 2019), we decided to test it for the sake of completeness. Conversely, in the Database of Individual Seismogenic Sources (DISS Working Group, 2021; Basili et al., 2008) the 1706 earthquake, being the only meaningful seismic event in that area may relate with the largest and proximal individual seismogenic source labelled ITIS027 SULMONA (see Fig. 7.2), although in the DISS database this structure is not associated to any specific seismic event. This seismogenic source is associated with the Mt. Morrone fault, a dip-slip fault with surface expression consistent with a maximum magnitude of 6.7±0.1 (Galli et al., 2015), and composed by two major sub-parallel WSW-dipping splays, extending approximately 24 km across the western slope of Mt. Morrone. Lastly, Bordoni et al. (2023) presented two seismic scenarios: one associated with the activation of the Mt. Morrone fault (labelled BORDONI23_1 in Fig. 7.2), and the second one associated with the synchronous activation of both the Mt. Morrone fault and the Mt. Porrara fault (POR, Fig. 7.1b), with a 43 km total fault length at the surface and an 860 km^2 maximum rupture area, which would generate an earthquake consistent with the 1706 seismic event (labelled BORDONI23_2 in Fig. 7.2). In this study we provide a comprehensive review of these hypotheses concerning the 1706 seismic source, along with another possible causative structure implying the dip-slip reactivation of the Mt.

Morrone fault plus the Palena fault (labelled TONDI24 in Fig. 7.2). As far as the Palena fault (PAL, Fig. 7.1b), Pizzi et al. (2010) hypothesized its Quaternary activity, with an almost pure dip-slip kinematics.

The seismogenic sources are shown in map view (Fig. 7.2a), in the form of seismogenic boxes (i.e., surface projection of the 3D structure) and in section view (Fig. 7.2b), where their actual down-dip expression, for the sake of simplicity, is directly over imposed to the interpreted seismic profile from Patacca et al. (2008). Their geometrical parameters are listed in table 7.1, including the following records: i) strike, ii) dip angle iii) dimension (i.e., length, width, area) and iv) the maximum moment magnitude derived from both the fault length at the surface (Mw1) and the total area (Mw2), applying the well-known fault scaling relationships from Wells and Coppersmith (1994). Following the approach proposed by Falcucci et al. (2018), the length refers to the mean of the rupture length at the surface and subsurface, and the fault width (down-dip length) is obtained from the mean dip angle reported in table 7.1. This assumption is valid for most modelled sources except for ITIS027 SULMONA and GALLI19. For the latter, the only source without a surface expression, the surface rupture length was first derived, calculated considering Wells and Coppersmith (1994) regression for a reverse fault and Mw 6.8. This choice was done for the sake of consistency in the modelling of the seismogenic sources. Whereas ITIS027 simply reports the same parameters present in the DISS, the main difference is that the geometry is calibrated from the solely surface rupture length, resulting in a smaller seismogenic source which corresponds to a lower maximum magnitude (Mw 6.4).

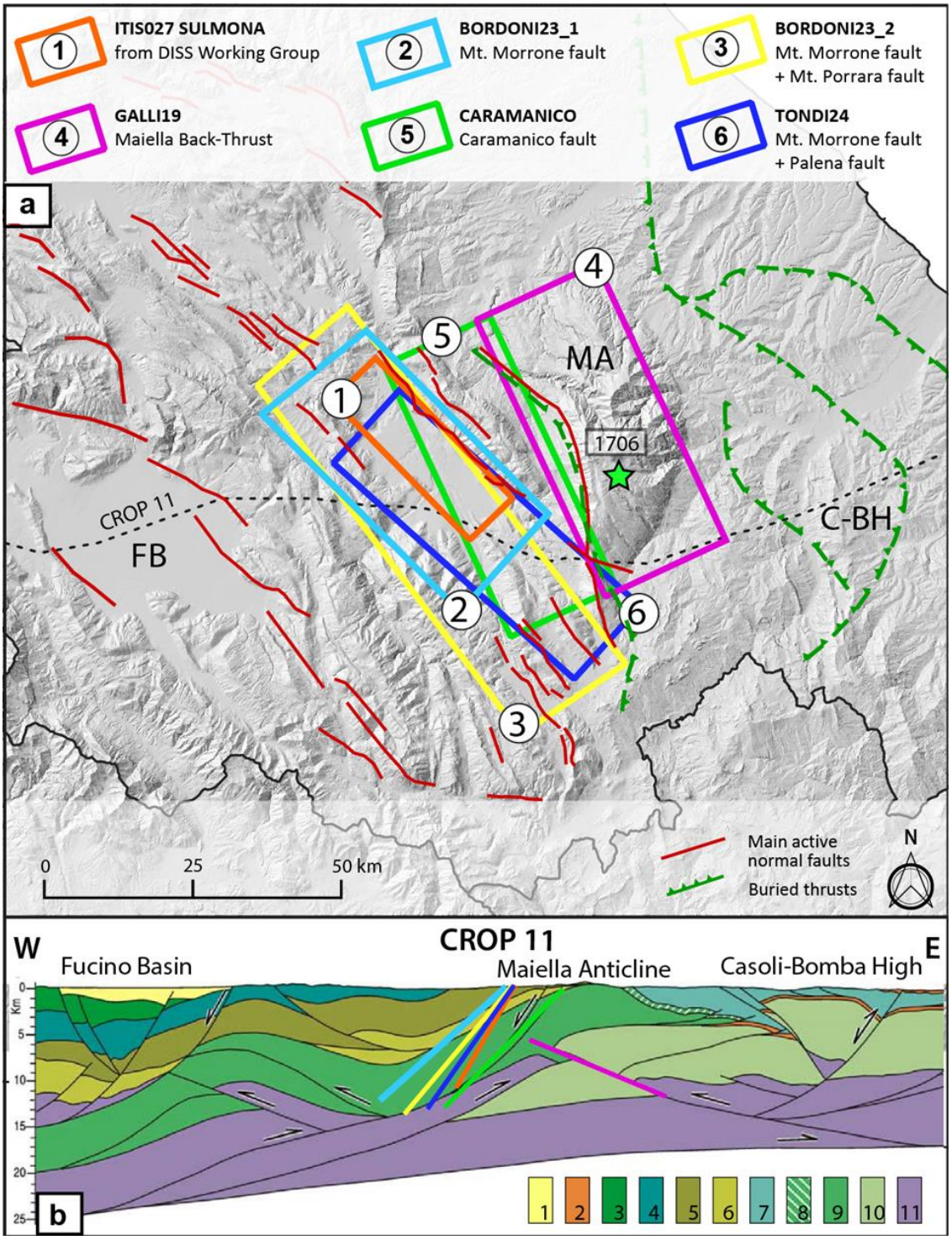

Figure 7.2. (a) Map of the main tectonic structures of the study area (Galadini and Galli, 2000; Pizzi et al., 2010; Galli et al., 2019) and the seismogenic boxes of the modelled seismogenic source hypothesis: (1) ITIS027 Sulmona from DISS database (DISS Working Group, 2021); (2) BORDONI23_1 associated with the Mt. Morrone fault, and (3) "BORDONI23_2 associated with the combination of Mt. Morrone and Mt. Porrara faults, from Bordoni et al. (2023); (4) GALLI19, Maiella back-thrust from Galli and Pallone (2019); (5) CARAMANICO, Seismogenic source related to the Caramanico normal fault from Ghisetti and Vezzani (2002) and Galli and Pallone (2019), and (6) TONDI_24 associated with the combination of Mt. Morrone fault and Palena fault. b) part of CROP-11 line interpreted by Patacca et al.

(2008): 1, Pliocene-Quaternary continental deposits of intramontane basins; 2, Pliocene marine deposits conformably overlying the Apulia carbonates; 3, Western Marsica-Meta Unit; 4, Mount Genzana unit; 5, Mount Morrone-Porrara unit; 6, Upper Cretaceous-Pliocene Mount Queglia unit; 7, Molise units; 8, Lower Pliocene flysch of Maiella unit; 9, Mesozoic-Tertiary carbonates of Maiella unit; 10, Mesozoic-Tertiary carbonates of Apulia Platform; 11, Paleozoic-Triassic deposits.

Table 7.1. List of the modelled seismogenic sources possibly associated with the 1706 earthquake (Mw 6.8).

FAULT_ID	TYPE	STRIKE [°]	DIP [°]	HYPO DEPTH [km]	DIMENSION			MAX MAGNITUDE		SOURCE VERTICIES (WGS84)	
					length [km]	width [km]	area [km^2]	Mw1	Mw2	TOP (lat-long)	BOTTOM (lat-long)
ITIS027 SULMONA	N	135	60	8.0	20	12.2	244	6.4	6.4	42.1773 - 13.8190 42.0501 - 13.9905	42.1385 - 13.7667 42.0114 - 13.9383
BORDONI23_1	N	145±10	45±5	8.4	27	18.7	505	6.6	6.7	42.2022 - 13.8058 42.0361 - 14.0347	42.1238 - 13.6786 41.9433 - 13.9280
BORDONI23_2	N	145±10	50±15	9.0	48.8	17.6	860	7.0	6.9	42.2316 - 13.7838 41.8842 - 14.1291	42.1710 - 13.6738 41.8237 - 14.0196
GALLI19	R	155±10	25±5	9.2	31.4	15.1	472	6.7	6.7	41.9409 - 14.1027 42.1959 - 13.9384	41.9942 - 14.2519 42.2493 - 14.0880
CARAMANICO	N	155±10	45±5	8.0	30.8	17	522	6.7	6.7	42.2185 - 13.9559 41.9674 - 14.1174	42.1724 - 13.8278 41.9215 - 13.9864
TONDI 24	N	135±10	55±5	8.3	38.5	15.3	588	6.8	6.7	42.1918 - 13.8047 41.9496 - 14.1377	42.1350 - 13.7304 41.8930 - 14.0634

Notes: the simulated fault types are, N, normal and, R, reverse; "hypo depth" is the hypocentral depth assumed at 2/3 along-dip of the fault plane. "length" stands for the mean length of surface and subsurface rupture length calculated from Wells and Coppersmith (1994) regressions; "width" stands for the fault down-dip length; "Mw1" and "Mw2" are the maximum moment magnitude derived from surface rupture length and fault area, respectively (Wells and Coppersmith, 1994); finally, the top and bottom coordinates of the seismogenic source vertices are expressed in decimals (WGS84).

7.3. Ground motion simulations of historical earthquakes

The primary focus of this study has been on the 1706 earthquake, the most significant seismic event in the Maiella region. In our pursuit to identify the most likely source of this event by exploiting the information of macroseismic intensity, we applied the procedure outlined by Gironelli et al. (2023) and summarized in the workflow of Figure 7.3. This workflow offers the advantage of testing various potential sources and quantitatively interpreting the earthquake-fault association.

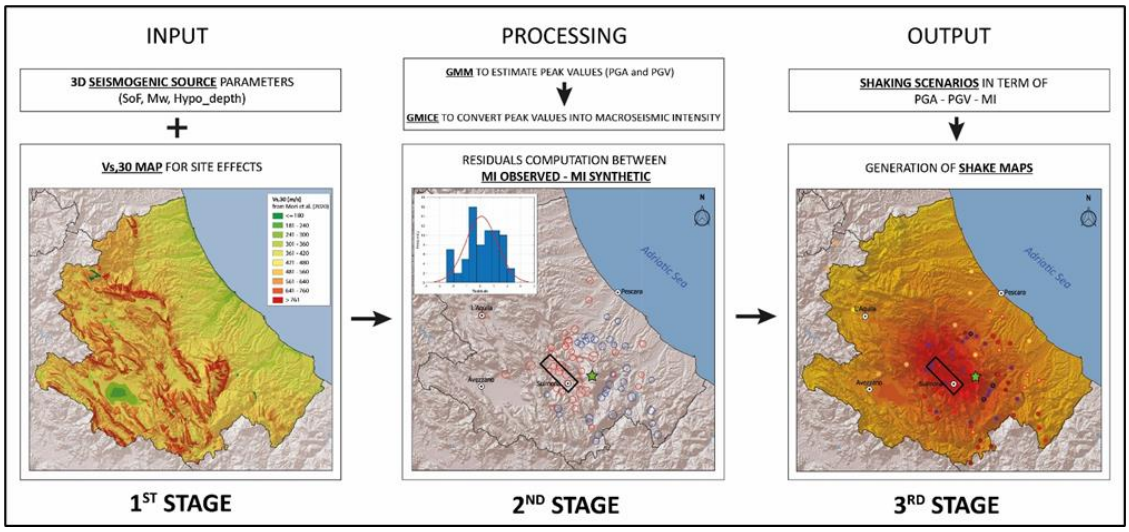

Figure 7.3. The workflow shows the main stages as explained in Gironelli et al. (2023).

The analysis relies on the computation of shaking scenarios regarding macroseismic intensity for the 1706 earthquake using different 3D source geometries. This is achieved by predicting the peak ground velocity (PGV), for each intensity data point of the 1706 macroseismic field, using the ground motion model ITA18 (Lanzano et al., 2019), which is specifically designed for the Italian territory, and it takes into account the closest distance from the rupture plane of the fault (Rrup) yielding to compute the 3D geometry of the seismogenic source. The analysed 3D fault geometries are modelled by assuming their hypocentral depth located at two-thirds along-dip of the fault plane (Table 7.1). Site amplification effects are incorporated into the computations by utilizing the shear wave velocity averaged within the uppermost 30 m (Vs,30) as parameter, obtained from a recent Vs,30 map of Italy by Mori et al. (2020). Subsequently, the peak ground velocity (PGV) is converted into macroseismic

intensities using empirical ground motion conversion relation by Gomez Capera et al. (2020) and approximated to the nearest half unit.

The best source model is determined by comparing the predicted macroseismic intensities with the observed ones. For each simulation, the mean of the residuals (i.e., the between-event error) and the root-mean square error (RMSE) are calculated. The accuracy of the prediction in reproducing the real macroseismic intensity distribution is evaluated through the between-event error, which is deemed reliable if it is less than 0.1. Consequently, the shaking scenarios in terms of peak values (i.e., PGA and PGV) and macroseismic intensities are calculated for the best source model. For reproducing the shaking scenario of the 1706 earthquake, we consider an equivalent magnitude value of 6.8 based on CPTI15 (Rovida et al., 2022). Whereas the analysed seismogenic sources and their characteristics are presented in Figure 7.2 and Table 7.1.

7.4. Results and Discussion

The residual analysis of synthetic and observed macroseismic intensities was crucial to validate the tested seismogenic sources. In figure 7.4, the distribution of residuals is shown in the form of a histogram and a map, with circles of different dimensions according to their absolute value. Positive residuals, marked by blue circles, indicate an underestimation of the predicted intensities compared to the macroseismic MCS values estimated from the historical accounts, while negative residuals in red indicate an overestimation of the predicted intensities. For each source model, the MEAN and RMSE of residuals are also reported in a box color-bounded, highlighting the quality of the results regarding source-macroseismic field matching (red indicates bad matching, green well matching).

The shaking scenario for the 1706 earthquake shown in Fig. 7.4a is performed using the individual seismogenic source "ITIS027" (DISS Working Group, 2021; Basili et al., 2008) corresponding to the NW-SE oriented seismogenic source calibrated with the surface fault length of the Mt. Morrone fault. The resulting scenario exhibits a residual RMSE of 1.66 and a mean of the residuals (between-event error) of 1.152 (Fig. 7.4a). In this case, we observed a slight overprediction of intensities in the western side of the

Maiella Massif. In contrast, the highest observed intensities around the Maiella Massif are overall underestimated. This discrepancy likely arises from the limited geometry of the source model proposed by the DISS database, which is associated with a maximum expected moment magnitude of 6.4. Therefore, it is plausible that the largest and nearest individual seismogenic source present in the DISS is unrelated to the 1706 earthquake.

Figure 7.4b presents the results of the seismogenic source hypothesis labelled TONDI24. This source hypothesis implies the simultaneous reactivation of the Mt. Morrone and Palena faults for a cumulative length of 32.2 km. The RMSE and mean of the residuals are 1.058 and 0.021, respectively, pointing out an optimal match between the simulated and observed macroseismic intensities. However, the histogram depicts a not-as-good distribution of the residuals, specifically evidencing a slight overestimation near the fault area, whereas the intensity points far from the fault are more likely underestimated. This aspect is particularly evident in the northern side of the Maiella Massif, where all points recording high intensities (i.e., X-XI MCS) are underestimated.

The seismic scenario computed using the source model BORDONI23_1, which implies the sole reactivation of the Mt. Morrone fault, also denotes an intensity underestimation with 0.347 residuals MEAN and 1.314 RMSE (Fig. 7.4c). Therefore, even considering the larger seismogenic source of the Mt. Morrone fault derived from the estimated subsurface rupture length we obtain more promising results. However, we are still not able to replicate the observed macroseismic field. Conversely, BORDONI23_2 results in a slight overprediction of the macroseismic field (residuals MEAN of -0.478, and RMSE of 1.222; Fig. 7.4d). This is likely related to the much larger source model size, which comprises both the Mt. Morrone and the Mt. Porrara fault, and therefore with the largest estimated moment magnitude (Mw 6.9-7.0; Table 7.1). Furthermore, similarly to TONDI24 this seismic scenario does not exhibit an optimal residuals distribution.

The source solutions GALLI19 and CARAMANICO, closer to the epicentral area of the 1706 Maiella earthquake, show similar results, both slightly underpredicting the macroseismic field, with residual means of 0.070 and 0.048, respectively, but, especially GALLI19, resulting in optimal residuals distribution (Fig. 7.4e, f), with the lowest RMSE value of 0.945. Although these seismogenic sources have similar dimensions, they differ in terms of kinematic and depth, with the latter resolved by a

high-angle normal fault crosscutting the surface and the former by a low-angle reverse fault at depth (Fig. 7.2b). However, it is worth noting that the Caramanico fault does not present clear evidence of Quaternary activity, except a possible surface break during the 1933 event, as documented by Galli and Pallone (2019).

The results of these simulations univocally indicated that the earthquake source might be shallower than the depth estimated by Sbarra et al. (2023). According to their approach, based on the intensity attenuation curve of macroseismic intensity data within 50 km distance from the epicentre, these authors attributed an inferred hypocentral depth of 19 km to the 1706 earthquake. This depth may relate to Composite Seismogenic Source ITCS078 (DISS Working Group, 2021), a deeper reverse structure we have not simulated for lack of geological constraints necessary for source modelling. However, a seismogenic source even deeper than GALLI19 would likely generate a much wider distribution of high intensities, resulting in an even higher intensity overprediction in areas more than 20 km away from the fault.

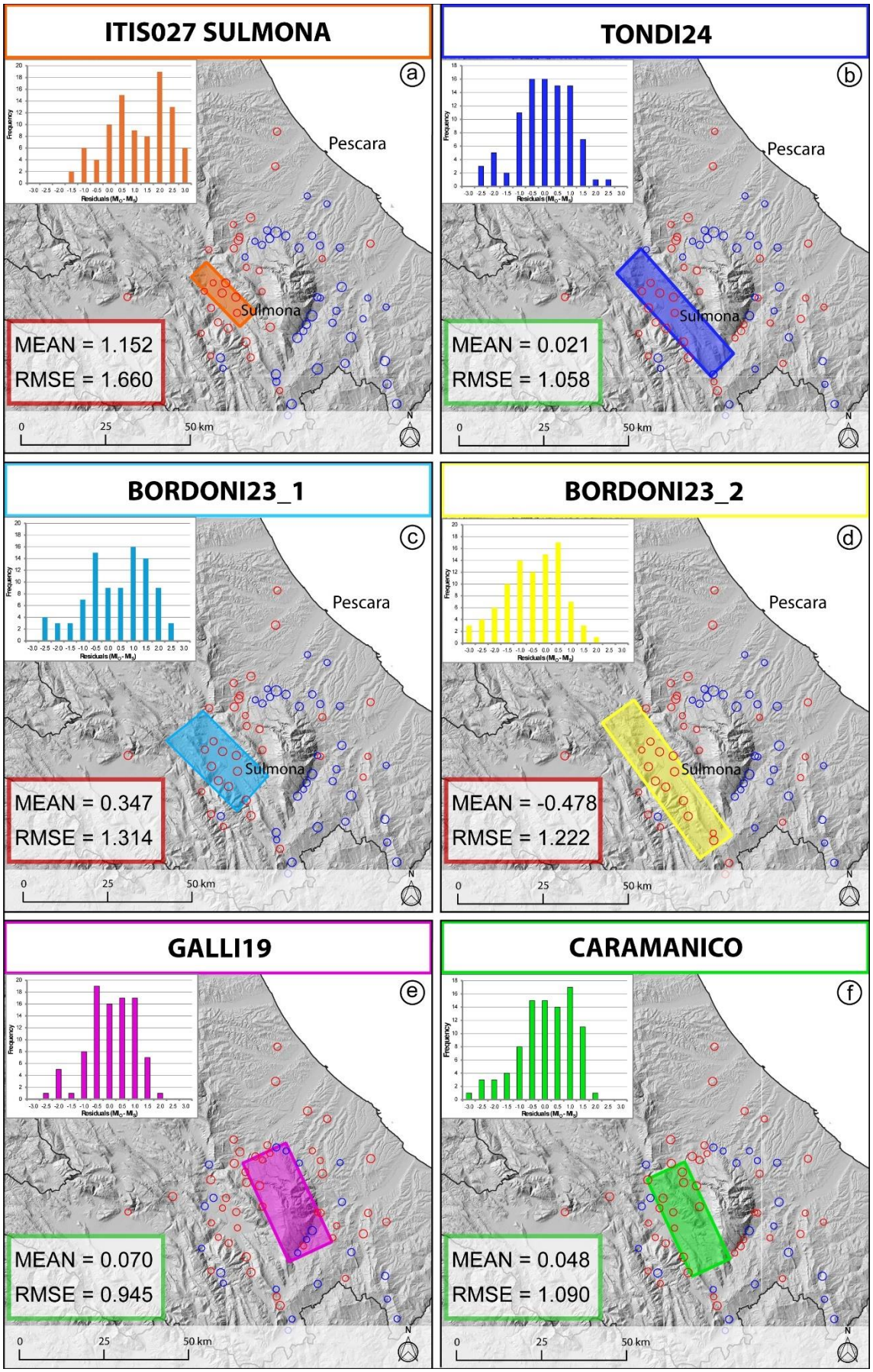
ITIS027 SULMONA
a
Pescara
Sulmona
MEAN = 1.152
RMSE = 1.660
0
25
50 km
N
TONDI24
b
Pescara
Sulmona
MEAN = 0.021
RMSE = 1.058
0
25
50 km
N
BORDONI23_1
c
Pescara
Sulmona
MEAN = 0.347
RMSE = 1.314
0
25
50 km
N
BORDONI23_2
d
Pescara
Sulmona
MEAN = -0.478
RMSE = 1.222
0
25
50 km
N
GALLI19
e
MEAN = 0.070
RMSE = 0.945
0
25
50 km
N
CARAMANICO
f
MEAN = 0.048
RMSE = 1.090
0
25
50 km
N

Figure 7.4. Spatial distribution of macroseismic intensity residuals (observed vs simulated, MI_O-MI_S). The blue and red circles indicate under-, and overestimation, respectively, given by the tested seismogenic source model in resolving the intensities of the, Mw6.8, 1706 Maiella earthquake. The histograms show the residual distribution, which is one of the main factors to validate a seismogenic source model, along with the residual mean, MEAN, and the residual root mean square error, RMSE. The analysis of residuals is computed for all modelled sources: (a) "ITIS027" (Mw 6.4) from DISS (DISS Working Group, 2021), (b) "TONDI24", which comprises the Mt. Morrone and Palena faults, (c) BORDONI23_1 and (d) BORDONI23_2, where the latter differently from the previous one extends beyond the Mt. Morrone fault comprising the Mt. Porrara fault (Bordoni et al., 2023); (e) GALLI19, seismogenic source associated to the Maiella back thrust as (Galli and Pallone, 2019); (f) CARAMANICO, normal fault bounding westward the Maiella Massif.

In conclusion, according to the analysis of residuals, the seismogenic sources GALLI19, CARAMANICO, and TONDI24 appear to best fit the observed macroseismic intensity distribution of the 1706 Maiella earthquake. For this reason, we produced the shaking scenario (PGA and macroseismic intensity) for these source hypotheses (Fig. 7.4).

GALLI19 results in a wide area surrounding the Maiella Massif with PGA ranging from 320 to 360 cm/s2. The macroseismic intensity map approximated to the half point highlights the impact of the site effect, giving a not homogeneous intensity distribution. This point is particularly evident in Pescara city, where red fringes of high intensity (8 MCS) can reach the coast due to terrains with lower S wave velocities. The over-imposed macroseismic field from the DBMI is hence counterproof for the intensity distribution described above. Specifically, the region surrounding the Maiella Massif characterized by the highest intensity is perfectly covered, whereas areas farther from the fault (e.g., coastal area) demonstrate an intensity overprediction. CARAMANICO, with similar dimensions but crosscutting the surface, results in higher PGA values in the near-fault area in the range of 400-440 cm/s2. A smaller areal distribution of high intensities (>7.5 MCS) better resolves the lower observed intensity points close to the coast. TONDI24 shows similar results in terms of PGA and intensity distribution, however, the highest intensities at the northern side of the Maiella Massif are not covered by resolving this seismogenic source due to its location and orientation apparently mismatching the epicentral area.

Given the settlement distribution, characteristics, and relative site effects, the latter source option and its misplaced position may be justified by a biased macroseismic field distribution. On the other hand, the first source option is supported by the absence of

any recent surface faulting evidence, with the last ground displacement documented by paleoseismological surveys in the northwestern sector of the Mt. Morrone Fault dating back to the 2nd century CE (Galli et al., 2015). However, despite determining which of these two plausible options is the most realistic, the main issue arising in the context of seismic hazard assessment is that given the typically medium to high seismic vulnerability of buildings in Italy, the occurrence of such a seismic event would "dramatically" fill this seismic gap in the central Apennines.

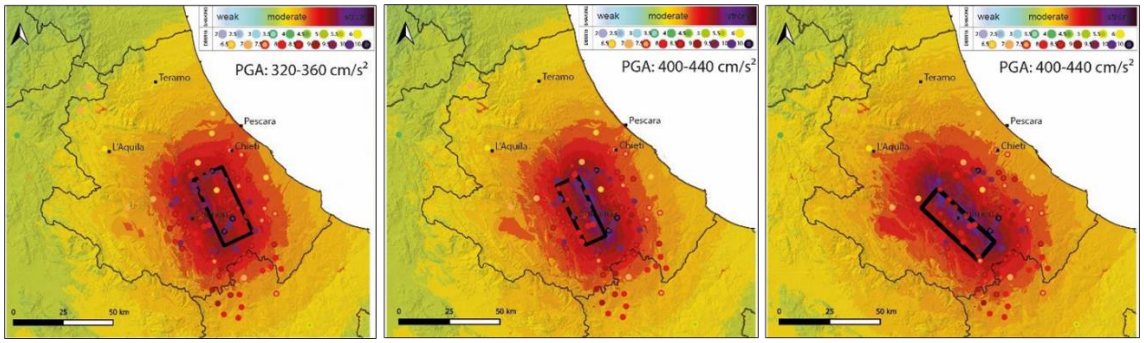

Figure 7.5. Ground motion simulations in terms of macroseismic intensities map approximated at the half for the best representative seismogenic sources of the 1706 Maiella earthquake, GALLI19, CARAMANICO, and TONDI24.

7.5. Conclusions

This study aims to comprehensively analyse the potential 3D seismogenic sources that could have generated the 1706 Maiella earthquake (Mw=6.8), one of the most significant seismic events in the Abruzzi region (central Italy). To identify the most plausible source geometry of this historical earthquake, we employed an analytical procedure based on the residuals of observed and predicted macroseismic intensities to identify the most probable seismogenic structures and rank various source hypotheses.

Our analysis considered six different seismogenic source models, including the "ITIS027" source from the DISS database (Diss Working Group, 2021; Basili et al., 2008) associated with a NW-SE oriented Mt. Morrone normal fault; the NW-SE oriented reverse fault (GALLI19) linked to the Maiella back-thrust, the Caramanico fault (CARAMANICO) westward bounding the Maiella Massif; the seismogenic sources from Bordoni et al. (2023) associated to the Morrone fault (BORDONI23_1) and to the Morrone-Porrara faults (BORDONI23_2), and the TONDI24 source hypothesis associated with the Morrone-Palena normal fault. The results of our simulations revealed several insights about the potential seismic source of this seismic event:

- Poor Fit of Mt Morrone seismogenic sources: The residual analysis showcasing the role of the modeled seismogenic sources in resolving the observed macroseismic field demonstrates a relevant underestimation using seismogenic sources of the solely Mt. Morrone Fault, both deriving its length from the surface (ITIS027 SULMONA, Mw 6.4) and subsurface rupture (BORDONI23_1, Mw 6.7), with similar hypocentral depth (8-9 km).
- Multiple-fault activation cases: the two-source hypothesis implying a synchronous activation of the Mt. Morrone fault along with the Mt. Porrara fault (BORDONI23_2, Mw 7.0) and the Palena fault (TONDI24, Mw 6.8), mainly diverging in size (850 km2 vs 588 km2 fault area), and orientation (10-30°), demonstrate clear divergences. The former is the only source hypothesis roughly overpredicting the intensity distribution, whereas the latter, with a lower RMSE of 1.058 and an optimal mean of the residuals (between-event error) of 0.021 well reproduces the observed macroseismic field. The shaking scenario using

this seismogenic structure revealed intense ground shaking in the epicentral area (PGA = 400-440 cm/s2). Unless this would be the best source, as paleoseismological studies exclude its activity after the 2nd century CE, we also discard it as a possible source.

- Good Performance of faults in the Maiella area: The NW-SE oriented reverse fault associated with the Maiella back thrust, simulated with a Mw 6.7 and 9.2 km hypocentral depth (z-top = 4.8 km), showed a low RMSE of 0.945 and a mean of the residuals of 0.07. This source demonstrates consistency with the observed macroseismic intensity distribution, particularly for areas bounding the Maiella Massif, but slightly overpredicting the intensities observed farther from the fault. On the other hand, the Caramanico normal fault, with similar dimensions but reaching the surface with a higher dip angle, better reproduces the observed intensity distribution, although no evidence of recent surface faulting has been attributed to this structure so far.

In conclusion, while this study has provided valuable insights into the potential seismogenic source of the 1706 earthquake, it is evident that despite the possibility that this study might shed light on this open issue within the Apennine seismicity, the complexities of seismic source modelling underscore the need for continued investigation and collaboration in seismic hazard assessment and risk reduction efforts in the Maiella region and beyond.

References

Akinci, A., Galadini, F., Pantosti, D., Petersen, M., Malagnini, L., & Perkins, D. (2009). Effect of time dependence on probabilistic seismic-hazard maps and deaggregation for the Central Apennines, Italy. Bulletin of the Seismological Society of America, 99(2A), 585-610.

Basili, R., Valensise, G., Vannoli, P., Burrato, P., Fracassi, U., Mariano, S., & Boschi, E. (2008). The Database of Individual Seismogenic Sources (DISS), version 3: summarizing 20 years of research on Italy's earthquake geology. Tectonophysics, 453(1-4), 20-43.

Boncio, P., Lavecchia, G., & Pace, B. (2004). Defining a model of 3D seismogenic sources for Seismic Hazard Assessment applications: the case of central Apennines (Italy). Journal of Seismology, 8, 407-425.

Boncio, P., Galli, P., Naso, G., & Pizzi, A. (2012). Surface fault rupture hazard along normal faults: Insight from the 2009 L'Aquila earthquake (Mw 6.3, central Italy), observations from global normal faulting earthquakes and implications for earthquake fault zoning. *Bull. Seismol. Soc. Am, 102*, 918-935.

Bordoni, P., Gori, S., Akinci, A., Visini, F., Sgobba, S., Pacor, F., & Doglioni, C. (2023). A site-specific earthquake ground response analysis using a fault-based approach and nonlinear modeling: The Case Pente site (Sulmona, Italy). Engineering Geology, 314, 106970.

Ceccaroni, E., Ameri, G., Gómez Capera, A. A., & Galadini, F. (2009). The 2nd century AD earthquake in central Italy: archaeoseismological data and seismotectonic implications. Natural hazards, 50, 335-359.

De Nardis, R., Garbin, M., Lavecchia, G., Pace, B., Peruzza, L., Priolo, E., ... & Vuan, A. (2011). A temporary seismic monitoring of the Sulmona area (Abruzzo, Italy) for seismotectonic purposes. Bollettino di Geofisica Teorica e Applicata, 52(4), 651-666.

DISS Working Group (2021). Database of Individual Seismogenic Sources (DISS), Version 3.3.0: A compilation of potential sources for earthquakes larger than M 5.5 in Italy and surrounding areas. Istituto Nazionale di Geofisica e Vulcanologia (INGV). https://doi.org/10.13127/diss3.3.0

Falcucci, E., Gori, S., Bignami, C., Pietrantonio, G., Melini, D., Moro, M., ... & Galadini, F. (2018). The Campotosto seismic gap in between the 2009 and 2016–2017 seismic sequences of central Italy and the role of inherited lithospheric faults in regional seismotectonic settings. Tectonics, 37(8), 2425-2445.

Galadini, F., & Galli, P. (1999). The Holocene paleoearthquakes on the 1915 Avezzano earthquake faults (central Italy): implications for active tectonics in the central Apennines. Tectonophysics, 308(1-2), 143-170.

Galadini, F., & Galli, P. (2000). Active tectonics in the central Apennines (Italy)–input data for seismic hazard assessment. Natural Hazards, 22, 225-268.

Galadini, F., & Galli, P. (2001). Archaeoseismology in Italy: case studies and implications on long-term seismicity. Journal of Earthquake Engineering, 5(01), 35-68.

Galadini, F., & Messina, P. (2004). Early–Middle Pleistocene eastward migration of the Abruzzi Apennine (central Italy) extensional domain. Journal of Geodynamics, 37(1), 57-81.

Galadini, F., & Galli, P. (2007). Inquadramento sismotettonico della regione interessata dai terremoti del 1703 e del 1706. Settecento Abruzzese: eventi sismici, mutamenti economico-sociali e ricerca storiografica.

Galli, P., Galadini, F., & Pantosti, D. (2008). Twenty years of paleoseismology in Italy. Earth-Science Reviews, 88(1-2), 89-117.

Galli, P., Giaccio, B., Peronace, E., & Messina, P. (2015). Holocene paleoearthquakes and early–late pleistocene slip rate on the Sulmona fault (central Apeninnes, Italy). Bulletin of the Seismological Society of America, 105(1), 1-13.

Galli, P., & Pallone, F. (2019). Reviewing the intensity distribution of the 1933 earthquake (Maiella, Central Italy). Clues on the seismogenic fault. Alpine and Mediterranean Quaternary, 32(2), 93-100.

Giaccio, B., Messina, P., Sposato, A., Voltaggio, M., Zanchetta, G., Galadini, F., ... & Santacroce, R. (2009). Tephra layers from Holocene Lake sediments of the Sulmona Basin, central Italy: implications for volcanic activity in Peninsular Italy and tephrostratigraphy in the central Mediterranean area. Quaternary Science Reviews, 28(25-26), 2710-2733.

Giaccio, B., Castorina, F., Nomade, S., Scardia, G., Voltaggio, M., & Sagnotti, L. (2013). Revised chronology of the Sulmona lacustrine succession, central Italy. Journal of Quaternary Science, 28(6), 545-551.

Gironelli, V., Volatili, T., Luzi, L., Brunelli, G., Zambrano, M., & Tondi, E. (2023). Ground motion simulations of historical earthquakes: the case study of the Fabriano (1741, Mw= 6.1) and Camerino (1799, Mw= 6.1) earthquakes in central Italy. *Bulletin of Earthquake Engineering*, *21*(13), 5809-5830.

Ghisetti, F., & Vezzani, L. (2002). Normal faulting, extension and uplift in the outer thrust belt of the central Apennines (Italy): role of the Caramanico fault. Basin Research, 14(2), 225-236.

Gomez-Capera, A. A., D'Amico, M., Lanzano, G., Locati, M., & Santulin, M. (2020). Relationships between ground motion parameters and macroseismic intensity for Italy. Bulletin of Earthquake Engineering, 18, 5143-5164.

Gori, S., Dramis, F., Galadini, F., & Messina, P. (2007). The use of geomorphological markers in the footwall of active faults for kinematic evaluations: examples from the central Apennines. BOLLETTINO-SOCIETA GEOLOGICA ITALIANA, 126(2), 365.

Gori, S., Giaccio, B., Galadini, F., Falcucci, E., Messina, P., Sposato, A., & Dramis, F. (2011). Active normal faulting along the Mt. Morrone south-western slopes (central Apennines, Italy). International journal of earth sciences, 100, 157-171.

Guidoboni, E., Ferrari, G., Mariotti, D., Comastri, A., Tarabusi, G., Sgattoni, G., & Valensise, G. (2018). CFTI5Med, Catalogo dei Forti Terremoti in Italia (461 aC-1997) e nell'area Mediterranea (760 aC-1500).

Lavecchia, G., & de Nardis, R. (2009, November). Seismogenic sources of major earthquakes of the Maiella area (Central Italy): constraints from macroseismic field simultaions and regional seimotectonics. UR 4.01-S1-29, Poster at the INGV-DPC meeting, Rome.

Lavecchia, G., R. de Nardis and F. Ferrarini (2010), Seismogenic sources of major earthquakes of the Maiella and Abruzzo foothill areas: constraints from macroseismic field simulation and regional seismotectonic data. Poster at DPC-INGV 2007-2009 Final Meeting, Rome 30 June-2 July 2010.

Locati M., Camassi R., Rovida A., Ercolani E., Bernardini F., Castelli V., Caracciolo C.H., Tertulliani A., Rossi A., Azzaro R., D'Amico S., Antonucci A. (2022). Database Macrosismico Italiano (DBMI15), versione 4.0. Istituto Nazionale di Geofisica e Vulcanologia (INGV). https://doi.org/10.13127/DBMI/DBMI15.4

Meletti C., Galadini F., Valensise G., Stucchi M., Basili R., Barba S., Vannucci G., Boschi E. (2004). Zonazione sismogenetica ZS9 [Data set]. Istituto Nazionale di Geofisica e Vulcanologia (INGV). https://doi.org/10.13127/sh/zs9

Meletti, C., Galadini, F., Valensise, G., Stucchi, M., Basili, R., Barba, S., & Boschi, E. (2008). A seismic source zone model for the seismic hazard assessment of the Italian territory. Tectonophysics, 450(1-4), 85-108.

Miccadei, E., Barberi, R., & Cavinato, G. P. (1999). La geologia quaternaria della Conca di Sulmona (Abruzzo, Italia centrale). *Geologica Romana, 34*, 58-86.

Mori, F., Mendicelli, A., Moscatelli, M., Romagnoli, G., Peronace, E., & Naso, G. (2020). A new Vs30 map for Italy based on the seismic microzonation dataset. Engineering Geology, 275, 105745.

Patacca, E., Sartori, R., & Scandone, P. (1990). Tyrrhenian basin and Apenninic arcs: kinematic relations since late Tortonian times. Memorie della Società Geologica Italiana, 45, 425-451.

Patacca, E., Scandone, P., Di Luzio, E., Cavinato, G. P., & Parotto, M. (2008). Structural architecture of the central Apennines: Interpretation of the CROP 11 seismic profile from the Adriatic coast to the orographic divide. Tectonics, 27(3).

Petricca, P., Barba, S., Carminati, E., Doglioni, C., & Riguzzi, F. (2015). Graviquakes in italy. Tectonophysics, 656, 202-214.

Pizzi, A., & Galadini, F. (2009). Pre-existing cross-structures and active fault segmentation in the northern-central Apennines (Italy). Tectonophysics, 476(1-2), 304-319.

Pizzi, A., Falcucci, E., Gori, S., Galadini, F., Messina, P., Di Vincenzo, M., Sposato, A. (2010). Active faulting in the Maiella massif (central Apennines, Italy). GeoActa, 3, 57-73. Pomposo, G., &

Pizzi, A. (2009). Evidenze di tettonica recente ed attiva nel settore esterno sepolto dell'Appennino centrale abruzzese. In Rendiconti online della Società Geologica Italiana (Vol. 5, pp. 176-178). Società Geologica Italiana.

Pomposo, G., & Pizzi, A. (2009). Evidenze di tettonica recente ed attiva nel settore esterno sepolto dell'Appennino centrale abruzzese. In *Rendiconti online della Società Geologica Italiana* (Vol. 5, pp. 176-178). Società Geologica Italiana.

Puliti, I., Pizzi, A., Gori, S., Falcucci, E., Galadini, F., Maceroni, D., & Moro, M. S. M. (2021). New paleoseismological constraints of late Holocene earthquakes along the Mt. Morrone fault (Sulmona basin, Abruzzi Apennines, Italy). In 90 CONGRESSO DELLA SOCIETÀ GEOLOGICA ITALIANA: ABSTRACT BOOK (pp. 217-217). Società Geologica Italiana.

Romano, M. A., De Nardis, R., Garbin, M., Peruzza, L., Priolo, E., Lavecchia, G., & Romanelli, M. (2013). Temporary seismic monitoring of the Sulmona area (Abruzzo, Italy): a quality study of microearthquake locations. Natural Hazards and Earth System Sciences, 13(11), 2727-2744.

Rovida A., Locati M., Camassi R., Lolli B., Gasperini P., Antonucci A. (2022). Catalogo Parametrico dei Terremoti Italiani (CPTI15), versione 4.0. Istituto Nazionale di Geofisica e Vulcanologia (INGV). https://doi.org/10.13127/CPTI/CPTI15.4

Sbarra, P., Burrato, P., De Rubeis, V., Tosi, P., Valensise, G., Vallone, R., & Vannoli, P. (2023). Inferring the depth and magnitude of pre-instrumental earthquakes from intensity attenuation curves. *Natural Hazards and Earth System Sciences*, *23*(3), 1007-1028.

Scisciani, V., Tavarnelli, E., & Calamita, F. (2002). The interaction of extensional and contractional deformations in the outer zones of the Central Apennines, Italy. Journal of Structural Geology, 24(10), 1647-1658.

Scisciani, V., Tavarnelli, E., Calamita, F., & Paltrinieri, W. (2002). Pre-thrusting normal faults within syn-orogenic basins of the Outer Central Apennines, Italy: implications for Apennine tectonics. B. Soc. Geol. It., Spec. Vol, 1, 295-304.

Vittori, E., Cavinato, G. P., Miccadei, E., Serva, L., & Slemmons, B. D. (1995). Active faulting along the northeastern edge of the Sulmona basin, central Apennines, Italy. Perspectives in Paleoseismology", Association of Engineering Geologists Bulletin, Special Publication, (6), 115-126.

Villani, M., Faccioli, E., Ordaz, M., & Stupazzini, M. (2014). High-resolution seismic hazard analysis in a complex geological configuration: the case of the Sulmona Basin in Central Italy. Earthquake Spectra, 30(4), 1801-1824.

Wells, D. L., and Coppersmith, K. J. (1994). New empirical relationships among magnitude, rupture length, rupture width, rupture area, and surface displacement. Bulletin of the seismological Society of America, 84(4), 974-1002. https://doi.org/10.1785/BSSA0840040974

8. General Conclusions

Studying moderate-to-large earthquakes before the era of instrumental recordings poses challenges, especially in seismically active continental regions like Italy. Within modern probabilistic seismic hazard assessment, a crucial aspect involves identifying and characterising earthquake seismogenic sources to estimate their potential impact on contemporary urban environments. However, this work remains highly challenging, especially for the sources of historical earthquakes. Particularly challenging are seismically silent areas with a lack of recent instrumental recordings (earthquakes with $Mw \geq 3$). The limited data from these areas makes it difficult to depict fault geometries accurately, thus hindering the identification of seismogenic sources of historical earthquakes. Thus, innovative methodologies are necessary.

In this regard, this doctoral thesis introduces a novel field in earthquake seismology, addressing the dual objective of identifying pre-instrumental earthquake sources and constructing reliable shaking scenarios. The study area selected as the focus area for this research is Central Italy, known for its active tectonics and extensive seismic history. Despite the consistent availability of macroseismic intensity data, the knowledge regarding the causative faults remains limited. The research focuses on three earthquakes: the 1741 Fabriano earthquake (Imax 9 MCS; Mw 6.17), the 1799 Camerino earthquake (Imax 9-10 MCS; Mw 6.18) in the Marche Region, and the 1706 Maiella earthquake (Imax 10-11 MCS; Mw 6.84) in the Abruzzi Region.

The primary goal of this PhD research is to compute shaking scenarios for the above-mentioned historical earthquakes. The proposed workflow for calculating historical earthquake scenarios involves: (i) identifying potential seismogenic sources using residual analysis, and (ii) calculating shaking scenarios in terms of peak values and macroseismic intensity utilizing both observations and predictions.
This is achieved by integrating macroseismic intensity observations, available Ground Motion Models (GMMs), and the empirical Ground Motion Intensity Conversion Equations (GMICEs) to convert macroseismic intensity and ground motion parameters.

The macroseismic data are obtained from the Italian Macroseismic Database (DBMI15; Locati et al. 2022), while the seismogenic sources are proposed in the Italian Database of Individual Seismogenic Sources (DISS; Working Group, 2021, Basili et al. 2008). The ground motion simulation is performed by using the most recent GMM for Italy (Lanzano et al. 2019), while the GMICEs by Gomez Capera et al. (2020) are used to convert the ground motion parameters into macroseismic intensities and vice versa.

In this research, different source geometries are explored by varying the fault parameters, such as location, strike, dip, depth, and fault mechanism. The 3D geometry of these earthquake sources is determined through residual analysis between observed and predicted macroseismic intensities, derived by converting Peak Ground Velocity (PGV) into macroseismic intensity. According to the residual analysis, the "best-fitting" seismogenic sources are the one that minimises the difference between observed and predicted macroseismic intensities.

The sensitivity of the results has been evaluated by calculating the mean of the residuals (between-event error) for each simulation. A threshold of 0.1 was set for the between-event error. This indicates low variability between the observed ground motion and the median prediction of the ground motion model for that specific earthquake. In cases where multiple potential seismic sources exhibited between-event errors smaller than 0.1, indicating equally good fits with observed data, the selection of the "best-fitting" source is further based on the regional tectonic context.

The shaking scenarios of historical earthquakes based on the seismogenic source are calculated at specific locations (i.e., site) in terms of Peak Ground Acceleration (PGA), Peak Ground Velocity (PGV), and macroseismic intensity. Additionally, to improve the accuracy of shaking scenarios the Vs,30 map is created to account for site amplifications in ground motion modelling.

This map has been calibrated for the Marche Region (see Chapter 5) by using Vs,30 values obtained from geophysical investigations carried out in the framework of the Italian seismic microzonation studies. These values are correlated with two common adopted geological and topographic proxies using mixed-effect regression. The results obtained from the regression analysis have been analysed to verify the dependence of

Vs,30 values from the lithology and topographic slope. The resulting Vs,30 map emphasize that the distribution of values well reflects the influence of the various lithologies. Whereas the contribution of the topography is associated with the variation within each lithological complex. Additionally, the influence of the map's resolution on the spatial variability of site amplification has been evaluated through a resampling of the map using various neighbourhoods. The analysis revealed that smaller neighbourhoods (e.g., 3x3, 5x5) exhibited similar variability and demonstrate that such 30 m resolution effectively captures local variations.

The application of the proposed methodology to two case studies in the Marche Region, presented in Chapter 6, identified the most fitting fault geometry for the 1741 Fabriano earthquake as a NE–SW oriented strike-slip fault at a focal depth of 20 km (RMSE = 1; Mean_res = -0.01). Conversely, the simulation that best matched the observed macroseismic data for the 1799 Camerino earthquake associates with a NW-SE normal fault with an enucleation point at a depth of 14 km (RMSE = 0.89; Mean_res = 0.06). The shaking scenarios obtained in this study for the 1741 Fabriano and 1799 Camerino earthquakes are coherent with macroseismic observations.

The methodology has also been applied (see Chapter 7) to identify the seismogenic source associated with the 1706 Maiella earthquake that occurred in the Abruzzo Region. The 1706 Maiella earthquake is associated with various seismogenic sources compared to the previous cases. Therefore, the outlined methodology was employed to quantitatively assess the reliability of existing source models. This study revealed that the fault geometry best replicating the macroseismic intensity distribution is an NW-SE oriented reverse fault associated with the Maiella back thrust, as proposed by Galli and Pallone (2019). This source geometry (labelled GALLI19), calibrated for the estimated magnitude of the 1706 earthquake (Mw = 6.8), showed a low RMSE of 0.945 and a Mean_res of 0.070. However, the TONDI24 source hypothesis also yielded promising results, suggesting a possible link to the Mt. Morrone-Palena normal fault system (RMSE = 1.058; Mean_res = 0.021). Furthermore, the Caramanico fault, a NW-SE oriented normal fault bounding the Maiella Massif westward, also demonstrated promising results in reproducing the observed intensity distribution (RMSE = 1.090;

Mean_res = 0.048). However, no recent surface faulting has been attributed to this structure.

For the analysed historical earthquakes, the macroseismic intensity data estimated with the proposed methodology have been compared with macroseismic observations from the DBMI15 (Locati et al., 2022). The comparison showed a good fit of the prediction to the observed data with a root mean square error (RMSE) value of approximately 1. However, the ground motion distribution, and consequently the intensity data, can be influenced by factors beyond those considered in this research, such as anisotropy in seismic wave propagation and/or the combined effects of directivity and radiation patterns. Therefore, future developments of the proposed methodology might involve more in-depth investigations into such aspects.

In conclusion, this PhD dissertation introduces an innovative methodology that combines geological knowledge, empirical ground motion models, and observed macroseismic intensity data to identify pre-instrumental earthquake sources and create shaking scenarios. The findings of this research significantly contribute to enhancing the understanding of the seismotectonic settings in the area, particularly in identifying active seismogenic sources and refining their faulting style. These insights serve as crucial inputs for probabilistic seismic hazard analysis and the development of shaking scenarios. Moreover, the proposed methodology can be applied to evaluate the history of ground motion shaking at any site, even if macroseismic observations are not available.

The outcomes of this study show promise, highlighting the need for future research endeavours to further identify seismogenic sources associated with historical earthquakes. This ongoing effort aims to produce an atlas of shaking scenarios, facilitating comprehensive hazard studies, effective emergency planning, and seismic risk reduction measures.

References

Albarello, D., & Mucciarelli, M. (2002). Seismic hazard estimates using ill-defined macroseismic data at site. pure and applied geophysics, 159, 1289-1304.

Albarello, D., & D'Amico, V. (2004). Attenuation relationship of macroseismic intensity in Italy for probabilistic seismic hazard assessment. Bollettino di Geofisica Teorica ed Applicata, 45(4), 271-284.

Allen, T. I., Wald, D. J., Hotovec, A. J., Lin, K., Earle, P. S., & Marano, K. D. (2008). An Atlas of ShakeMaps for selected global earthquakes (p. 35). US Department of the Interior, US Geological Survey.

Akkar, S., & Bommer, J. J. (2010). Empirical equations for the prediction of PGA, PGV, and spectral accelerations in Europe, the Mediterranean region, and the Middle East. Seismological Research Letters, 81(2), 195-206.

Antonellini, M., Tondi, E., Agosta, F., Aydin, A., & Cello, G. (2008). Failure modes in deep-water carbonates and their impact for fault development: Majella Mountain, Central Apennines, Italy. Marine and Petroleum Geology, 25(10), 1074-1096.

Aochi, H., & Douglas, J. (2006). Testing the validity of simulated strong ground motion from the dynamic rupture of a finite fault, by using empirical equations. Bulletin of Earthquake Engineering, 4(3), 211-229.

Atik, L. A., Abrahamson, N., Bommer, J. J., Scherbaum, F., Cotton, F., & Kuehn, N. (2010). The variability of ground-motion prediction models and its components. Seismological Research Letters, 81(5), 794-801.

Atkinson, G. M., & Kaka, S. I. (2007). Relationships between felt intensity and instrumental ground motion in the central United States and California. Bulletin of the Seismological Society of America, 97(2), 497-510.

Baker, J., Bradley, B., & Stafford, P. (2021). Seismic hazard and risk analysis. Cambridge University Press.

Bakun, W. U., & Wentworth, C. M. (1997). Estimating earthquake location and magnitude from seismic intensity data. Bulletin of the Seismological Society of America, 87(6), 1502-1521.

Bakun, W. H. (2006). Estimating locations and magnitudes of earthquakes in southern California from modified Mercalli intensities. Bulletin of the Seismological Society of America, 96(4A), 1278-1295.

Bakun, W. H., & Scotti, O. (2006). Regional intensity attenuation models for France and the estimation of magnitude and location of historical earthquakes. Geophysical Journal International, 164(3), 596-610.

Barchi, M. R., Galadini, F., Lavecchia, G., Messina, P., Michetti, A. M., Peruzza, L., ... & Vittori, E. (2000). Sintesi delle conoscenze sulle faglie attive in Italia Centrale: parametrizzazione ai fini della caratterizzazione della pericolosità sismica.

Basili, R., Valensise, G., Vannoli, P., Burrato, P., Fracassi, U., Mariano, S., ... & Boschi, E. (2008). The Database of Individual Seismogenic Sources (DISS), version 3: summarizing 20 years of research on Italy's earthquake geology. Tectonophysics, 453(1-4), 20-43.

Bindi, D., Parolai, S., Oth, A., Abdrakhmatov, K., Muraliev, A., & Zschau, J. (2011). Intensity prediction equations for Central Asia. Geophysical Journal International, 187(1), 327-337.

Bindi, D., Massa, M., Luzi, L., Ameri, G., Pacor, F., Puglia, R., & Augliera, P. (2014). Pan-European ground-motion prediction equations for the average horizontal component of PGA, PGV, and 5%-damped PSA at spectral periods up to 3.0 s using the RESORCE dataset. Bulletin of Earthquake Engineering, 12, 391-430.

Bisch, P., Carvalho, E., Degee, H., Fajfar, P., Fardis, M., Franchin, P., ... & Tsionis, G. (2012). Eurocode 8: seismic design of buildings worked examples. Luxembourg: Publications Office of the European Union.

Boore, D. M., Joyner, W. B., & Fumal, T. E. (1997). Equations for estimating horizontal response spectra and peak acceleration from western North American earthquakes: A summary of recent work. Seismological research letters, 68(1), 128-153.

Boore, D. M., & Atkinson, G. M. (2008). Ground-motion prediction equations for the average horizontal component of PGA, PGV, and 5%-damped PSA at spectral periods between 0.01 s and 10.0 s. Earthquake spectra, 24(1), 99-138.

Borcherdt, R. D. (1994). Estimates of site-dependent response spectra for design (methodology and justification). Earthquake spectra, 10(4), 617-653.

Bordoni, P., Gori, S., Akinci, A., Visini, F., Sgobba, S., Pacor, F., ... & Doglioni, C. (2023). A site-specific earthquake ground response analysis using a fault-based approach and nonlinear modeling: The Case Pente site (Sulmona, Italy). Engineering Geology, 314, 106970.

Boschi E., Gasperini P., Valensise G., Camassi R., Castelli V., Stucchi M., Rebez A., Monachesi G., Barbano M. S., Albini P., Guidoboni E., Ferrari G., Mariotti D., Comastri A., Molin D. (1999). Catalogo Parametrico dei Terremoti Italiani (CPTI99) [Data set]. Istituto Nazionale di Geofisica e Vulcanologia (INGV). https://doi.org/10.6092/ingv.it-cpti99

Butler, R. W., Tavarnelli, E., & Grasso, M. (2006). Structural inheritance in mountain belts: an Alpine–Apennine perspective. Journal of structural geology, 28(11), 1893-

1908.Campbell, K. W. (1981). Near-source attenuation of peak horizontal acceleration. Bulletin of the Seismological Society of America, 71(6), 2039-2070.

Campbell, K. W. (1985). Strong motion attenuation relations: a ten-year perspective. Earthquake spectra,1(4), 759-804.

Campbell, K. W., & Bozorgnia, Y. (2003). Updated near-source ground-motion (attenuation) relations for the horizontal and vertical components of peak ground acceleration and acceleration response spectra. Bulletin of the Seismological Society of America, 93(1), 314-331.

Campbell, K. W., & Bozorgnia, Y. (2008). NGA ground motion model for the geometric mean horizontal component of PGA, PGV, PGD and 5% damped linear elastic response spectra for periods ranging from 0.01 to 10 s. Earthquake spectra, 24(1), 139-171.

Campbell, K. W., & Bozorgnia, Y. (2014). NGA-West2 ground motion model for the average horizontal components of PGA, PGV, and 5% damped linear acceleration response spectra. Earthquake Spectra, 30(3), 1087-1115.

Cancani, A. (1904). Sur l'emploi d'une double échelle sismique des intensités, empirique et absolue. Gerlands Beitrage Geophysik, 2, 281-283.

Cantore, L., Convertito, V., & Zollo, A. (2010). Development of a site conditions map for the Campania-Lucania region (southern Apennines, Italy). Annals Geophysics.

Carminati, E., & Doglioni, C. (2012). Alps vs. Apennines: The paradigm of a tectonically asymmetric Earth. Earth-Science Reviews, 112(1-2), 67-96.

Cello, G., Mazzoli, S., Tondi, E., & Turco, E. (1997). Active tectonics in the central Apennines and possible implications for seismic hazard analysis in peninsular Italy. Tectonophysics, 272(1), 43-68.

Cello, G., Deiana, G., Ferelli, L., Marchegiani, L., Maschio, L., Mazzoli, S., ... & Vittori, T. (2000). Geological constraints for earthquake faulting studies in the Colfiorito area (central Italy). Journal of Seismology, 4, 357-364.

Centamore, E., & Rossi, D. (2009). Neogene-Quaternary tectonics and sedimentation in the Central Apennines. Italian Journal of Geosciences, 128(1), 73-88.Code, P. (2005). Eurocode 8: Design of structures for earthquake resistance-part 1: general rules, seismic actions and rules for buildings. Brussels: European Committee for Standardization.

Collettini, C., & Barchi, M. R. (2002). A low-angle normal fault in the Umbria region (Central Italy): a mechanical model for the related microseismicity. Tectonophysics, 359(1-2), 97-115.

Collettini, C., Barchi, M. R., Chiaraluce, L., Mirabella, F., & Pucci, S. (2003). The Gubbio fault: can different methods give pictures of the same object?. Journal of Geodynamics, 36(1-2), 51-66.

Cosentino, D., Cipollari, P., Marsili, P., & Scrocca, D. (2010). Geology of the central Apennines: a regional review. Journal of the virtual explorer, 36(11), 1-37.

Code, P. (2005). Eurocode 8: Design of structures for earthquake resistance-part 1: general rules, seismic actions and rules for buildings. Brussels: European Committee for Standardization.

Crowley, H., Dabbeek, J., Despotaki, V., Rodrigues, D., Martins, L., Silva, V., Romão X., Pereira N., Weatherill G., Danciu, L. (2021). European seismic risk model (ESRM20). EFEHR Technical Report, 2. https://doi.org/10.7414/EUC-EFEHR-TR002-ESRM20

Danciu L., Nandan S., Reyes C., Basili R., Weatherill G., Beauval C., Rovida A., Vilanova S., Sesetyan K., Bard P-Y., Cotton F., Wiemer S., Giardini D. (2021) - The 2020 update of the European Seismic Hazard Model: Model Overview. EFEHR Technical Report 001, v1.0.0, https://doi.org/10.12686/a15

Dangkua, D. T., & Cramer, C. H. (2011). Felt intensity versus instrumental ground motion: A difference between California and eastern North America. Bulletin of the Seismological Society of America, 101(4), 1847-1858

De Nardis, R., Garbin, M., Lavecchia, G., Pace, B., Peruzza, L., Priolo, E., ... & Vuan, A. (2011). A temporary seismic monitoring of the Sulmona area (Abruzzo, Italy) for seismotectonic purposes. Bollettino di Geofisica Teorica e Applicata, 52(4), 651-666.

D'Amico, V., & Albarello, D. (2008). SASHA: a computer program to assess seismic hazard from intensity data. Seismological Research Letters, 79(5), 663-671.

Di Domenica, A., Petricca, P., Trippetta, F., Carminati, E., & Calamita, F. (2014). Investigating fault reactivation during multiple tectonic inversions through mechanical and numerical modeling: An application to the Central-Northern Apennines of Italy. Journal of Structural Geology, 67, 167-185.DISS Working Group (2021). Database of Individual Seismogenic Sources (DISS), Version 3.3.0: A compilation of potential sources for earthquakes larger than M 5.5 in Italy and surrounding areas. Istituto Nazionale di Geofisica e Vulcanologia (INGV).

Douglas, J., & Aochi, H. (2008). A survey of techniques for predicting earthquake ground motions for engineering purposes. Surveys in geophysics, 29, 187-220.

Dowrick, D. J. (1977). Earthquake resistant design. A manual for engineers and architects (No. Monograph).

Fabbrocino, S., Lanzano, G., Forte, G., de Magistris, F. S., & Fabbrocino, G. (2015). SPT blow count vs. shear wave velocity relationship in the structurally complex formations of the Molise Region (Italy). Engineering Geology, 187, 84-97.

Faccioli, E., & Cauzzi, C. (2006, September). Macroseismic intensities for seismic scenarios, estimated from instrumentally based correlations. In Proc. First European Conference on Earthquake Engineering and Seismology (Vol. 569). Swiss Society for Earthquake Engineering and Structural Dynamics (SGEB).

Faenza, L., & Michelini, A. (2010). Regression analysis of MCS intensity and ground motion parameters in Italy and its application in ShakeMap. Geophysical Journal International, 180(3), 1138-1152.Farr, T. G., Rosen, P. A., Caro, E., Crippen, R., Duren, R., Hensley, S., & Alsdorf, D. (2007). The shuttle radar topography mission. Reviews of geophysics, 45(2).

Faenza, L., & Michelini, A. (2011). Regression analysis of MCS intensity and ground motion spectral accelerations (SAs) in Italy. Geophysical Journal International, 186(3), 1415-1430.

FEMA (1997) NEHRP Guidelines for the Seismic Rehabilitation of Buildings. Report No. 273, Federal Emergency Management Agency, Washington DC.

Forte, G., Chioccarelli, E., De Falco, M., Cito, P., Santo, A., & Iervolino, I. (2019). Seismic soil classification of Italy based on surface geology and shear-wave velocity measurements. Soil Dynamics and Earthquake Engineering, 122, 79-93.

Galadini, F., & Galli, P. (2000). Active tectonics in the central Apennines (Italy)–input data for seismic hazard assessment. Natural Hazards, 22, 225-268.

Galli, P., Galadini, F., & Pantosti, D. (2008). Twenty years of paleoseismology in Italy. Earth-Science Reviews, 88(1-2), 89-117.

Galli, P., Giaccio, B., Peronace, E., & Messina, P. (2015). Holocene paleoearthquakes and early–late pleistocene slip rate on the Sulmona fault (central Apeninnes, Italy). Bulletin of the Seismological Society of America, 105(1), 1-13.

Galli, P., & Pallone, F. (2019). Reviewing the intensity distribution of the 1933 earthquake (Maiella, Central Italy). Clues on the seismogenic fault. Alpine and Mediterranean Quaternary, 32(2), 93-100.

Galli, P., Galderisi, A., Messina, P., & Peronace, E. (2022). The Gran Sasso fault system: Paleoseismological constraints on the catastrophic 1349 earthquake in Central Italy. Tectonophysics, 822, 229156.

Gasperini, P., Bernardini, F., Valensise, G., & Boschi, E. (1999). Defining seismogenic sources from historical earthquake felt reports. Bulletin of the Seismological Society of America, 89(1), 94-110.

Gasperini, P., Vannucci, G., Tripone, D., & Boschi, E. (2010). The location and sizing of historical earthquakes using the attenuation of macroseismic intensity with distance. Bulletin of the Seismological Society of America, 100(5A), 2035-2066.

Gómez, C., & Augusto, A. (2006). Seismic hazard map for the Italian territory using macroseismic data. Earth Sciences Research Journal, 10(2), 67-90.

Gomez Capera, A. A., Locati, M., Fiorini, E., Bazurro, P., Luzi, L., Massa, M., ... & Santulin, M. (2015). D3. 1 Macroseismic and ground motion: site specific conversion rules. DPC-INGV-S2 Project-2015, Deliverable 3.1, https://sites. google. com/site/ingvdpc2014progettos2/deliverables/. Accessed Dec.

Gomez Capera, A. A., Santulin, M., D'Amico, M., D'Amico, V., Locati, M., Luzi, L., ... & Puglia, R. (2018). Macroseismic intensity to ground motion empirical relationships for Italy. In Proceedings (Vol. 37, pp. 289-291).

Gomez-Capera, A. A., D'Amico, M., Lanzano, G., Locati, M., & Santulin, M. (2020). Relationships between ground motion parameters and macroseismic intensity for Italy. Bulletin of Earthquake Engineering, 18, 5143-5164.

Graves, R. W., & Pitarka, A. (2010). Broadband ground-motion simulation using a hybrid approach. Bulletin of the Seismological Society of America, 100(5A), 2095-2123.

Grünthal G (ed) (1998) European Macroseismic Scale 1998. Cahiers du Centre Europèen de Gèodynamique et de Seismologie. Conseil de l'Europe, Conseil de l'Europe

Guatteri, M., Mai, P. M., Beroza, G. C., & Boatwright, J. (2003). Strong ground-motion prediction from stochastic-dynamic source models. Bulletin of the Seismological Society of America, 93(1), 301-313.

Guatteri, M., Mai, P. M., & Beroza, G. C. (2004). A pseudo-dynamic approximation to dynamic rupture models for strong ground motion prediction. Bulletin of the Seismological Society of America, 94(6), 2051-2063.

Guidoboni, E., Ferrari, G., Mariotti, D., Comastri, A., Tarabusi, G., & Valensise, G. (2007). Catalogue of Strong Earthquakes in Italy (461 BC-1997) and Mediterranean Area (760 BC-1500).

Guidoboni, E., Ferrari, G., Mariotti, D., Comastri, A., Tarabusi, G., Sgattoni, G., & Valensise, G. (2018). CFTI5Med, Catalogo dei Forti Terremoti in Italia (461 aC-1997) e nell'area Mediterranea (760 aC-1500).

Guidoboni, E., Ferrari, G., Tarabusi, G., Sgattoni, G., Comastri, A., Mariotti, D., ... & Valensise, G. (2019). CFTI5Med, the new release of the catalogue of strong earthquakes in Italy and in the Mediterranean area. Scientific Data, 6(1), 80.

Hartzell, S., Harmsen, S., Frankel, A., & Larsen, S. (1999). Calculation of broadband time histories of ground motion: Comparison of methods and validation using strong-ground motion from the 1994 Northridge earthquake. Bulletin of the Seismological Society of America, 89(6), 1484-1504.

Hartzell, S., Guatteri, M., Mai, P. M., Liu, P. C., & Fisk, M. (2005). Calculation of broadband time histories of ground motion, Part II: Kinematic and dynamic modeling using theoretical Green's functions and comparison with the 1994 Northridge earthquake. Bulletin of the Seismological Society of America, 95(2), 614-645.

Herrero, A., & Bernard, P. (1994). A kinematic self-similar rupture process for earthquakes. Bulletin of the Seismological Society of America, 84(4), 1216-1228.

Housner, G. W. (1947). Characteristics of strong-motion earthquakes. Bulletin of the Seismological Society of America, 37(1), 19-31.

Huang, J., Motha, J., Tarbali, K., Lee, R., Bae, S., Polak, V., & Bradley, B. (2020). Cybershake NZ v19. 5: New Zealand simulation-based probabilistic seismic hazard analysis.

Hutchings, L. (1994). Kinematic earthquake models and synthesized ground motion using empirical Green's functions. Bulletin of the Seismological Society of America, 84(4), 1028-1050.

ITHACA Working Group (2019). ITHACA (ITaly HAzard from CApable faulting), A database of active capable faults of the Italian territory. Version December 2019.

Iwahashi, J., Kamiya, I., & Matsuoka, M. (2010). Regression analysis of Vs30 using topographic attributes from a 50-m DEM. Geomorphology, 117(1-2), 202-205.

Joyner, W. B., & Boore, D. M. (1981). Peak horizontal acceleration and velocity from strong-motion records including records from the 1979 Imperial Valley, California, earthquake. Bulletin of the seismological Society of America, 71(6), 2011-2038.

Joyner, W. B., & Boore, D. M. (1986). On simulating large earthquakes by Green's–Function addition of smaller earthquakes. Earthquake source mechanics, 37, 269-274.

Joyner, W. B., & Boore, D. M. (1988, June). Measurement, characterization, and prediction of strong ground motion. In Earthquake Engineering and Soil Dynamics II, Proc. Am. Soc. Civil Eng. Geotech. Eng. Div. Specialty Conf (pp. 27-30).

Kaka, S. I., & Atkinson, G. M. (2004). Relationships between instrumental ground-motion parameters and modified Mercalli intensity in eastern North America. Bulletin of the Seismological Society of America, 94(5), 1728-1736.

Kircher, C. A., Whitman, R. V., & Holmes, W. T. (2006). HAZUS earthquake loss estimation methods. Natural Hazards Review, 7(2), 45-59.

Komatitsch, D., & Tromp, J. (2002). Spectral-element simulations of global seismic wave propagation—I. Validation. Geophysical Journal International, 149(2), 390-412.

Kozdon, J. E., & Dunham, E. M. (2013). Rupture to the trench: Dynamic rupture simulations of the 11 March 2011 Tohoku earthquake. Bulletin of the Seismological Society of America, 103(2B), 1275-1289.

Lanzano, G., Luzi, L., Pacor, F., Felicetta, C., Puglia, R., Sgobba, S., & D'Amico, M. (2019). A revised ground-motion prediction model for shallow crustal earthquakes in Italy. Bulletin of the Seismological Society of America, 109(2), 525-540.

Lavecchia, G., Boncio, P., Creati, N., & Brozzetti, F. (2004). Stile strutturale, stato termo-meccanico e significato sismogenetico del thrust Adriatico; dati e spunti da una revisione del profilo CROP 03 integrata con l'analisi di dati sismologici. Bollettino della Società geologica italiana, 123(2), 111-125.

Lee, C. T., & Tsai, B. R. (2008). Mapping Vs30 in Taiwan. TAO: Terrestrial, Atmospheric and Oceanic Sciences, 19(6), 6.

Locati M., Camassi R., Rovida A., Ercolani E., Bernardini F., Castelli V., Caracciolo C.H., Tertulliani A., Rossi A., Azzaro R., D'Amico S., Antonucci A. (2022). Database Macrosismico Italiano (DBMI15), versione 4.0. Istituto Nazionale di Geofisica e Vulcanologia (INGV). https://doi.org/10.13127/DBMI/DBMI15.4

Mai, P. M., Imperatori, W., & Olsen, K. B. (2010). Hybrid broadband ground-motion simulations: Combining long-period deterministic synthetics with high-frequency multiple S-to-S backscattering. Bulletin of the Seismological Society of America, 100(5A), 2124-2142.

Margottini, C., Molin, D., & Serva, L. (1992). Intensity versus ground motion: a new approach using Italian data. Engineering Geology, 33(1), 45-58.

Materazzi, M., Bufalini, M., Dramis, F., Pambianchi, G., Gentili, B., & Di Leo, M. (2022). Active tectonics and paleoseismicity of a transverse lineament in the Fabriano valley, Umbria-Marche Apennine (central Italy). International Journal of Earth Sciences, 111(5), 1539-1549.

Mazzoli, S., Deiana, G., Galdenzi, S., & Cello, G. (2002). Miocene fault-controlled sedimentation and thrust propagation in the previously faulted external zones of the Umbria-Marche Apennines, Italy. EGU Stephan Mueller Special Publication Series, 1, 195-209.

McCallen, D., Petrone, F., Miah, M., Pitarka, A., Rodgers, A., & Abrahamson, N. (2021). EQSIM—A multidisciplinary framework for fault-to-structure earthquake simulations on exascale computers, part II: Regional simulations of building response. Earthquake Spectra, 37(2), 736-761.

Medvedev S, Sponheuer W, Karník V (1964) Neue seismische Skala Intensity scale of earthquakes, 7. Tagung der Europäischen Seismologischen Kommission vom 24.9. bis 30.9.1962. In: Jena, Veröff. Institut für Bodendynamik und Erdbebenforschung in Jena, vol 77. Deutsche Akademie der Wissenschaften zu Berlin, pp 69–76

Meletti, C., Montaldo, V., Stucchi, M., Martinelli, F. (2006). Database della pericolosità sismica MPS04. Istituto Nazionale di Geofisica e Vulcanologia (INGV). DOI: 10.13127/SH/MPS04/DB

Michelini, A., Faenza, L., Lanzano, G., Lauciani, V., Jozinović, D., Puglia, R., & Luzi, L. (2020). The new ShakeMap in Italy: Progress and advances in the last 10 yr. Seismological Research Letters, 91(1), 317-333.

Monachesi G. (1987). Revisione della sismicità di riferimento per i comuni di Cerreto d'Esi (AN), Esanatoglia (MC), Serra San Quirico (AN). Osservatorio Geofisico Sperimentale, Macerata, Internal report, 240 pp.

Monachesi, G., Castelli, V., & Camassi, R. (2016). Aggiornamento delle conoscenze sul terremoto del 28 luglio 1799 nel sub-Appennino maceratese. Quaderni di Geofisica (INGV).

Monachesi G, Ladina C, Calamita C, Pantaleo D, Cattaneo M, Marzorati S, Frapiccini M, D'Alema E, Carannante S (2021) Beach Balls in central-eastern Italy. Istituto Nazionale di Geofisica e Vulcanologia (INGV).

Mori, F., Mendicelli, A., Moscatelli, M., Romagnoli, G., Peronace, E., & Naso, G. (2020). A new Vs30 map for Italy based on the seismic microzonation dataset. Engineering Geology, 275, 105745.

Motazedian, D., & Atkinson, G. M. (2005). Stochastic finite-fault modeling based on a dynamic corner frequency. Bulletin of the Seismological Society of America, 95(3), 995-1010.

Murphy, J. U., & O'brien, L. J. (1977). The correlation of peak ground acceleration amplitude with seismic intensity and other physical parameters. Bulletin of the Seismological Society of America, 67(3), 877-915.

Musson, R. M. W., & Jiménez, M. J. (2008). Macroseismic estimation of earthquake parameters.

Oliveti, I., Faenza, L., & Michelini, A. (2022). New reversible relationships between ground motion parameters and macroseismic intensity for Italy and their application in ShakeMap. Geophysical Journal International, 231(2), 1117-1137.

Oliveti, I., Faenza, L., Antonucci, A., Locati, M., Rovida, A., & Michelini, A. (2023). The ShakeMap Atlas of Historical Earthquakes in Italy: Configuration and Validation. Seismological Research Letters.

Oros, E., Placinta, A. O., Popa, M., Rogozea, M., & Paulescu, D. (2019, November). Attenuation of macroseismic intensity for crustal romanian earthquakes: Calibrating the bakun-wentworth's method. In IOP Conference Series: Earth and Environmental Science (Vol. 362, No. 1, p. 012026).

Panza, G. F., Cazzaro, R., & Vaccari, F. (1997). Correlation between macroseismic intensities and seismic ground motion parameters.

Park, S., & Elrick, S. (1998). Predictions of shear-wave velocities in southern California using surface geology. Bulletin of the Seismological Society of America, 88(3), 677-685.

Pasolini, C., Albarello, D., Gasperini, P., D'Amico, V., & Lolli, B. (2008). The attenuation of seismic intensity in Italy, Part II: Modeling and validation. Bulletin of the Seismological Society of America, 98(2), 692-708.

Patacca, E., Sartori, R., & Scandone, P. (1990). Tyrrhenian basin and Apenninic arcs: kinematic relations since late Tortonian times. Memorie della Società Geologica Italiana, 45, 425-451.

Patacca, E., Scandone, P., Di Luzio, E., Cavinato, G. P., & Parotto, M. (2008). Structural architecture of the central Apennines: Interpretation of the CROP 11 seismic profile from the Adriatic coast to the orographic divide. Tectonics, 27(3).

Pauselli, C., Barchi, M. R., Federico, C., Magnani, M. B., & Minelli, G. (2006). The crustal structure of the Northern Apennines (Central Italy): an insight by the CROP03 seismic line. American Journal of Science, 306(6), 428-450.

Pierantoni, P., Deiana, G., & Galdenzi, S. (2013). Stratigraphic and structural features of the Sibillini mountains (Umbria-Marche Apennines, Italy). Italian Journal of Geosciences, 132(3), 497-520.

Pizzi, A., & Galadini, F. (2009). Pre-existing cross-structures and active fault segmentation in the northern-central Apennines (Italy). Tectonophysics, 476(1-2), 304-319.

Pousse, G., Bonilla, L. F., Cotton, F., & Margerin, L. (2006). Nonstationary stochastic simulation of strong ground motion time histories including natural variability: Application to the K-net Japanese database. Bulletin of the Seismological Society of America, 96(6), 2103-2117.

Provost, L., & Scotti, O. (2020). QUake-MD: Open-source code to quantify uncertainties in magnitude–depth estimates of earthquakes from macroseismic intensities. Seismological Research Letters, 91(5), 2520-2530.

Roberts, G. P., & Michetti, A. M. (2004). Spatial and temporal variations in growth rates along active normal fault systems: an example from The Lazio–Abruzzo Apennines, central Italy. Journal of Structural Geology, 26(2), 339-376.

Rovida A., Locati M., Antonucci A., Camassi R. (a cura di) (2017). Archivio Storico Macrosismico Italiano (ASMI). Istituto Nazionale di Geofisica e Vulcanologia (INGV). https://doi.org/10.13127/asmi

Rovida A., Locati M., Camassi R., Lolli, B., Gasperini P., Antonucci A., 2022. Catalogo Parametrico dei Terremoti Italiani (CPTI15), versione 4.0. Istituto Nazionale di Geofisica e Vulcanologia (INGV). https:// doi. org/ 10. 13127/ cpti/ cpti15.4

Ruiz, J., Baumont, D., Bernard, P., & Berge-Thierry, C. (2007). New approach in the kinematic k− 2 source model for generating physical slip velocity functions. Geophysical Journal International, 171(2), 739-754.

Sbarra, P., Burrato, P., Tosi, P., Vannoli, P., De Rubeis, V., & Valensise, G. (2019). Inferring the depth of pre-instrumental earthquakes from macroseismic intensity data: a case-history from Northern Italy. Scientific Reports, 9(1), 15583.

Sbarra, P., Burrato, P., De Rubeis, V., Tosi, P., Valensise, G., Vallone, R., & Vannoli, P. (2023). Inferring the depth and magnitude of pre-instrumental earthquakes from intensity attenuation curves. Natural Hazards and Earth System Sciences, 23(3), 1007-1028.

Schmedes, J., Archuleta, R. J., & Lavallée, D. (2010). Correlation of earthquake source parameters inferred from dynamic rupture simulations. Journal of Geophysical Research: Solid Earth, 115(B3).

Sgobba, S., Lanzano, G., Pacor, F., Puglia, R., D'Amico, M., Felicetta, C., & Luzi, L. (2019). Spatial correlation model of systematic site and path effects for ground-motion fields in northern Italy. Bulletin of the Seismological Society of America, 109(4), 1419-1434.

Sgobba, S., Felicetta, C., Lanzano, G., Ramadan, F., D'Amico, M., & Pacor, F. (2021). NESS2. 0: An updated version of the worldwide dataset for calibrating and adjusting ground-motion models in near source. Bulletin of the Seismological Society of America, 111(5), 2358-2378.

Sibol, M. S., Bollinger, G. A., & Birch, J. B. (1987). Estimation of magnitudes in central and eastern North America using intensity and felt area. Bulletin of the Seismological Society of America, 77(5), 1635-1654.

Sieberg, A. H., & Gutenberg, B. (1923). Geologische, physikalische und angewandte Erdbebenkunde. G. Fischer.

Sørensen, M. B., Stromeyer, D., & Grünthal, G. (2010). Intensity attenuation in the Campania region, Southern Italy. Journal of seismology, 14, 209-223.

Spudich, P. A., & Hartzell, S. H. (1985). Predicting earthquake ground-motion time-histories. Evaluating Earthquake Hazards in the Los Angeles Region, 1360, 249-260.

Stover CW, Coffman JL (1993) Seismicity of the United States, 1568–1989 (revised). United States Government Printing Office, Washington

Strasser, F. O., Abrahamson, N. A., & Bommer, J. J. (2009). Sigma: Issues, insights, and challenges. Seismological Research Letters, 80(1), 40-56.

Stromeyer, D., & Grünthal, G. (2009). Attenuation relationship of macroseismic intensities in Central Europe. Bulletin of the Seismological Society of America, 99(2A), 554-565.

Thráinsson, H., & Kiremidjian, A. S. (2002). Simulation of digital earthquake accelerograms using the inverse discrete Fourier transform. Earthquake engineering & structural dynamics, 31(12), 2023-2048.

Tinsley, J. C., Fumal, T. E., & Ziony, J. I. (1985). Mapping Quaternary sedimentary deposits for areal variations in shaking response. Evaluating Earthquake Hazards in the Los Angeles Region—An Earth Science Perspective, 1360, 101-126.

Tondi, E. (2000). Geological analysis and seismic hazard in the central Apennines (Italy). Journal of Geodynamics, 29(3-5), 517-533.

Tondi, E., Jablonská, D., Volatili, T., Michele, M., Mazzoli, S., & Pierantoni, P. P. (2021). The Campotosto linkage fault zone between the 2009 and 2016 seismic sequences of central Italy: Implications for seismic hazard analysis. Bulletin, 133(7-8), 1679-1694.

Trifunac, M. D., & Brady, A. G. (1975a). On the correlation of seismic intensity scales with the peaks of recorded strong ground motion. Bulletin of the Seismological Society of America, 65(1), 139-162.

Trifunac, M. D., & Brady, A. G. (1975b). On correlation of seismoscope response with earthquake magnitude and Modified Mercalli Intensity. Bulletin of the Seismological Society of America, 65(2), 307-321.

Tumarkin, A. G., Archuleta, R. J., & Madariaga, R. (1994). Scaling relations for composite earthquake models. Bulletin of the Seismological Society of America, 84(4), 1279-1283.

Vezzani, L., Ghisetti, F., 1998. Carta geologica dell'Abruzzo: S.EL.CA. Firenze (Ed).

Zeng, Y., Anderson, J. G., & Yu, G. (1994). A composite source model for computing realistic synthetic strong ground motions. Geophysical Research Letters, 21(8), 725-728.

Wald, D. J., Quitoriano, V., Heaton, T. H., & Kanamori, H. (1999). Relationships between peak ground acceleration, peak ground velocity, and modified Mercalli intensity in California. Earthquake spectra, 15(3), 557-564.

Wald, D. J., & Allen, T. I. (2007). Topographic slope as a proxy for seismic site conditions and amplification. Bulletin of the Seismological Society of America, 97(5), 1379-1395.

Wald, D. J., Worden, C. B., Thompson, E. M., & Hearne, M. (2022). ShakeMap operations, policies, and procedures. Earthquake Spectra, 38(1), 756-777.

Worden, C. B., Thompson, E. M., Hearne, M., & Wald, D. J. (2020). ShakeMap Manual Online: technical manual, user's guide, and software guide, US Geological Survey.

Wells, D. L., & Coppersmith, K. J. (1994). New empirical relationships among magnitude, rupture length, rupture width, rupture area, and surface displacement. Bulletin of the seismological Society of America, 84(4), 974-1002.

Yong, A., Hough, S. E., Abrams, M. J., Cox, H. M., Wills, C. J., & Simila, G. W. (2008). Site characterization using integrated imaging analysis methods on satellite data of the Islamabad, Pakistan, region. Bulletin of the Seismological Society of America, 98(6), 2679-2693.

Yong, A., Hough, S. E., Iwahashi, J., & Braverman, A. (2012). A terrain-based site-conditions map of California with implications for the contiguous United States. Bulletin of the Seismological Society of America, 102(1), 114-128.

APPENDIX A

Historical and instrumental earthquakes affecting central Apennines from CPTI15 (Rovida et al., 2022).

Year	Latitude	Longitude	Mw	Imax	Epicentral zone
1269-09	43.566	13.567	5.6	VIII	Costa Anconetana
1279-04-	43.093	12.872	6.2	IX	Appennino umbro-
1315-12-	42.350	13.398	5.6	VIII	Aquilano
1328-12-	42.856	13.018	6.5	X	Valnerina
1352-12-	43.469	12.127	6.3	IX	Alta Valtiberina
1389-10-	43.527	12.298	6.0	IX	Alta Valtiberina
1458-04-	43.463	12.236	5.8	VIII-IX	Alta Valtiberina
1461-11-	42.308	13.542	6.5	X	Aquilano
1599-11-	42.723	13.021	6.0	IX	Valnerina
1639-10-	42.639	13.260	6.2	IX-X	Monti della Laga
1646-04-	42.615	13.247	5.9	IX	Monti della Laga
1690-12-	43.549	13.593	5.6	VIII	Costa Anconetana
1703-01-	42.708	13.071	6.9	XI	Valnerina
1703-02-	42.434	13.292	6.6	X	Aquilano
1706-11-	42.076	14.080	6.8	X-XI	Maiella
1719-06-	42.875	13.047	5.6	VIII	Valnerina
1730-05-	42.753	13.119	6.0	IX	Valnerina
1741-04-	43.424	13.005	6.1	IX	Fabrianese
1747-04-	43.204	12.769	6.0	IX	Appennino umbro-
1751-07-	43.225	12.739	6.4	X	Appennino umbro-
1762-10-	42.308	13.585	5.5	VIII	Aquilano
1781-06-	43.596	12.512	6.5	X	Cagliese
1789-09-	43.509	12.217	5.9	IX	Alta Valtiberina
1791-10-	42.950	12.861	5.6	VIII	Appennino umbro-
1799-07-	43.192	13.151	6.1	IX	Appennino
1815-09-	42.832	13.015	5.6	VIII	Valnerina
1832-01-	42.979	12.605	6.4	X	Valle Umbra
1854-02-	43.055	12.542	5.6	VIII	Valle Umbra
1859-08-	42.825	13.097	5.7	VIII-IX	Valnerina
1873-03-	43.088	13.244	5.8	VIII	Appennino
1879-02-	42.765	13.042	5.6	VIII	Valnerina
1915-01-	42.014	13.530	7.0	XI	Marsica
1916-11-	42.646	13.169	5.5	VIII	Alto Reatino
1917-04-	43.466	12.129	6.0	IX-X	Alta Valtiberina
1930-10-	43.689	13.385	5.8	VIII	Senigallia
1933-09-	42.079	14.093	5.9	IX	Maiella
1950-09-	42.546	13.457	5.7	VIII	Gran Sasso
1979-09-	42.729	12.956	5.8	VIII-IX	Valnerina
1984-04-	43.626	12.525	5.6	VII	Umbria
1997-09-	43.021	12.891	5.6	VII-VIII	Appennino umbro-
1997-09-	43.014	12.853	6.0	VIII-IX	Appennino umbro-

1997-10-	42.898	12.898	5.7	VII-VIII	Valnerina
2009-04-	42.308	13.510	5.5	VII	Aquilano
2009-04-	42.302	13.486	6.3	IX-X	Aquilano
2016-08-	42.698	13.233	6.0	X	Monti della Laga
2016-08-	42.792	13.150	5.5	VII-VIII	Valnerina
2016-10-	42.904	13.090	6.1	X	Valnerina
2016-10-	42.830	13.109	6.5	X	Valnerina
2017-01-	42.530	13.282	5.6	/	Aquilano
2017-01-	42.503	13.276	5.7	/	Aquilano

APPENDIX B

Dataset of Vs,30 for the calibration of the Vs,30 map of the Marche Region.

ID	Point_ID	Coord_X	Coord_Y	Survey_Type	Vs,30
1	043006L7MASW7	355381	4778044	MASW	493
2	043005L3MASW3	354820	4762026	MASW	610
3	043005L5MASW5	355639	4761437	MASW	573
4	043005L1MASW1	355292	4761920	MASW	612
5	043005L2MASW2	355033	4762020	MASW	510
6	043005L8MASW8	355605	4761074	MASW	647
7	043006L1MASW1	355419	4778459	MASW	579
8	043005L7MASW7	355759	4761306	MASW	549
9	044007L47MASW98	383971	4744502	MASW	485
10	109003L1MASW1	380810	4772163	MASW	594
11	044007L45MASW94	383807	4743745	MASW	405
12	044007L46MASW96	384076	4744288	MASW	369
13	109003L4MASW4	381651	4772345	MASW	380
14	109003L5MASW5	381286	4772117	MASW	457
15	109003L2MASW2	381588	4772233	MASW	370
16	109003L3MASW3	381709	4772099	MASW	559
17	044007L39MASW84	382125	4746640	MASW	614
18	044007L40MASW85	382189	4746404	MASW	431
19	044007L37MASW37	389069	4744520	MASW	515
20	044007L38MASW38	390520	4744692	MASW	431
21	044007L43MASW91	382092	4745423	MASW	416
22	044007L44MASW93	381987	4745350	MASW	430
23	044007L41MASW87	382083	4746101	MASW	399
24	044007L42MASW89	382478	4746301	MASW	639
25	044006L30MASW31	360914	4737194	MASW	411
26	044006L31MASW32	360850	4737047	MASW	577
27	044006L26MASW27	360001	4737415	MASW	381
28	044006L27MASW28	360313	4737349	MASW	400
29	044006L36MASW37	362013	4737089	MASW	483
30	044006L37MASW38	361706	4737004	MASW	398
31	044006L34MASW35	361702	4737129	MASW	698
32	044006L35MASW36	361882	4737122	MASW	373
33	044006L9MASW15	362209	4737069	MASW	342
34	044006L10MASW10	361305	4740040	MASW	324
35	044006L5MASW5	360547	4735238	MASW	481
36	044006L6MASW6	361695	4732060	MASW	600
37	044006L13MASW13	358339	4734713	MASW	610
38	044006L14MASW14	355623	4733269	MASW	541
39	044006L11MASW11	360473	4737498	MASW	413
40	044006L12MASW12	359578	4735621	MASW	488
41	044005L5MASW5	390935	4750556	MASW	467

42	044006L3MASW3	360749	4735780	MASW	383
43	044006L4MASW4	360922	4735460	MASW	492
44	044006L1MASW1	360168	4737378	MASW	362
45	044006L2MASW2	358151	4733822	MASW	486
46	043002L16REMI32	348642	4805854	REMI	373
47	043002L17MASW33	347463	4806530	MASW	289
48	043002L15REMI30	348533	4805703	REMI	329
49	043002L16MASW31	348642	4805854	MASW	373
50	043002L18REMI36	347095	4807550	REMI	429
51	044005L1MASW1	390981	4750582	MASW	385
52	043002L17REMI34	347463	4806530	REMI	265
53	043002L18MASW35	347095	4807550	MASW	429
54	043007L15MASW15	342285	4777021	MASW	317
55	043007L16MASW16	342854	4778479	MASW	225
56	043007L13MASW13	342861	4776841	MASW	301
57	043007L7MASW7	342041	4779008	MASW	239
58	043007L8MASW8	343016	4778242	MASW	269
59	044007L4MASW55	383221	4746170	MASW	662
60	043007L6MASW6	341859	4778885	MASW	262
61	043007L12MASW12	342443	4777169	MASW	389
62	043007L9MASW9	342650	4777815	MASW	294
63	043007L10MASW10	342616	4778023	MASW	261
64	044006L60MASW61	356354	4732836	MASW	474
65	044006L61MASW62	356920	4733036	MASW	623
66	044006L58MASW59	355959	4733048	MASW	447
67	044006L59MASW60	356089	4732910	MASW	572
68	044007L2MASW51	383027	4746147	MASW	734
69	044007L3MASW53	387436	4745329	MASW	334
70	044006L62MASW63	357038	4732965	MASW	432
71	044007L1MASW49	382887	4746020	MASW	815
72	044006L43MASW44	360715	4735824	MASW	392
73	044006L45MASW46	360874	4735694	MASW	332
74	044006L39MASW40	361533	4736648	MASW	293
75	044006L41MASW42	361467	4736632	MASW	391
76	044006L54MASW55	358622	4734370	MASW	512
77	044006L57MASW58	355769	4733084	MASW	532
78	044006L46MASW47	359368	4735089	MASW	443
79	044006L47MASW48	358573	4734846	MASW	338
80	109002L2MASW2	366379	4760131	MASW	444
81	109002L1MASW1	366537	4760153	MASW	498
82	109002L5MASW5	365600	4759262	MASW	515
83	109002L6MASW6	366047	4760129	MASW	749
84	109002L3MASW3	366608	4759925	MASW	455
85	109002L4MASW4	366701	4760050	MASW	520
86	044001L33MASW35	369782	4736323	MASW	462
87	044001L32MASW34	369963	4736377	MASW	513
88	044001L37MASW39	370314	4733558	MASW	463

89	044001L30MASW32	370255	4736634	MASW	458
90	042011L26REMI26	340128	4829602	REMI	289
91	044001L19MASW19	369878	4736318	MASW	517
92	044001L17MASW17	369909	4736369	MASW	620
93	044001L18MASW23	369958	4736372	MASW	612
94	043002L12REMI24	348442	4806244	REMI	343
95	043002L13MASW25	349240	4806454	MASW	629
96	043002L11REMI22	340722	4806146	REMI	338
97	043002L12MASW23	348442	4806244	MASW	343
98	043002L14REMI28	349104	4806290	REMI	694
99	043002L15MASW29	348533	4805703	MASW	329
100	043002L13REMI26	349240	4806454	REMI	629
101	043002L14MASW27	349104	4806290	MASW	694
102	043002L8REMI16	348762	4804999	REMI	345
103	043002L9MASW17	348697	4805894	MASW	385
104	043002L7REMI14	348783	4805366	REMI	271
105	043002L8MASW15	348762	4804999	MASW	345
106	043002L10REMI20	348535	4806113	REMI	616
107	043002L11MASW21	340722	4806146	MASW	338
108	043002L9REMI18	348697	4805894	REMI	385
109	043002L10MASW19	348535	4806113	MASW	616
110	043002L4REMI8	346188	4809397	REMI	257
111	043002L5MASW9	346814	4808490	MASW	407
112	043002L3REMI6	346114	4809339	REMI	334
113	043002L4MASW7	346188	4809397	MASW	257
114	043002L6REMI12	346812	4808657	REMI	342
115	043002L7MASW13	348783	4805366	MASW	271
116	043002L5REMI10	346814	4808490	REMI	407
117	043002L6MASW11	346812	4808657	MASW	342
118	043002L1MASW1	345475	4809443	MASW	431
119	109002L7MASW7	366307	4760007	MASW	451
120	109002L8MASW8	365992	4759808	MASW	500
121	043002L2REMI4	345554	4809353	REMI	408
122	043002L3MASW5	346114	4809339	MASW	334
123	043002L1REMI2	345475	4809443	REMI	431
124	043002L2MASW3	345554	4809353	MASW	408
125	043009L30MASW30	345282	4784364	MASW	322
126	043009L31MASW31	342300	4786048	MASW	491
127	043009L28MASW28	340559	4786214	MASW	404
128	043009L29MASW29	340344	4786258	MASW	373
129	042010L11MASW11	384551	4813088	MASW	333
130	042010L12MASW12	381936	4811496	MASW	294
131	043009L32MASW32	342214	4785838	MASW	285
132	043009L33MASW33	342123	4785588	MASW	533
133	043009L22MASW22	341655	4785875	MASW	271
134	043009L23MASW23	341805	4785866	MASW	282
135	043009L15MASW15	344372	4786974	MASW	659

136	043009L26MASW26	341906	4785765	MASW	263
137	043009L27MASW27	341662	4785298	MASW	337
138	043009L24MASW24	341905	4785801	MASW	417
139	043009L25MASW25	342091	4785942	MASW	480
140	043010L9MASW9	350260	4749925	MASW	538
141	043010L10MASW10	349065	4751522	MASW	466
142	043010L7MASW7	350711	4750327	MASW	461
143	043010L8MASW8	350723	4750501	MASW	598
144	043010L13MASW13	349112	4749650	MASW	463
145	043009L10MASW10	341565	4786276	MASW	316
146	043010L11MASW11	350124	4749508	MASW	417
147	043010L12MASW12	349138	4750742	MASW	400
148	041066P111DH157	299398	4837301	DH	556
149	041050P201DH250	330638	4846764	DH	333
150	041067P126DH167	309511	4844550	DH	534
151	043010L6MASW6	349006	4748815	MASW	461
152	041066P114DH162	298994	4837918	DH	495
153	041067P120DH160	309920	4844133	DH	486
154	042011L20REMI20	336867	4827994	REMI	289
155	042011L21REMI21	337812	4829233	REMI	259
156	042011L19REMI19	336702	4828910	REMI	198
157	042011L25REMI25	339631	4830148	REMI	270
158	042011L22REMI22	338296	4828995	REMI	281
159	042011L23REMI23	337894	4829678	REMI	276
160	042011L13REMI13	338785	4830786	REMI	298
161	042011L10REMI10	337178	4830990	REMI	262
162	042011L11REMI11	337499	4831267	REMI	319
163	042011L4REMI4	336678	4830076	REMI	307
164	042011L5REMI5	336499	4830168	REMI	356
165	042011L7REMI7	337095	4830275	REMI	324
166	042010L13MASW13	384487	4814217	MASW	225
167	042010L14MASW14	384247	4814197	MASW	243
168	042010L22MASW22	382647	4813260	MASW	393
169	042010L21MASW21	382334	4812890	MASW	324
170	044006P204DH205	360543	4737495	DH	512
171	044006P205DH206	361187	4739828	DH	475
172	044006P202DH203	360784	4737257	DH	612
173	044006P203DH204	360434	4737395	DH	335
174	044006P208DH209	358513	4734733	DH	352
175	044006P209DH210	357913	4733648	DH	439
176	044006P206DH207	360806	4735637	DH	308
177	109002P209DH280	366180	4759972	DH	395
178	044006P236DH239	360413	4737336	DH	327
179	044006P201DH202	360682	4736937	DH	753
180	044006P231DH232	360964	4738626	DH	380
181	044006P233DH235	359463	4735558	DH	514
182	042010P227DH315	382727	4815735	DH	233

183	042045P9512MASW1	354809	4843673	MASW	303
184	041067P9513MASW1	312213	4847536	MASW	459
185	044001P89DH103	370271	4736637	DH	395
186	044001P91ESAC_SPAC105	370319	4736734	ESAC_SPAC	458
187	042002P9504MASW1	376425	4828924	MASW	249
188	042011P9505DH1	339799	4831608	DH	319
189	042002P9501MASW1	377039	4828272	MASW	296
190	042002P9502MASW1	377003	4828532	MASW	221
191	042002P9508MASW1	377633	4829114	MASW	265
192	042002P9510MASW1	376107	4829417	MASW	191
193	042002P9506MASW1	377472	4828994	MASW	233
194	042002P9507MASW1	376223	4829212	MASW	227
195	109034P95DH113	397945	4792308	DH	239
196	042045P489DH628	356500	4842358	DH	253
197	109032P15SR37	390689	4772964	SR	424
198	041034P105DH125	325627	4844764	DH	520
199	042045P79DH176	356824	4841306	DH	221
200	042045P80DH178	356420	4841657	DH	279
201	042045P75DH168	361983	4837290	DH	230
202	042018P325DH403	369986	4830411	DH	231
203	042018P291DH362	367738	4833708	DH	385
204	042018P329DH408	371566	4830203	DH	270
205	043047P485DH622	353060	4787460	DH	234
206	043006P387DH388	355579	4777963	DH	575
207	043035P61DH76	371776	4768350	DH	395
208	043054P236DH321	362496	4796846	DH	321
209	043055P108DH158	367914	4783401	DH	444
210	043052P313DH314	333581	4770977	DH	578
211	044054P6065DH126	393751	4754272	DH	396
212	044054P6066DH127	394069	4753713	DH	323
213	044073P6069DH130	376689	4749101	DH	463
214	044007P7032MASW40	382578	4745576	MASW	504
215	044064P6067DH128	375359	4746289	DH	377
216	044065P6068DH129	382356	4756589	DH	693
217	044032P6058DH119	386394	4760253	DH	375
218	044034P6059DH120	385078	4758958	DH	678
219	044021P6056DH117	376885	4758288	DH	439
220	044027P6057DH118	391469	4744123	DH	390
221	044013P6049DH110	396083	4750250	DH	350
222	044014P6050DH111	397694	4747910	DH	375
223	044020P6054DH115	388371	4742013	DH	528
224	044021P6055DH116	376897	4758076	DH	683
225	044016P6186DH244	393040	4759926	DH	555
226	044020P6053DH114	388378	4743451	DH	302
227	044011P5942DH5	394347	4747696	DH	230
228	044011P5945DH8	394530	4747135	DH	336
229	044012P6048DH109	388281	4755149	DH	304

230	044011P5943DH6	394168	4747658	DH	417
231	044011P5944DH7	394133	4746030	DH	352
232	109026P5982DH43	376835	4775415	DH	321
233	109029P5983DH44	386444	4765296	DH	318
234	109020P5980DH41	380624	4763940	DH	448
235	109021P5981DH42	384251	4764842	DH	358
236	109039P5986DH47	370647	4762921	DH	421
237	109033P9458REMI1	401902	4781718	REMI	336
238	109036P5984DH45	377145	4764693	DH	448
239	109038P5985DH46	377168	4770871	DH	438
240	109013P5975DH36	375882	4777551	DH	374
241	109014P6160DH218	374166	4760849	DH	988
242	109011P5973DH34	375959	4778268	DH	465
243	109012P5974DH35	382468	4769351	DH	323
244	109017P5978DH39	381078	4776633	DH	364
245	109019P5979DH40	380257	4767211	DH	474
246	044007P7044MASW52	390520	4744692	MASW	431
247	042013P5987DH48	336533	4798063	DH	435
248	044007P7043MASW51	389069	4744520	MASW	515
249	109005P5972DH33	375658	4773871	DH	470
250	044007P7035MASW43	384156	4745538	MASW	631
251	044007P7041MASW49	387395	4744292	MASW	553
252	044007P7039MASW47	384786	4744850	MASW	410
253	043021P6011DH72	364748	4769645	DH	393
254	043019P6009DH70	332045	4783610	DH	168
255	043020P6010DH71	342944	4787021	DH	509
256	043023P6015DH76	374376	4795201	DH	355
257	043022P6013DH74	371405	4780512	DH	472
258	043023P6014DH75	373358	4795070	DH	331
259	043008P5998DH59	358962	4776906	DH	457
260	043007P5995DH56	342853	4776819	DH	306
261	043007P5996DH57	342894	4777710	DH	805
262	043017P6007DH68	349793	4766370	DH	320
263	043015P6005DH66	377256	4790662	DH	406
264	043016P6006DH67	333255	4790784	DH	531
265	042017P6166DH224	329920	4799840	DH	522
266	043005P5991DH52	355737	4761266	DH	583
267	043006P5992DH53	355579	4777963	DH	575
268	043004P5989DH50	357067	4780794	DH	326
269	043011P6000DH61	355766	4773030	DH	502
270	043012P6001DH62	354953	4804123	DH	390
271	043015P6004DH65	378443	4789563	DH	325
272	043012P6002DH63	360128	4800657	DH	628
273	043014P6003DH64	366335	4780212	DH	560
274	043058P6043DH104	343926	4769531	DH	455
275	044005P6176DH234	390954	4750553	DH	334
276	043054P6039DH100	362496	4796846	DH	321

277	043054P6040DH101	364342	4793793	DH	410
278	043049P6175DH233	359262	4762640	DH	374
279	043048P6030DH91	367604	4774854	DH	576
280	043053P5938DH1	361192	4785289	DH	375
281	043051P6033DH94	352938	4782072	DH	438
282	043052P6034DH95	333581	4770977	DH	578
283	043040P6023DH84	344793	4803773	DH	568
284	043041P6024DH85	365935	4791887	DH	492
285	043039P6022DH83	336344	4782578	DH	294
286	043046P6028DH89	363586	4774069	DH	473
287	043046P6029DH90	363200	4774268	DH	510
288	043041P6025DH86	363418	4791598	DH	345
289	043046P6027DH88	363499	4774180	DH	445
290	043032P6019DH80	373151	4765603	DH	276
291	043038P6170DH228	340967	4767393	DH	716
292	043038P6171DH229	341025	4767204	DH	613
293	043036P6021DH82	375555	4786579	DH	399
294	041067L65MASW68	308708	4843462	MASW	655
295	041012L1MASW1	316670	4854387	MASW	486
296	041067L63MASW66	312638	4853039	MASW	371
297	041067L64MASW67	307954	4851785	MASW	383
298	041012L4MASW4	316662	4855314	MASW	331
299	041012L2MASW2	318183	4855027	MASW	418
300	041012L3MASW3	316020	4853781	MASW	513
301	041067L46MASW48	310403	4847838	MASW	477
302	041067L47MASW49	310678	4847918	MASW	585
303	041067L44MASW46	304766	4842048	MASW	472
304	041067L45MASW47	305220	4842156	MASW	570
305	041067L55MASW57	307064	4841984	MASW	496
306	041067L58MASW61	309064	4844694	MASW	329
307	041067L48MASW50	309783	4846574	MASW	440
308	041067L49MASW51	309015	4844948	MASW	543
309	041004L36REMI36	333023	4837677	REMI	348
310	041004L35REMI35	333079	4837580	REMI	309
311	041066L1MASW1	296617	4839063	MASW	623
312	041064L1MASW1	306912	4857356	MASW	251
313	041065L1MASW1	319915	4863246	MASW	295
314	041059L5MASW6	297548	4850671	MASW	598
315	041061L1MASW1	320327	4816867	MASW	380
316	041004L32REMI32	329631	4841365	REMI	330
317	041065L2MASW2	319940	4862976	MASW	287
318	041065L3MASW3	319148	4862072	MASW	412
319	041058L1MASW1	328416	4840900	MASW	337
320	041058L3MASW3	328376	4838564	MASW	395
321	041059L3MASW4	298373	4850546	MASW	325
322	041059L4MASW5	298706	4850077	MASW	447
323	041059L1MASW1	298477	4850981	MASW	343

324	041059L2MASW3	299277	4853248	MASW	607
325	041054L10MASW10	334382	4830005	MASW	371
326	041054L12MASW12	334169	4830047	MASW	458
327	041054L8MASW8	334431	4830211	MASW	357
328	041054L9MASW9	332086	4831143	MASW	290
329	041057L4MASW4	291049	4837839	MASW	594
330	041057L2MASW2	291459	4838157	MASW	504
331	041067L38MASW40	308494	4842590	MASW	445
332	041067L39MASW41	308578	4845530	MASW	502
333	041067L36MASW38	306984	4841743	MASW	417
334	041067L37MASW39	303788	4848476	MASW	603
335	041067L42MASW44	315304	4840049	MASW	418
336	041067L43MASW45	314768	4840068	MASW	617
337	041067L40MASW42	309906	4843242	MASW	352
338	041067L41MASW43	312043	4851769	MASW	447
339	041067L30MASW31	309120	4844402	MASW	695
340	041067L31MASW32	309098	4844436	MASW	690
341	041067L20REMI21	309445	4844959	REMI	793
342	041067L29MASW30	308705	4845745	MASW	864
343	041067L34MASW35	307013	4847333	MASW	480
344	041067L35MASW37	308569	4846911	MASW	322
345	041067L32MASW33	309509	4843146	MASW	454
346	041067L33MASW34	314852	4839881	MASW	560
347	041067L12MASW12	310101	4843821	MASW	602
348	041067L15MASW15	311449	4846953	MASW	309
349	041067L10MASW10	310263	4843217	MASW	706
350	041067L11MASW11	310071	4843760	MASW	304
351	041067L18MASW19	309642	4844690	MASW	556
352	041067L19MASW20	309364	4845106	MASW	396
353	041067L16MASW16	311490	4847016	MASW	406
354	041067L17MASW17	309280	4843845	MASW	391
355	041066L6MASW6	300079	4838971	MASW	576
356	041066L2MASW2	299569	4837940	MASW	478
357	041066L13MASW13	300440	4836814	MASW	276
358	041067L1MASW1	311203	4844551	MASW	753
359	041066L9MASW9	300717	4837504	MASW	713
360	041040L4MASW4	330269	4842635	MASW	354
361	041040L5MASW5	337031	4839262	MASW	264
362	041040L2MASW2	336178	4839293	MASW	311
363	041040L3MASW3	332100	4841854	MASW	458
364	041041L1MASW1	298256	4841094	MASW	484
365	041041L2MASW2	299011	4841236	MASW	601
366	041040L6MASW6	330869	4842948	MASW	338
367	041040L7MASW7	336165	4839666	MASW	473
368	041038L36REMI36	340685	4841540	REMI	268
369	041038L37REMI37	343625	4841760	REMI	211
370	041038L40REMI40	344427	4840560	REMI	291

371	041040L1MASW1	334809	4838387	MASW	392
372	041038L39REMI39	344603	4840730	REMI	237
373	041038L28REMI28	341548	4839840	REMI	216
374	041038L32REMI32	342357	4839570	REMI	198
375	041038L30REMI30	340613	4839190	REMI	219
376	041038L21REMI21	342516	4839600	REMI	286
377	041038L18SASW18	342485	4839210	SASW	251
378	041038L23REMI23	342337	4839240	REMI	255
379	041054L2MASW2	334645	4830297	MASW	419
380	041054L3MASW3	331970	4828972	MASW	573
381	041052L6MASW6	337790	4841910	MASW	459
382	041052L9MASW9	337275	4842940	MASW	353
383	041054L6MASW6	331786	4830514	MASW	355
384	041054L7MASW7	329675	4828256	MASW	516
385	041054L4MASW4	334255	4829677	MASW	434
386	041054L5MASW5	335325	4829972	MASW	393
387	041050L4MASW4	332945	4847176	MASW	372
388	041052L1MASW1	337283	4843290	MASW	369
389	041052L4MASW4	337558	4842300	MASW	384
390	041052L5MASW5	336588	4842200	MASW	284
391	041052L2MASW2	336555	4841000	MASW	531
392	041052L3MASW3	340714	4841600	MASW	330
393	041047L1MASW1	291639	4844434	MASW	514
394	041047L2MASW2	290472	4844107	MASW	325
395	041045L8MASW8	317094	4850284	MASW	367
396	041045L9MASW9	315430	4851656	MASW	387
397	041049L2MASW2	299297	4829191	MASW	795
398	041047L3MASW3	290329	4844019	MASW	726
399	041047L4MASW4	292672	4844289	MASW	432
400	041045L2MASW2	316445	4850946	MASW	545
401	041045L3MASW3	317773	4849132	MASW	221
402	041041L3MASW3	299269	4841462	MASW	515
403	041045L1MASW1	315934	4850709	MASW	338
404	041045L6MASW6	317164	4850945	MASW	413
405	041045L7MASW7	316628	4851045	MASW	509
406	041045L4MASW4	315913	4850667	MASW	433
407	041045L5MASW5	315871	4850688	MASW	423
408	041029L13MASW13	351955	4845727	MASW	419
409	041029L14MASW14	349015	4846439	MASW	372
410	041029L5MASW5	347525	4844447	MASW	346
411	041029L18MASW18	350081	4847883	MASW	348
412	041029L15MASW15	348037	4847330	MASW	295
413	041029L16MASW16	351323	4846786	MASW	527
414	041028L4MASW4	335707	4838000	MASW	396
415	041028L5MASW5	336859	4836958	MASW	423
416	041028L2MASW2	338341	4836738	MASW	290
417	041028L3MASW3	336939	4835180	MASW	232

418	041029L2MASW2	350000	4847660	MASW	452
419	041029L4MASW4	346847	4845129	MASW	586
420	041028L6MASW6	336861	4836712	MASW	472
421	041027L3MASW3	327661	4850923	MASW	395
422	041027L4MASW4	327278	4851361	MASW	467
423	041027L1MASW1	326982	4853554	MASW	512
424	041027L2MASW2	328288	4851800	MASW	419
425	041028L1MASW1	336485	4838003	MASW	435
426	041027L5MASW5	327510	4851644	MASW	726
427	041027L6MASW6	326934	4853113	MASW	578
428	041023L4MASW4	294409	4855106	MASW	609
429	041020L6MASW6	320546	4867038	MASW	371
430	041020L7MASW7	319062	4868209	MASW	235
431	041025L3MASW3	286714	4835897	MASW	638
432	041025L4MASW4	285004	4836399	MASW	646
433	041025L1MASW1	285162	4836357	MASW	664
434	041025L2MASW2	285645	4835522	MASW	987
435	041038L10REMI10	342383	4841060	REMI	202
436	041038L16REMI16	343105	4839600	REMI	340
437	041038L17REMI17	342739	4839190	REMI	206
438	041038L3REMI3	343633	4840420	REMI	263
439	041034L1MASW1	327865	4842640	MASW	490
440	041034L2MASW2	327070	4842350	MASW	529
441	041032L1MASW1	326540	4855523	MASW	319
442	041032L2MASW2	321977	4852370	MASW	373
443	041034L5REMI5	325525	4844620	REMI	316
444	041038L1REMI1	344992	4841640	REMI	289
445	041034L3MASW3	327665	4842560	MASW	540
446	041034L4MASW4	328127	4843210	MASW	436
447	041029L21MASW21	350567	4845386	MASW	354
448	041030L1MASW1	309214	4853782	MASW	528
449	041029L19MASW19	350479	4847325	MASW	451
450	041029L20MASW20	349746	4848337	MASW	364
451	041030L4MASW4	312135	4854256	MASW	300
452	041030L5MASW5	312475	4854407	MASW	367
453	041030L2MASW2	312179	4854518	MASW	372
454	041030L3MASW3	307960	4853374	MASW	291
455	041013L37MASW37	341282	4853445	MASW	394
456	041013L38MASW38	336921	4852517	MASW	422
457	041013L35MASW35	338547	4856759	MASW	312
458	041013L36MASW36	338219	4856209	MASW	341
459	041013L41MASW41	342241	4854086	MASW	476
460	041014L1MASW1	309816	4839197	MASW	463
461	041013L39MASW39	339133	4857718	MASW	361
462	041013L40MASW40	340660	4856170	MASW	386
463	041013L29MASW29	348315	4849217	MASW	319
464	041013L30MASW30	347948	4848711	MASW	266

465	041013L27MASW27	348176	4849806	MASW	275
466	041013L33MASW33	331661	4854356	MASW	321
467	041013L34MASW34	338921	4857569	MASW	463
468	041013L31MASW31	348648	4848289	MASW	289
469	041013L32MASW32	348790	4848844	MASW	294
470	041013L21MASW21	340696	4857094	MASW	317
471	041013L22MASW22	341382	4855874	MASW	395
472	041013L19MASW19	340090	4857149	MASW	350
473	041013L20MASW20	336505	4851935	MASW	476
474	041013L25MASW25	342218	4855724	MASW	329
475	041013L26MASW26	343120	4855216	MASW	345
476	041013L23MASW23	341952	4855640	MASW	378
477	041013L24MASW24	342081	4855515	MASW	309
478	041013L13MASW13	339602	4855825	MASW	312
479	041013L14MASW14	340154	4855457	MASW	568
480	041013L11MASW11	339403	4855355	MASW	411
481	041013L12MASW12	339007	4856012	MASW	360
482	041013L17MASW17	340423	4855870	MASW	446
483	041013L18MASW18	340727	4856070	MASW	438
484	041013L15MASW15	340542	4855622	MASW	310
485	041017L5MASW5	287069	4850777	MASW	235
486	041017L3MASW3	287226	4850692	MASW	483
487	041017L4MASW4	287383	4848166	MASW	480
488	041020L4MASW4	320897	4867067	MASW	286
489	041020L5MASW5	320723	4867043	MASW	394
490	041020L2MASW2	320529	4867686	MASW	437
491	041020L3MASW3	321132	4867655	MASW	617
492	041016L1MASW1	330435	4833884	MASW	302
493	041016L2MASW2	331037	4833190	MASW	371
494	041015L7MASW7	325276	4841142	MASW	424
495	041015L11MASW11	323779	4839652	MASW	339
496	041017L1MASW1	288623	4849038	MASW	455
497	041017L2MASW2	289009	4849056	MASW	517
498	041014L12MASW12	310961	4840707	MASW	658
499	041014L10MASW10	306730	4836223	MASW	429
500	041014L11MASW11	310121	4839066	MASW	603
501	041015L2MASW2	326596	4836196	MASW	486
502	041015L6MASW6	325353	4841084	MASW	363
503	041014L14MASW14	309761	4839634	MASW	390
504	041014L15MASW15	309855	4839607	MASW	398
505	041014L4MASW4	310651	4838123	MASW	380
506	041014L5MASW5	310225	4837468	MASW	424
507	041014L2MASW2	310313	4838338	MASW	573
508	041014L3MASW3	318677	4837616	MASW	377
509	041014L8MASW8	306110	4836035	MASW	421
510	041014L9MASW9	309657	4839682	MASW	384
511	041014L6MASW6	309241	4838187	MASW	388

512	041014L7MASW7	310904	4840720	MASW	694
513	041008L1MASW1	311377	4813865	MASW	597
514	041008L2MASW2	308355	4815983	MASW	492
515	041007L18MASW18	309286	4824309	MASW	509
516	041007L19MASW19	310078	4823660	MASW	586
517	041008L5MASW9	311118	4813506	MASW	471
518	041008L6MASW10	307085	4811838	MASW	640
519	041008L3MASW5	310845	4813536	MASW	372
520	041008L4MASW7	308146	4816645	MASW	432
521	041007L12MASW12	310400	4824926	MASW	784
522	041007L13MASW13	310698	4824869	MASW	626
523	041007L10MASW10	310182	4825661	MASW	507
524	041007L11MASW11	310207	4825033	MASW	750
525	041007L16MASW16	309826	4824120	MASW	552
526	041007L17MASW17	309534	4823916	MASW	590
527	041007L14MASW14	310865	4824763	MASW	271
528	041007L15MASW15	310797	4824811	MASW	310
529	041007L4MASW4	311135	4826378	MASW	385
530	041007L5MASW5	311300	4826667	MASW	528
531	041007L2MASW2	310992	4824099	MASW	408
532	041007L3MASW3	310856	4824288	MASW	302
533	041007L8MASW8	311810	4828313	MASW	520
534	041007L9MASW9	311242	4827556	MASW	449
535	041007L6MASW6	312133	4828137	MASW	638
536	041007L7MASW7	311326	4826801	MASW	628
537	041005L6MASW6	289031	4844225	MASW	352
538	041006L1MASW1	281790	4837778	MASW	411
539	041005L4MASW4	288359	4844448	MASW	423
540	041005L5MASW5	288331	4844616	MASW	348
541	041006L4MASW4	281822	4837448	MASW	489
542	041007L1MASW1	310980	4823964	MASW	478
543	041006L2MASW2	277246	4836922	MASW	608
544	041013L5MASW5	340120	4852081	MASW	323
545	041013L6MASW6	340157	4852310	MASW	496
546	041013L3MASW3	337064	4851639	MASW	362
547	041013L9MASW9	338608	4855071	MASW	294
548	041013L10MASW10	339183	4855175	MASW	416
549	041013L7MASW7	338899	4850406	MASW	470
550	041013L8MASW8	339463	4854765	MASW	404
551	041037L8MASW8	333123	4844570	MASW	488
552	041037L9MASW9	334641	4846330	MASW	384
553	041037L6MASW6	333736	4845280	MASW	432
554	041037L7MASW7	333250	4845172	MASW	489
555	041013L1MASW1	335239	4851322	MASW	232
556	041013L2MASW2	336862	4851811	MASW	349
557	041062L1MASW1	327972	4847029	MASW	422
558	041009L11MASW11	287076	4850752	MASW	235

559	041037L1MASW1	332976	4845533	MASW	496
560	041009L9MASW9	285809	4851067	MASW	436
561	041009L10MASW10	284914	4850875	MASW	434
562	041037L4MASW4	333437	4844617	MASW	488
563	041037L5MASW5	334504	4844450	MASW	351
564	041037L2MASW2	334231	4844658	MASW	368
565	041037L3MASW3	335846	4845414	MASW	420
566	041008L9MASW15	308502	4814059	MASW	594
567	041008L10MASW16	307955	4817193	MASW	527
568	041008L7MASW12	308108	4816930	MASW	425
569	041008L8MASW13	307478	4812144	MASW	573
570	041008L13MASW19	310867	4814051	MASW	481
571	041008L14MASW21	311249	4813777	MASW	565
572	041008L11MASW17	309633	4814769	MASW	346
573	041008L12MASW18	310185	4814495	MASW	440
574	043028L1MASW1	389504	4796844	MASW	358
575	043026L3MASW3	374870	4801417	MASW	368
576	043026L6MASW7	374391	4799939	MASW	351
577	043030L7MASW7	385576	4802330	MASW	238
578	043030L8MASW8	385172	4802133	MASW	269
579	043030L4MASW4	385557	4802581	MASW	444
580	043013L1MASW2	397412	4795703	MASW	300
581	043013L2MASW4	396093	4797518	MASW	369
582	043003L1MASW1	366093	4802263	MASW	307
583	043003L2MASW2	365937	4802836	MASW	255
584	043013L5MASW7	394651	4794409	MASW	516
585	043026L1MASW1	375468	4800492	MASW	407
586	043013L3MASW5	394680	4794006	MASW	552
587	043013L4MASW6	394569	4794308	MASW	540
588	109004L2MASW2	402806	4770828	MASW	369
589	109004L10MASW10	405437	4770007	MASW	340
590	042050L8MASW8	347841	4840271	MASW	416
591	109004L1MASW1	402044	4770528	MASW	516
592	109023L3MASW3	386399	4783548	MASW	319
593	109032L1MASW1	388228	4776234	MASW	439
594	109023L1MASW1	382826	4785509	MASW	337
595	109023L2MASW2	384745	4783466	MASW	328
596	042050L1MASW1	351204	4836327	MASW	368
597	042050L2MASW2	346121	4843194	MASW	408
598	042049L3MASW3	355354	4811173	MASW	292
599	042049L4MASW4	356405	4813906	MASW	350
600	042050L6MASW6	348846	4835847	MASW	342
601	042050L7MASW7	346213	4843033	MASW	368
602	042050L3MASW3	346517	4840339	MASW	235
603	042050L4MASW4	346927	4835181	MASW	323
604	041002L3MASW3	297107	4824517	MASW	701
605	041002L4MASW4	291444	4826017	MASW	567

606	041002L1MASW1	296740	4825384	MASW	682
607	041002L2MASW2	297123	4824541	MASW	391
608	041005L2MASW2	288392	4843900	MASW	476
609	041002L5MASW5	297846	4823944	MASW	473
610	041005L1MASW1	288615	4843827	MASW	477
611	041001L1MASW1	312198	4832640	MASW	487
612	043044L9MASW9	382754	4805680	MASW	313
613	043044L11MASW11	383748	4806218	MASW	278
614	041001L7MASW7	312144	4832910	MASW	446
615	041001L8MASW8	315554	4834180	MASW	576
616	041001L4MASW4	311991	4832460	MASW	692
617	041001L6MASW6	313930	4834460	MASW	598
618	043042L5MASW5	389571	4808337	MASW	473
619	043043L1MASW1	386705	4803697	MASW	377
620	043042L3MASW3	391559	4806904	MASW	250
621	043042L4MASW4	392532	4807305	MASW	353
622	043044L7MASW7	382569	4806606	MASW	330
623	043044L8MASW8	383291	4806281	MASW	393
624	043044L5MASW5	383612	4807338	MASW	233
625	043044L6MASW6	348873	4809814	MASW	244
626	043031L3MASW3	384916	4790403	MASW	230
627	043031L1MASW1	386229	4790918	MASW	268
628	043031L2MASW2	385659	4790370	MASW	212
629	043042L1MASW1	390522	4813258	MASW	527
630	043042L2MASW2	390797	4806990	MASW	289
631	043031L7MASW7	384999	4789423	MASW	224
632	043031L9MASW9	385532	4790143	MASW	264
633	042044L2MASW2	326775	4810800	MASW	1110
634	042044L3MASW3	327164	4807615	MASW	783
635	042043L5MASW5	363931	4816198	MASW	310
636	042044L1MASW1	325682	4812904	MASW	576
637	042045L6MASW6	361422	4836719	MASW	276
638	042045L1MASW1	354116	4840503	MASW	217
639	042045L4MASW4	355541	4842990	MASW	255
640	042041L7MASW7	352391	4821524	MASW	331
641	042041L6MASW6	351772	4822408	MASW	276
642	042043L3MASW3	363500	4817536	MASW	305
643	042043L4MASW4	365035	4816271	MASW	314
644	042043L1MASW1	363786	4817067	MASW	405
645	042043L2MASW2	363353	4817313	MASW	299
646	042035L3MASW3	350274	4833065	MASW	270
647	042035L5MASW5	349053	4830388	MASW	250
648	042035L1MASW1	348509	4832534	MASW	289
649	042035L2MASW2	349326	4831917	MASW	301
650	042038L3MASW3	367797	4821289	MASW	226
651	042041L3MASW3	354836	4826871	MASW	271
652	042038L1MASW1	367252	4821183	MASW	285

653	042038L2MASW2	368814	4820580	MASW	318
654	042034L33MASW33	376939	4814892	MASW	284
655	042034L31MASW31	376481	4815412	MASW	253
656	042034L32MASW32	376847	4814663	MASW	243
657	042034L38MASW38	378445	4816217	MASW	257
658	042034L36MASW36	376941	4816190	MASW	366
659	042046L5MASW5	341279	4823458	MASW	427
660	042046L6MASW6	340792	4822682	MASW	535
661	042046L3MASW3	340043	4822507	MASW	551
662	042049L1MASW1	355406	4813294	MASW	324
663	042049L2MASW2	354620	4811127	MASW	440
664	042048L1MASW1	385761	4817807	MASW	333
665	042048L2MASW2	386427	4817257	MASW	273
666	042047L14MASW14	343121	4812180	MASW	460
667	042047L15MASW15	339936	4811080	MASW	468
668	042047L12MASW12	343144	4812520	MASW	522
669	042047L13MASW13	343194	4807300	MASW	289
670	042046L1MASW1	341443	4823749	MASW	485
671	042046L2MASW2	340042	4823507	MASW	462
672	042047L16MASW16	339945	4812120	MASW	552
673	042047L17MASW17	338698	4813790	MASW	404
674	042047L1MASW1	343148	4812720	MASW	591
675	042047L2MASW2	343913	4810280	MASW	280
676	042047L10MASW10	339183	4812590	MASW	327
677	042047L11MASW11	343821	4810480	MASW	370
678	042047L3MASW3	339960	4812230	MASW	449
679	042047L4MASW4	340952	4811740	MASW	413
680	042045L9MASW9	359225	4839723	MASW	276
681	042045L10MASW10	355639	4841496	MASW	314
682	042045L7MASW7	354654	4843834	MASW	335
683	042045L11MASW11	355682	4841720	MASW	239
684	042032L19MASW19	389618	4814878	MASW	204
685	042032L15MASW15	388121	4816239	MASW	325
686	042033L1MASW1	373587	4819843	MASW	289
687	042033L2MASW2	375030	4820764	MASW	413
688	042032L25MASW25	386611	4815375	MASW	322
689	042032L26MASW26	388505	4818244	MASW	321
690	042027L1MASW1	364670	4833994	MASW	250
691	042026L1MASW1	342750	4821283	MASW	363
692	042026L9MASW9	343035	4821400	MASW	419
693	042027L6MASW6	363763	4833325	MASW	314
694	042027L4MASW4	363233	4836553	MASW	347
695	042030L15MASW15	360062	4827879	MASW	248
696	042030L16MASW16	360346	4828005	MASW	302
697	042030L13MASW13	363432	4827043	MASW	349
698	042030L14MASW14	361580	4829283	MASW	346
699	042030L3MASW3	360633	4828929	MASW	389

700	042029L6MASW6	353112	4816400	MASW	402
701	042030L1MASW1	364153	4828368	MASW	587
702	042034L25MASW25	380842	4814366	MASW	305
703	042034L26MASW26	378032	4814544	MASW	299
704	042034L23MASW23	379397	4814497	MASW	293
705	042034L24MASW24	379506	4814734	MASW	292
706	042034L29MASW29	376730	4814891	MASW	214
707	042034L27MASW27	378663	4814612	MASW	451
708	042034L28MASW28	376814	4814551	MASW	290
709	042034L17MASW17	372640	4811701	MASW	275
710	042034L18MASW18	375239	4814001	MASW	336
711	042034L15MASW15	370089	4815983	MASW	368
712	042034L16MASW16	373794	4811859	MASW	379
713	042034L21MASW21	379626	4813048	MASW	269
714	042034L22MASW22	379872	4814171	MASW	248
715	042034L19MASW19	373203	4814693	MASW	497
716	042034L20MASW20	378039	4813205	MASW	345
717	042034L9MASW9	378632	4819322	MASW	321
718	042034L10MASW10	378709	4819378	MASW	325
719	042034L7MASW7	381017	4817398	MASW	223
720	042034L8MASW8	378607	4820820	MASW	262
721	042034L13MASW13	373407	4817832	MASW	257
722	042034L14MASW14	371926	4816177	MASW	302
723	042034L11MASW11	378471	4818742	MASW	301
724	042034L12MASW12	375042	4818857	MASW	325
725	042034L1MASW1	382498	4817090	MASW	274
726	042034L2MASW2	381372	4816148	MASW	255
727	042033L3MASW3	374493	4822182	MASW	324
728	042033L4MASW4	373789	4820604	MASW	484
729	042034L5MASW5	382542	4817147	MASW	261
730	042034L6MASW6	382316	4817219	MASW	236
731	042034L3MASW3	378681	4818958	MASW	302
732	042034L4MASW4	382162	4816376	MASW	276
733	042012L5MASW5	344813	4817265	MASW	371
734	042012L6MASW6	344752	4817460	MASW	368
735	042012L3MASW3	346173	4817972	MASW	507
736	042012L4MASW4	344647	4816484	MASW	531
737	042015L1MASW1	343375	4833817	MASW	497
738	042012L7MASW7	347594	4818562	MASW	339
739	042012L8MASW8	346320	4817156	MASW	416
740	042010L8MASW8	381340	4811037	MASW	352
741	042010L9MASW9	386293	4814195	MASW	273
742	042010L6MASW6	385185	4813360	MASW	374
743	042010L7MASW7	384741	4814034	MASW	281
744	042012L1MASW1	347809	4818665	MASW	441
745	042012L2MASW2	346877	4817985	MASW	358
746	042010L10MASW10	382254	4813554	MASW	347

747	042008L2MASW2	351313	4817105	MASW	324
748	042010L1MASW1	383399	4814366	MASW	249
749	042008L1MASW1	350722	4818444	MASW	485
750	042010L4MASW4	383730	4811311	MASW	254
751	042010L5MASW5	384445	4815181	MASW	254
752	042010L2MASW2	381474	4812331	MASW	312
753	042010L3MASW3	382780	4813417	MASW	291
754	042006L37REMI37	384027	4818006	REMI	282
755	042006L38REMI38	384253	4818372	REMI	255
756	042006L35REMI35	384130	4819048	REMI	278
757	042006L36REMI36	384194	4819794	REMI	190
758	042006L41MASW41	383585	4820834	MASW	382
759	042006L42MASW42	382566	4820716	MASW	295
760	042006L39REMI39	382351	4819381	REMI	228
761	042025L5MASW5	361409	4825460	MASW	459
762	042025L6MASW6	358262	4824460	MASW	286
763	042025L3MASW3	358651	4824910	MASW	306
764	042025L4MASW4	359511	4824880	MASW	291
765	042029L2MASW2	349619	4815900	MASW	345
766	042022L14MASW14	388616	4810520	MASW	280
767	042022L15MASW15	388420	4810400	MASW	277
768	042021L37MASW37	359479	4818777	MASW	372
769	042021L39MASW39	356750	4821312	MASW	347
770	042023L3MASW3	349108	4818256	MASW	471
771	042025L1MASW1	360950	4823750	MASW	408
772	042022L16MASW16	387518	4811810	MASW	258
773	042023L1MASW1	348213	4818633	MASW	268
774	042021L16MASW16	359652	4821473	MASW	464
775	042021L19MASW19	360173	4819517	MASW	251
776	042019L4MASW5	366565	4810353	MASW	324
777	042019L5MASW6	366553	4810506	MASW	435
778	042021L32MASW32	355878	4821092	MASW	282
779	042021L35MASW35	362853	4824216	MASW	421
780	042021L21MASW21	358529	4819710	MASW	547
781	042021L31MASW31	355826	4818281	MASW	380
782	042018L4MASW4	371978	4831226	MASW	311
783	042019L2MASW2	366427	4810857	MASW	271
784	042019L3MASW4	366114	4808939	MASW	321
785	042018L13MASW13	370602	4831229	MASW	298
786	042003L3MASW3	332262	4822863	MASW	434
787	042003L4MASW4	334392	4828860	MASW	371
788	042003L1MASW1	337137	4820969	MASW	448
789	042003L2MASW2	337831	4823162	MASW	440
790	042004L1MASW1	341111	4827833	MASW	347
791	042005L1MASW1	351960	4827228	MASW	241
792	042003L5MASW5	333907	4818764	MASW	548
793	042003L6MASW6	338405	4818264	MASW	462

794	044023L42REMI67	408243	4757641	REMI	254
795	044023L43MASW68	405858	4759900	MASW	287
796	044023L41REMI65	408649	4757565	REMI	225
797	044023L44REMI71	405869	4759857	REMI	350
798	042001L1MASW1	370333	4822709	MASW	229
799	044023L43REMI69	405858	4759900	REMI	286
800	044023L44MASW70	405869	4759857	MASW	373
801	044023L38REMI59	407991	4759348	REMI	313
802	044023L39MASW60	408448	4758512	MASW	276
803	044023L37REMI57	407726	4760432	REMI	263
804	044023L38MASW58	407991	4759348	MASW	322
805	044023L40REMI63	408055	4758317	REMI	319
806	044023L41MASW64	408649	4757565	MASW	236
807	044023L39REMI61	408448	4758512	REMI	245
808	044023L40MASW62	408055	4758317	MASW	334
809	044023L34REMI51	407676	4761069	REMI	341
810	044023L33REMI49	407679	4761634	REMI	277
811	044023L34MASW50	407676	4761069	MASW	349
812	044023L36REMI55	407996	4760374	REMI	270
813	044023L37MASW56	407726	4760432	MASW	263
814	044023L36MASW54	407996	4760374	MASW	283
815	042006L29REMI29	381335	4819224	REMI	196
816	042006L30REMI30	381058	4819629	REMI	213
817	042006L27REMI27	382958	4817888	REMI	181
818	042006L28REMI28	381964	4818991	REMI	266
819	042006L31REMI31	382081	4820223	REMI	246
820	042006L20REMI20	382077	4822266	REMI	187
821	042006L19REMI19	381137	4822766	REMI	240
822	042006L16REMI16	381046	4821304	REMI	244
823	042006L14REMI14	380732	4820824	REMI	198
824	042006L15REMI15	380841	4821076	REMI	262
825	044023L1MASW1	407304	4758061	MASW	484
826	044023L3MASW3	407974	4757714	MASW	311
827	044023L4MASW4	408322	4757553	MASW	271
828	041021L15REMI15	322278	4845109	REMI	215
829	041021L13REMI13	321721	4845204	REMI	385
830	041021L8REMI8	318683	4843400	REMI	372
831	044023L30REMI43	405765	4759436	REMI	265
832	044023L31MASW44	406069	4760022	MASW	261
833	044023L29REMI41	406604	4759186	REMI	341
834	044023L30MASW42	405765	4759436	MASW	273
835	044023L32REMI47	406819	4759547	REMI	282
836	044023L33MASW48	407679	4761634	MASW	291
837	044023L31REMI45	406069	4760022	REMI	262
838	044023L32MASW46	406819	4759547	MASW	293
839	044023L26REMI35	406696	4759009	REMI	353
840	044023L27MASW36	407145	4758941	MASW	353

841	044023L25REMI33	407778	4758878	REMI	329
842	044023L26MASW34	406696	4759009	MASW	375
843	044023L28REMI39	407576	4759396	REMI	344
844	044023L29MASW40	406604	4759186	MASW	339
845	044023L27REMI37	407145	4758941	REMI	356
846	044023L28MASW38	407576	4759396	MASW	347
847	044023L21REMI25	406845	4759987	REMI	305
848	044023L22MASW26	404737	4759123	MASW	360
849	044023L21MASW24	406845	4759987	MASW	341
850	044023L24REMI31	407169	4758249	REMI	376
851	044023L25MASW32	407778	4758878	MASW	342
852	044023L22REMI27	404737	4759123	REMI	331
853	044023L24MASW30	407169	4758249	MASW	395
854	044023L18MASW18	406932	4760905	MASW	491
855	044023L19REMI21	406733	4760428	REMI	397
856	044023L20MASW22	405851	4759606	MASW	336
857	044023L18REMI19	406932	4760905	REMI	451
858	044023L19MASW20	406733	4760428	MASW	392
859	043053L26MASW26	361401	4785438	MASW	415
860	043054L1MASW1	365477	4794511	MASW	373
861	043053L24MASW24	359822	4785342	MASW	376
862	043053L25MASW25	360228	4785313	MASW	479
863	043054L5MASW5	363157	4796568	MASW	619
864	043054L6MASW6	362709	4796873	MASW	595
865	043054L2MASW2	365415	4794478	MASW	366
866	043054L4REMI4	363154	4796566	REMI	607
867	043053L18MASW18	361442	4786607	MASW	311
868	043053L19MASW19	361789	4786575	MASW	245
869	043053L16MASW16	359547	4788143	MASW	494
870	043053L17MASW17	360993	4786454	MASW	248
871	043053L22MASW22	361060	4785804	MASW	453
872	043053L23MASW23	360043	4786163	MASW	268
873	043053L20MASW20	362469	4786262	MASW	437
874	043053L21MASW21	361357	4786096	MASW	319
875	043053L10MASW10	362106	4785086	MASW	452
876	043053L11MASW11	359295	4785040	MASW	321
877	043053L8MASW8	361833	4785505	MASW	516
878	043053L14MASW14	359329	4787972	MASW	341
879	043053L15MASW15	359643	4788076	MASW	329
880	043053L12MASW12	361052	4786151	MASW	318
881	043053L13MASW13	362724	4786234	MASW	324
882	043053L2MASW2	364028	4786523	MASW	430
883	043053L1MASW1	364996	4786870	MASW	462
884	043053L7MASW7	361884	4785204	MASW	397
885	043053L4MASW4	360451	4785614	MASW	347
886	044073L5MASW5	376598	4749091	MASW	397
887	044073L6MASW6	376732	4748910	MASW	330

888	043058L9MASW9	344143	4769545	MASW	429
889	043058L10MASW2	343890	4769421	MASW	347
890	041021L1REMI1	319812	4846925	REMI	326
891	041021L2REMI2	321456	4845104	REMI	250
892	044073L7MASW7	376269	4748594	MASW	603
893	044073L8MASW8	375853	4748463	MASW	433
894	043058L2MASW3	343849	4769975	MASW	378
895	043058L3MASW4	344098	4769579	MASW	329
896	043055L7MASW7	368093	4784020	MASW	313
897	043058L1MASW1	343711	4769916	MASW	306
898	043058L6MASW7	344304	4766794	MASW	478
899	043058L8MASW8	344111	4769265	MASW	395
900	043058L4MASW5	343964	4766466	MASW	448
901	043058L5MASW6	344079	4766452	MASW	567
902	043054L20MASW20	363179	4795587	MASW	359
903	043055L2MASW2	368343	4784306	MASW	447
904	043054L18MASW18	364321	4793781	MASW	424
905	043054L19MASW19	361605	4797512	MASW	318
906	043055L3MASW3	368076	4783798	MASW	487
907	043055L4MASW4	368031	4783597	MASW	346
908	043054L12REMI12	364264	4793472	REMI	478
909	043054L13MASW13	362499	4796570	MASW	464
910	043054L8REMI8	363278	4796752	REMI	357
911	043054L10MASW10	364311	4799902	MASW	399
912	043054L16MASW16	363050	4795830	MASW	425
913	043054L17MASW17	363973	4793275	MASW	371
914	043054L14MASW14	362706	4797126	MASW	456
915	043054L15MASW15	363103	4796494	MASW	412
916	043049L1MASW1	361030	4765801	MASW	373
917	043049L2MASW2	361537	4766131	MASW	462
918	043049L3MASW3	361507	4766094	MASW	465
919	043049L4MASW4	358432	4763271	MASW	411
920	109036L3MASW3	377826	4761027	MASW	420
921	043052L18MASW18	333988	4771222	MASW	486
922	109036L1MASW1	377803	4764269	MASW	318
923	109036L6MASW6	377240	4765058	MASW	375
924	109036L7MASW7	378555	4761190	MASW	478
925	109036L4MASW4	376490	4766302	MASW	361
926	109036L5MASW5	377155	4764657	MASW	477
927	043052L8MASW8	331161	4765501	MASW	853
928	043052L9MASW9	330976	4760402	MASW	621
929	043052L6MASW6	334517	4771302	MASW	548
930	043052L7MASW7	329589	4762615	MASW	551
931	043052L14MASW14	337333	4772257	MASW	363
932	043051L13MASW13	353072	4781969	MASW	505
933	043051L11MASW11	353166	4781987	MASW	263
934	043051L20MASW20	353328	4779008	MASW	593

935	043051L14MASW14	352864	4781922	MASW	614
936	043051L15MASW15	352758	4781892	MASW	659
937	109038L5MASW5	377297	4767893	MASW	410
938	043050L8MASW8	335169	4778640	MASW	581
939	043052L19MASW19	333386	4770834	MASW	248
940	109038L3MASW3	377585	4770705	MASW	393
941	109038L4MASW4	378346	4770550	MASW	300
942	109038L1MASW1	377543	4770543	MASW	313
943	109038L2MASW2	377638	4771026	MASW	616
944	043049L24MASW24	361636	4766224	MASW	852
945	043050L6MASW6	333215	4779335	MASW	588
946	043050L7MASW7	333420	4779382	MASW	354
947	043050L5MASW5	333241	4779050	MASW	192
948	043047L8MASW8	351023	4787529	MASW	696
949	043047L9MASW9	352213	4788078	MASW	439
950	043047L7MASW7	351735	4787922	MASW	591
951	043046L8MASW8	358276	4769298	MASW	631
952	043046L9MASW9	359165	4769056	MASW	619
953	043046L6MASW6	362236	4772387	MASW	369
954	043046L7MASW7	358503	4768144	MASW	453
955	043046L12MASW12	363233	4774238	MASW	519
956	043047L1MASW1	351918	4788195	MASW	510
957	043046L10MASW10	359560	4771209	MASW	636
958	043046L11MASW11	358896	4772804	MASW	385
959	043046L1MASW1	363572	4774170	MASW	410
960	044065L5MASW5	382343	4756584	MASW	613
961	043046L4MASW4	362947	4774200	MASW	289
962	043046L5MASW5	362799	4774340	MASW	352
963	043046L2MASW2	363527	4774018	MASW	355
964	043046L3MASW3	362061	4778504	MASW	388
965	044064L4MASW4	375368	4746305	MASW	355
966	044064L2MASW2	374559	4747427	MASW	642
967	044064L3MASW3	375662	4746283	MASW	833
968	043051L4MASW4	352165	4778211	MASW	837
969	043051L2MASW2	353883	4783021	MASW	456
970	043051L8MASW8	353835	4782271	MASW	401
971	043051L6MASW6	350647	4782439	MASW	803
972	043051L7MASW7	356774	4783174	MASW	587
973	043047L28MASW28	351667	4788003	MASW	432
974	043047L26MASW26	351938	4787767	MASW	381
975	043047L27MASW27	351634	4787989	MASW	505
976	043047L32MASW32	352911	4787650	MASW	328
977	043047L30MASW30	351369	4787936	MASW	764
978	043047L31MASW31	350973	4788089	MASW	1151
979	043047L20MASW20	351430	4788265	MASW	406
980	043047L21MASW21	351795	4787570	MASW	525
981	043047L18MASW18	350940	4787612	MASW	509

982	043047L22MASW22	353039	4787901	MASW	464
983	043047L23MASW23	352918	4787552	MASW	281
984	043047L12MASW12	352178	4788011	MASW	526
985	043047L13MASW13	352827	4788277	MASW	409
986	043047L10MASW10	351652	4788619	MASW	481
987	043047L11MASW11	351679	4787903	MASW	844
988	043047L16MASW16	352063	4788819	MASW	355
989	043047L17MASW17	352081	4788613	MASW	324
990	043047L14MASW14	352583	4788016	MASW	579
991	043047L15MASW15	352585	4788332	MASW	374
992	043038L7MASW7	341310	4762601	MASW	414
993	043038L8MASW8	342058	4762565	MASW	622
994	043038L5MASW5	341310	4762601	MASW	495
995	043038L6MASW6	340829	4764081	MASW	676
996	043038L11MASW11	343597	4760207	MASW	856
997	043038L12MASW12	343653	4759925	MASW	516
998	043038L9MASW9	340829	4764081	MASW	730
999	043038L10MASW10	343429	4760186	MASW	571
1000	043036L4MASW4	375477	4786678	MASW	410
1001	043036L5MASW5	376376	4787083	MASW	500
1002	043036L2MASW2	374930	4786276	MASW	585
1003	043036L3MASW3	375523	4786579	MASW	392
1004	043038L3MASW3	340813	4767353	MASW	445
1005	043038L4MASW4	341036	4769203	MASW	490
1006	043038L1MASW1	341345	4767964	MASW	520
1007	043038L2MASW2	340967	4767554	MASW	765
1008	043035L0MASW0	371796	4768348	MASW	655
1009	044056L9MASW9	374589	4753110	MASW	432
1010	044056L10MASW10	375548	4753443	MASW	478
1011	043035L4MASW4	369973	4769905	MASW	345
1012	043036L1MASW1	374828	4786652	MASW	550
1013	043035L3MASW3	369089	4768122	MASW	334
1014	109029L7MASW7	385944	4764959	MASW	361
1015	044056L7MASW7	376042	4751767	MASW	557
1016	044056L8MASW8	374709	4752903	MASW	651
1017	044056L6MASW6	375233	4751815	MASW	349
1018	043045L2MASW2	367069	4777771	MASW	345
1019	043041L10MASW10	364155	4792417	MASW	397
1020	043045L1MASW1	367226	4777977	MASW	536
1021	043045L6MASW6	369572	4777301	MASW	375
1022	044064L1MASW1	375533	4746437	MASW	669
1023	043045L4MASW4	368097	4777907	MASW	277
1024	043045L5MASW5	367780	4777906	MASW	398
1025	043041L4MASW4	366066	4791764	MASW	432
1026	043041L5MASW5	365766	4792286	MASW	484
1027	043041L8MASW8	366523	4791590	MASW	265
1028	043041L9MASW9	362963	4791663	MASW	293

1029	043041L6MASW6	365524	4791521	MASW	315
1030	043041L7MASW7	366309	4791585	MASW	299
1031	043040L1MASW1	344326	4804150	MASW	762
1032	043039L9MASW9	336294	4782292	MASW	569
1033	043039L10MASW10	338559	4783013	MASW	668
1034	043040L4MASW4	345046	4804795	MASW	375
1035	043040L2MASW2	344799	4803802	MASW	529
1036	043040L3MASW3	345271	4803716	MASW	415
1037	043039L3MASW3	339201	4781536	MASW	158
1038	043039L4MASW4	339500	4781530	MASW	464
1039	043039L1MASW1	335702	4782829	MASW	208
1040	043039L2MASW2	335682	4782769	MASW	158
1041	043039L7MASW7	335468	4783081	MASW	509
1042	043039L8MASW8	336344	4782597	MASW	299
1043	043039L5MASW5	338421	4782931	MASW	233
1044	043039L6MASW6	336233	4782218	MASW	335
1045	109020L7MASW8	381682	4763207	MASW	314
1046	109020L5MASW6	380831	4763738	MASW	335
1047	109020L6MASW7	380773	4763978	MASW	326
1048	044044L1MASW1	363391	4751010	MASW	1015
1049	044044L2MASW2	362128	4747753	MASW	548
1050	041004L29REMI29	335061	4836193	REMI	243
1051	109020L2MASW3	381812	4763305	MASW	360
1052	109020L3MASW4	380779	4763802	MASW	461
1053	041004L31REMI31	329322	4840904	REMI	289
1054	109020L1MASW1	380860	4763847	MASW	439
1055	041004L22REMI22	332248	4838630	REMI	279
1056	041004L23REMI23	334258	4836558	REMI	285
1057	041004L14REMI14	331651	4840050	REMI	229
1058	041004L11REMI11	331082	4835920	REMI	228
1059	041004L12REMI12	330251	4839717	REMI	278
1060	041004L18REMI18	332281	4837049	REMI	262
1061	041004L16REMI16	329918	4841361	REMI	263
1062	044054L1MASW1	393676	4753886	MASW	369
1063	043034L20MASW20	341966	4770928	MASW	493
1064	043034L21MASW21	342046	4771098	MASW	372
1065	109029L6MASW6	386388	4765233	MASW	463
1066	044054L2MASW2	394142	4754269	MASW	225
1067	109029L1MASW1	387744	4764899	MASW	330
1068	043034L14MASW14	340568	4771560	MASW	424
1069	043034L12MASW12	340509	4771777	MASW	413
1070	043034L13MASW13	340499	4771725	MASW	392
1071	043034L18MASW18	340744	4772157	MASW	295
1072	043034L19MASW19	340910	4771755	MASW	388
1073	043034L16MASW16	340574	4772201	MASW	399
1074	043034L17MASW17	340839	4772365	MASW	467
1075	109021L1MASW1	384252	4764372	MASW	261

1076	044044L11MASW11	365085	4752024	MASW	935
1077	044044L12MASW12	358698	4748484	MASW	602
1078	043034L11MASW11	342130	4771029	MASW	607
1079	044044L5MASW5	365662	4749671	MASW	558
1080	044044L6MASW6	361557	4750172	MASW	1077
1081	044044L3MASW3	358630	4748487	MASW	664
1082	044044L4MASW4	361832	4752067	MASW	469
1083	044044L9MASW9	364280	4751233	MASW	862
1084	044044L10MASW10	365719	4749540	MASW	398
1085	044044L7MASW7	363452	4748954	MASW	704
1086	044044L8MASW8	363744	4752565	MASW	467
1087	109014L2MASW2	374388	4759663	MASW	580
1088	109014L3MASW3	374495	4759765	MASW	357
1089	044034L4MASW4	385221	4759006	MASW	445
1090	109014L1MASW1	374326	4763046	MASW	451
1091	109014L4MASW4	374382	4760676	MASW	1262
1092	109014L5MASW5	374170	4760827	MASW	866
1093	043027L8MASW9	338398	4762518	MASW	576
1094	043027L9MASW10	338025	4763304	MASW	610
1095	043027L6MASW7	337534	4761070	MASW	455
1096	043027L7MASW8	337549	4760722	MASW	874
1097	044034L1MASW1	384337	4759068	MASW	181
1098	044034L3MASW3	384048	4758355	MASW	553
1099	043027L10MASW11	338152	4763394	MASW	590
1100	043027L11MASW12	337426	4763562	MASW	504
1101	043027L1MASW1	338381	4762401	MASW	576
1102	043027L4MASW5	333966	4762504	MASW	399
1103	043027L5MASW6	336442	4760686	MASW	612
1104	043027L2MASW3	337124	4761962	MASW	585
1105	043027L3MASW4	333999	4760718	MASW	899
1106	109013L3MASW3	375426	4777318	MASW	548
1107	109013L4MASW4	374692	4777030	MASW	463
1108	109013L1MASW1	375581	4776894	MASW	353
1109	109013L2MASW2	375603	4777366	MASW	580
1110	109026L1MASW1	377051	4774660	MASW	254
1111	109026L2MASW2	375461	4775560	MASW	380
1112	109013L5MASW5	375423	4776720	MASW	631
1113	109013L6MASW6	375505	4776405	MASW	505
1114	041004L8REMI8	335047	4836946	REMI	245
1115	041065L5MASW5	318441	4858367	MASW	513
1116	041065L6MASW6	324594	4861811	MASW	302
1117	109019L3MASW3	379951	4769304	MASW	384
1118	041065L4MASW4	321248	4864202	MASW	297
1119	041004L1REMI1	333611	4837356	REMI	279
1120	109017L2MASW2	381238	4776865	MASW	293
1121	109017L3MASW3	380238	4776086	MASW	232
1122	109017L1MASW1	381241	4776392	MASW	235

1123	109019L2MASW2	380184	4767202	MASW	569
1124	109017L4MASW4	380918	4776602	MASW	316
1125	044027L6MASW8	392481	4742963	MASW	383
1126	044027L7MASW6	393429	4743003	MASW	330
1127	043023L43MASW43	374596	4794863	MASW	348
1128	043023L44MASW44	372917	4793944	MASW	355
1129	109011L2MASW2	376022	4778620	MASW	418
1130	109011L3MASW3	376097	4779288	MASW	170
1131	044027L8MASW7	391479	4744132	MASW	295
1132	109011L1MASW1	376906	4780009	MASW	335
1133	043023L37MASW37	372118	4797438	MASW	259
1134	043023L36MASW36	371050	4790292	MASW	441
1135	043023L41MASW41	373389	4795101	MASW	272
1136	043023L40MASW40	375129	4794519	MASW	455
1137	043023L27MASW27	375179	4796174	MASW	373
1138	043023L28MASW28	374201	4794781	MASW	243
1139	043023L34MASW34	373129	4795505	MASW	308
1140	043023L32MASW32	373371	4794507	MASW	238
1141	043023L21MASW21	373238	4795421	MASW	349
1142	043023L22MASW22	375618	4796544	MASW	415
1143	043023L20MASW20	375041	4795430	MASW	304
1144	043023L26MASW26	373615	4795274	MASW	307
1145	109012L2MASW2	382862	4769412	MASW	540
1146	109012L3MASW3	382723	4769319	MASW	412
1147	043025L5MASW5	375982	4782260	MASW	495
1148	043025L6MASW6	376470	4781800	MASW	300
1149	109012L6MASW6	382823	4766800	MASW	341
1150	044032L2MASW2	384898	4761531	MASW	337
1151	109012L4MASW4	382340	4769335	MASW	318
1152	109012L5MASW5	382333	4769351	MASW	315
1153	043024L28MASW28	337853	4789771	MASW	366
1154	043024L29MASW29	337844	4789812	MASW	489
1155	043024L26MASW26	341572	4792625	MASW	686
1156	043024L27MASW27	338953	4795633	MASW	392
1157	043025L3MASW3	376556	4782621	MASW	482
1158	043025L4MASW4	377000	4782805	MASW	414
1159	043025L1MASW1	376961	4782759	MASW	464
1160	043025L2MASW2	375439	4782587	MASW	435
1161	043024L20MASW20	338522	4791031	MASW	635
1162	043024L21MASW21	338748	4791053	MASW	462
1163	043024L18MASW18	338247	4790042	MASW	482
1164	043024L19MASW19	337760	4789999	MASW	492
1165	043024L24MASW24	338735	4791185	MASW	422
1166	043024L25MASW25	338329	4789857	MASW	291
1167	043024L22MASW22	338434	4790713	MASW	528
1168	043024L23MASW23	337330	4793821	MASW	544
1169	043024L2MASW2	337301	4794090	MASW	519

1170	043024L3MASW3	338290	4791355	MASW	571
1171	109011L4MASW4	376123	4778001	MASW	380
1172	043024L1MASW1	339191	4791104	MASW	392
1173	043024L16MASW16	338216	4790540	MASW	523
1174	043024L17MASW17	338178	4790915	MASW	442
1175	043024L4MASW4	337906	4790299	MASW	524
1176	043024L15MASW15	340386	4797524	MASW	640
1177	043019L1MASW1	332054	4784041	MASW	251
1178	043019L2MASW2	332076	4783907	MASW	267
1179	043019L5MASW5	331811	4784201	MASW	801
1180	043019L6MASW6	331180	4783004	MASW	196
1181	043019L3MASW3	331993	4783889	MASW	417
1182	043019L4MASW4	331939	4783817	MASW	1069
1183	109005L9MASW9	375416	4772594	MASW	308
1184	043017L1MASW1	347101	4772551	MASW	343
1185	109005L7MASW7	377386	4773660	MASW	316
1186	109005L8MASW8	375590	4773296	MASW	326
1187	043017L2MASW2	347127	4772621	MASW	393
1188	109005L1MASW1	378342	4772775	MASW	385
1189	109005L4MASW4	378047	4772527	MASW	516
1190	109005L5MASW5	377686	4772440	MASW	332
1191	109005L2MASW2	377237	4772746	MASW	437
1192	109005L3MASW3	376755	4771998	MASW	427
1193	042017L23MASW26	330948	4799763	MASW	335
1194	043023L14MASW14	371716	4797008	MASW	342
1195	043023L11MASW11	378685	4792734	MASW	373
1196	043023L12MASW12	371553	4790245	MASW	364
1197	043023L17MASW17	375933	4794170	MASW	421
1198	043023L18MASW18	374589	4795318	MASW	364
1199	043023L15MASW15	372228	4797797	MASW	328
1200	043023L16MASW16	374351	4795203	MASW	433
1201	043022L6MASW6	371017	4780335	MASW	309
1202	043022L7MASW7	370248	4779640	MASW	404
1203	043022L4MASW4	371868	4779981	MASW	392
1204	043022L5MASW5	371210	4780495	MASW	377
1205	043023L7MASW7	375006	4794834	MASW	331
1206	043022L8MASW8	371527	4780612	MASW	309
1207	043023L6MASW6	374781	4794070	MASW	345
1208	043020L4MASW4	343433	4789179	MASW	520
1209	043020L5MASW5	342971	4786823	MASW	416
1210	043020L2MASW2	342614	4789479	MASW	703
1211	043020L3MASW3	343348	4789311	MASW	469
1212	043022L2MASW2	370188	4779714	MASW	270
1213	043022L3MASW3	371468	4780482	MASW	265
1214	043020L6MASW6	343084	4787019	MASW	700
1215	043022L1MASW1	371158	4780311	MASW	403
1216	044021L3MASW3	376906	4757954	MASW	393

1217	044021L11MASW11	377147	4755226	MASW	312
1218	043019L7MASW7	331209	4782746	MASW	575
1219	043019L8MASW8	331791	4783732	MASW	490
1220	044021L14MASW14	376955	4758362	MASW	304
1221	043020L1MASW1	342816	4786824	MASW	391
1222	044021L12MASW12	376122	4756566	MASW	322
1223	044021L13MASW13	376760	4757672	MASW	345
1224	043011L6MASW6	358047	4774211	MASW	462
1225	043011L4MASW4	358295	4774414	MASW	467
1226	043011L11MASW11	357949	4775612	MASW	508
1227	043011L8MASW8	355552	4774102	MASW	871
1228	043011L9MASW9	355354	4773867	MASW	476
1229	042013L15MASW17	337232	4797578	MASW	455
1230	042013L16MASW18	337164	4798987	MASW	306
1231	042013L13MASW15	336612	4797123	MASW	545
1232	042013L14MASW16	336556	4796879	MASW	509
1233	043011L2MASW2	355726	4773056	MASW	611
1234	043011L3MASW3	357343	4773141	MASW	442
1235	042013L17MASW19	336505	4798062	MASW	668
1236	042013L18MASW20	336870	4797052	MASW	331
1237	042013L7MASW8	337044	4798916	MASW	388
1238	042013L8MASW9	337060	4798284	MASW	354
1239	042013L4MASW5	336963	4798092	MASW	902
1240	042013L6MASW7	337460	4797885	MASW	381
1241	042013L11MASW13	337313	4798941	MASW	342
1242	042013L12MASW14	336654	4797556	MASW	542
1243	042013L9MASW10	336917	4798787	MASW	511
1244	042013L10MASW12	336705	4798610	MASW	464
1245	044012L1MASW1	385507	4753574	MASW	379
1246	044012L2MASW2	386753	4752730	MASW	517
1247	043009L34MASW34	341785	4786212	MASW	604
1248	043009L35MASW35	341855	4785285	MASW	269
1249	044013L10MASW10	396410	4750597	MASW	452
1250	042013L3MASW3	337052	4798962	MASW	397
1251	044013L8MASW8	396023	4749759	MASW	475
1252	044013L9MASW9	396100	4750217	MASW	468
1253	042017L16MASW19	328886	4801188	MASW	483
1254	043057L21MASW21	340119	4753992	MASW	422
1255	043057L19MASW19	343443	4755209	MASW	424
1256	043012L9MASW9	355186	4804247	MASW	495
1257	043012L10MASW10	354678	4803949	MASW	1200
1258	043012L7MASW7	354135	4804176	MASW	510
1259	043057L16MASW16	343780	4754468	MASW	508
1260	043057L17MASW17	343853	4754967	MASW	353
1261	043012L11MASW11	355494	4803897	MASW	469
1262	043012L1MASW1	354858	4804439	MASW	439
1263	043012L2MASW2	359743	4807563	MASW	240

1264	043011L13MASW13	356065	4769500	MASW	580
1265	043012L5MASW5	359602	4800762	MASW	508
1266	043012L6MASW6	353789	4804497	MASW	1400
1267	043012L3MASW3	362248	4804403	MASW	319
1268	043014L5MASW5	368195	4782089	MASW	425
1269	043014L6MASW6	366448	4780116	MASW	277
1270	043014L3MASW3	366987	4781193	MASW	511
1271	043014L4MASW4	367839	4780891	MASW	283
1272	044015L4MASW4	370376	4757358	MASW	406
1273	044015L5MASW5	370470	4757398	MASW	546
1274	044015L2MASW2	370022	4756775	MASW	592
1275	044015L3MASW3	370291	4757088	MASW	570
1276	044014L2MASW2	397487	4747901	MASW	357
1277	044014L3MASW3	397233	4748324	MASW	267
1278	044014L1MASW1	397650	4747865	MASW	349
1279	043014L1MASW1	366406	4780016	MASW	227
1280	043014L2MASW2	366768	4780721	MASW	437
1281	044014L4MASW4	398139	4747727	MASW	327
1282	044014L5MASW5	397779	4747662	MASW	383
1283	043007L4MASW4	342517	4776928	MASW	273
1284	043007L5MASW5	342598	4778794	MASW	339
1285	043007L2MASW2	342744	4777071	MASW	415
1286	043007L3MASW3	342607	4778982	MASW	272
1287	044011L3MASW3	393822	4748577	MASW	570
1288	043006L12MASW12	355474	4777847	MASW	357
1289	043006L10MASW10	355607	4777470	MASW	264
1290	043007L1MASW1	342007	4778551	MASW	398
1291	042017L6MASW7	330383	4800215	MASW	381
1292	042017L7MASW8	333772	4803978	MASW	518
1293	042017L3MASW4	331410	4799598	MASW	456
1294	042017L5MASW6	332321	4801568	MASW	681
1295	042017L8MASW10	323723	4797766	MASW	476
1296	043016L7MASW7	334219	4790969	MASW	451
1297	043016L4MASW4	333110	4790779	MASW	456
1298	042017L1MASW1	332377	4801526	MASW	647
1299	042017L2MASW3	329826	4800021	MASW	516
1300	043016L9MASW9	334963	4792766	MASW	362
1301	044016L23MASW23	393114	4760135	MASW	304
1302	044016L24MASW24	392242	4759773	MASW	300
1303	043015L14MASW14	378646	4788173	MASW	499
1304	043016L2MASW2	333541	4790510	MASW	465
1305	043016L3MASW3	333113	4790687	MASW	392
1306	044016L25MASW25	391713	4758352	MASW	359
1307	043016L1MASW1	333332	4791303	MASW	589
1308	043015L6MASW6	379457	4788762	MASW	300
1309	043015L9MASW9	378546	4789575	MASW	357
1310	044015L6MASW6	371481	4758046	MASW	555

1311	043015L5MASW5	377098	4790600	MASW	447
1312	043015L13MASW13	379146	4789273	MASW	354
1313	043015L10MASW10	377605	4790911	MASW	471
1314	043015L11MASW11	378397	4790330	MASW	318
1315	044007L31MASW31	385593	4746144	MASW	485
1316	044007L32MASW32	387000	4745436	MASW	489
1317	044007L29MASW29	384156	4745538	MASW	631
1318	044007L30MASW30	384760	4745405	MASW	474
1319	044007L35MASW35	387395	4744292	MASW	553
1320	044007L36MASW36	388852	4746728	MASW	386
1321	044007L33MASW33	384786	4744850	MASW	410
1322	044007L34MASW34	387527	4745804	MASW	587
1323	044007L23MASW23	383959	4746266	MASW	538
1324	044007L24MASW24	383488	4746316	MASW	593
1325	044007L21MASW21	384908	4745830	MASW	632
1326	044007L22MASW22	383982	4746296	MASW	538
1327	044007L27MASW27	383932	4746130	MASW	704
1328	044007L28MASW28	384291	4746116	MASW	666
1329	044007L25MASW25	385268	4745642	MASW	884
1330	044007L26MASW26	382578	4745576	MASW	504
1331	044007L13MASW69	390552	4744456	MASW	401
1332	044007L15MASW73	395008	4745590	MASW	416
1333	044007L8MASW63	382404	4745583	MASW	656
1334	044007L9MASW65	382589	4746747	MASW	418
1335	044007L18MASW79	384089	4742744	MASW	572
1336	044007L19MASW81	385461	4743973	MASW	399
1337	044007L16MASW75	382997	4746253	MASW	570
1338	044007L17MASW77	389046	4746269	MASW	414
1339	043008L4MASW4	358802	4776500	MASW	270
1340	043008L5MASW5	358746	4776451	MASW	300
1341	044007L6MASW59	385079	4744880	MASW	416
1342	044007L7MASW61	387958	4744999	MASW	687
1343	044007L5MASW57	384621	4745066	MASW	646
1344	043006L5MASW5	355429	4777937	MASW	350
1345	043006L2MASW2	355853	4778884	MASW	437
1346	043006L3MASW3	351312	4777439	MASW	589
1347	043006L8MASW8	355509	4778327	MASW	620
1348	043006L9MASW9	355534	4777908	MASW	501

Dual-proxy estimation of Vs30: the case study of the Marche Region (central Italy)

Veronica Gironelli[1,2], Tiziano Volatili[1], Lucia Luzi[3], Giulio Brunelli[1,3], Emanuele Tondi[1,2]

[1] School of Science and Technology – Geology Division, University of Camerino, Italy

[2] National Institute of Geophysics and Volcanology, Seismology and Tectonophysics Division, Camerino, Italy

[3] National Institute of Geophysics and Volcanology, Milan, Italy

ISTITUTO NAZIONALE DI GEOFISICA E VULCANOLOGIA

300049 337555 375061 412567 450073

4838285

4800779

4763273

Pesaro
Urbino
Ancona
Macerata
Fermo
Ascoli Piceno

Foglia River
Metauro River
Cesano River
Misa River
Esino River
Musone River
Potenza River
Chienti River
Tenna River
Aso River
Tronto River

Adriatic Sea

Italy
Thyrrenian Sea

Vs30 [m/s]

- ≤ 320
- 321 - 370
- 371 - 420
- 421 - 470
- 471 - 520
- 521 - 570
- 571 - 620
- 621 - 670
- 671 - 720
- > 720

Lithology

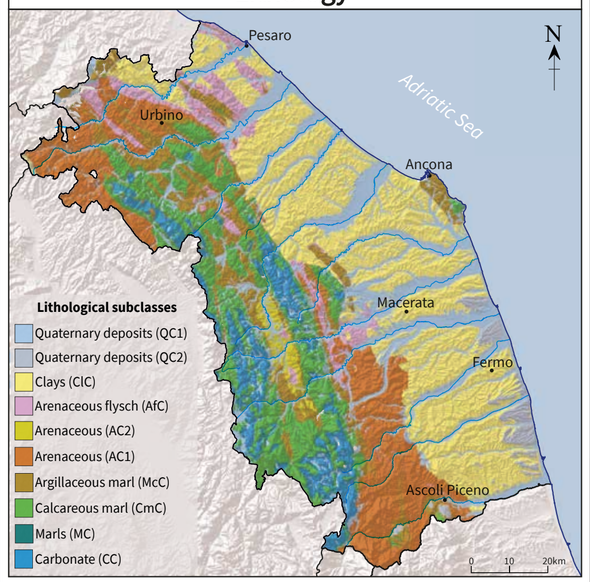

Lithological subclasses

- Quaternary deposits (QC1)
- Quaternary deposits (QC2)
- Clays (ClC)
- Arenaceous flysch (AfC)
- Arenaceous (AC2)
- Arenaceous (AC1)
- Argillaceous marl (McC)
- Calcareous marl (CmC)
- Marls (MC)
- Carbonate (CC)

Topographic slope

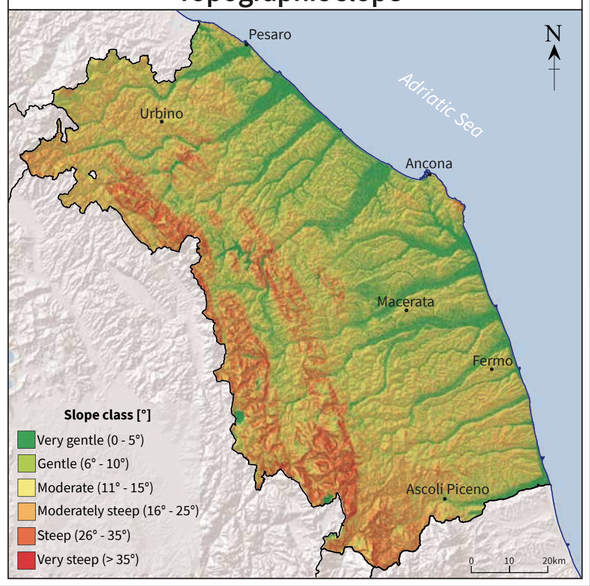

Slope class [°]

- Very gentle (0 - 5°)
- Gentle (6° - 10°)
- Moderate (11° - 15°)
- Moderately steep (16° - 25°)
- Steep (26° - 35°)
- Very steep (> 35°)

N

1 : 250.000
(if printed at A1)

0 10 20
kilometers

Basemaps: 1) World Shaded Relief - Source Esri, Shaded relief; 2) Hydrographic network from vectorial maps at 1:10.000 scale from Regione Marche

Coordinate System: UTM Zone 33N

Datum: WGS84

Unit: meters